# The role of TRPC6 channel in the dentate gyrus and pathophysiology of traumatic brain injury.

Dissertation

to obtain the degree

"Doctor of the natural sciences (Dr. rer. nat.)"

in Pharmacology and Toxicology

submitted to the faculty of Chemistry, Pharmaceutical Sciences, Geography, and Geosciences of the Johannes Gutenberg University Mainz

by

Salma Hamed

born in Beheira

Mainz,   March 2023

# The role of TRPC6 channel in the dentate gyrus and the pathophysiology of traumatic brain injury

Dean: Prof. Dr██████████████

Name of 1st reviewer: ███████████████

Name of 2nd reviewer: ██████████████

Name of 3rd reviewer: ████████████

Name of 4th reviewer: ——————————

Date of submission: 7.03.2023

*D77 (Dissertation Universität Mainz)*

## Declaration of Authorship

"I, Salma Hamed, herewith declare that the presented work and thesis titled "The role of TRPC6 channel in hippocampal plasticity and pathophysiology of traumatic brain injury" are composed by myself and without any use other than the cited sources and aids.

I confirm that:

- This work was done wholly in candidature for a research degree at the Johannes Gutenberg University, Mainz
- Sentences or parts of sentences quoted literally are marked as such; other references with regard to the statement and scope are indicated by full details of the publications concerned.
- The thesis in the same or similar form has not been submitted to any examination body and has not been published.
- Where the thesis is based on work, I did jointly with others, I have clarified exactly what others did and what I have contributed to myself.

Date:_____

Sign:_____

*"If we knew what it was we were doing, it would not be called research, would it?"*

– Albert Einstein

Johannes Gutenberg University Mainz

# Abstract

Department of Pharmacology and Toxicology at the Institute of Pharmaceutical and Biomedical Sciences

Dr. rer. nat.

**The role of TRPC6 channel in the dentate gyrus and pathophysiology of traumatic brain injury.**

Salma Hamed

The TRPC6 channel, a member of the TRP superfamily, is widely expressed in various brain regions, including the dentate gyrus (DG), where its expression is exceptionally high. This research focuses on the significance of TRPC6 in normal hippocampal function and its potential protective role in traumatic brain injury (TBI). The TRPC6 has been shown to play a crucial role in synaptic plasticity processes, including changes in dendritic growth, spine morphology, and an increase in excitatory synapses. Recent evidence suggests that TRPC6 may act as a protective mechanism during ischemic strokes, as its expression is dramatically lessened in neurons following ischemia, leading to neuronal death. The pathological role of TRPC6 in the brain was investigated using a combination of TRPC6 wild-type (WT) and knockout mice (KO), along with various molecular, immunohistology, and electrophysiology techniques. The controlled cortical impact method (CCI) was also used to induce TBI for further study. The research findings demonstrate that deletion of TRPC6 leads to altered hippocampus function, including aberrant maturation of granular cells (GC) in the DG and morphological and electrophysiological modifications, including hypo-excitability and lack of long-term potentiation (LTP). These modifications are accompanied by molecular changes, including alterations in protein phosphorylation and gene expression, which are crucial for synaptic plasticity and neuronal survival, such as CREB, mTOR, and AKT. Additionally, this thesis shows for the first time how deletion of TRPC6 increases the pathogenicity of TBI, manifested as a larger lesion volume. In conclusion, this research sheds light on the critical role of the TRPC6 in maintaining normal brain function and highlights its potential as a target for new approaches in mitigating TBI.

Johannes Gutenberg Universität Mainz

# Zusammenfassung

Department Pharmakologie und Toxikologie am Institut für Pharmazeutische und Biomedizinische Wissenschaften

Dr. rer. nat.

## Die Rolle des TRPC6-Kanals im Gyrus dentatus und die Pathophysiologie von traumatischen Hirnverletzungen

Salma Hamed

Der TRPC6-Kanal, ein Mitglied der TRP-Superfamilie, ist in verschiedenen Hirnregionen weit verbreitet, darunter auch im Gyrus dentatus (DG), wo seine Expression außergewöhnlich hoch ist. Diese Forschungsarbeit konzentriert sich auf die Bedeutung von TRPC6 für die normale Funktion des Hippocampus und seine potenzielle Schutzfunktion bei traumatischen Hirnverletzungen (TBI). Es hat sich gezeigt, dass TRPC6 eine entscheidende Rolle bei synaptischen Plastizitätsprozessen spielt, einschließlich Veränderungen des dendritischen Wachstums, der Stachelmorphologie und einer Zunahme der erregenden Synapsen. Jüngste Erkenntnisse deuten darauf hin, dass TRPC6 bei ischämischen Schlaganfällen als Schutzmechanismus fungieren könnte, da seine Expression in Neuronen nach einer Ischämie dramatisch abnimmt, was zum Absterben von Neuronen führt. Die pathologische Rolle von TRPC6 im Gehirn wurde mit einer Kombination aus TRPC6-Wildtyp (WT) und Knockout-Mäusen (KO) sowie mit verschiedenen molekularen, immunhistologischen und elektrophysiologischen Techniken untersucht. Zur weiteren Untersuchung wurde auch die Methode der kontrollierten kortikalen Einwirkung (CCI) verwendet, um ein Schädel-Hirn-Trauma zu induzieren. Die Forschungsergebnisse zeigen, dass die Abwesenheit von TRPC6 zu einer veränderten Funktion des Hippocampus führt, einschließlich einer abnormalen Reifung der granularen Zellen (GC) in der DG und morphologischer und elektrophysiologischer Veränderungen, einschließlich Hypoerregbarkeit und fehlender Langzeitpotenzierung (LTP).

Diese Modifikationen werden von molekularen Veränderungen begleitet, einschließlich Veränderungen der Proteinphosphorylierung und der Genexpression, die für die synaptische Plastizität und das neuronale Überleben entscheidend sind, wie CREB, mTOR und AKT. Darüber hinaus zeigt diese Arbeit zum ersten Mal, wie die Absenz von TRPC6 die Pathogenität von TBI erhöht, was sich in einem größeren Läsionsvolumen manifestiert. Zusammenfassend lässt sich sagen, dass diese Forschungsarbeit die kritische Rolle von TRPC6 bei der Aufrechterhaltung der normalen Gehirnfunktion beleuchtet und sein Potenzial als Ziel für neue Ansätze zur Linderung von Schädel-Hirn-Traumata hervorhebt.

## Acknowledgments

████████████████████████████████████vii████████████████████████████████████

████████████████████████████████████████████████████████████████████████████

████████████████████████████████████████████████████████████████████████████

██████████████████████████████████████████████.

- ████████████████████████████████████████████████████████████████████████

████████████████████████████████████████████████████████████████████

████████████████████████████████████████████████████████████████████

████████████████████████████████████████████████████████████████████

████████████████████████████████████████████████████████████████████

████████████████████████████████████████████████████████████████████

████████████████████████████████████████████████████████████████████

████████████████████████████████████████████████████████████████████

████████████████████████████████████████████████████████████████████

████████████████████████████████████████████████████████████████████

██████████████████████████████████████████████████████████████.

- ████████████████████████████████████████████████████████████████████████

████████████████████████████████████████████████████████████████████

████████████████████████████████████████████████████████████████████

████████████████████████████████████████████████████████████████████

████████████████████████████████████████████████████████████████████

████████████████████████████████████████████████████████████████████

████████████████████████████████████████████████████████████████████

████████████████████████████████████████████████████████████████████

████████████████████████████████████████████████████████████████████

████████████████████████████████████████████████████████████████████

███████████████████████████████████████████████████████████████████.

████████████████████████████████████████████████████████████

████████████████████████████████████████████████████████

████████████████████████████████████████████████████████

████████████████████████████████████████████████████████

████████████████████████████████████████████████████████

████████████████████████████████████████████████████████

████████████████████████████████████████████████████████

████████████████████████████████████████████████████████

████████████████████████████████████████████████████████

████████████████████████████████████████████████████████

████████████████████████████████████████████████████████

████████████████████████████████████████████████████████

███

███████████████████████████████████████████████████████████████

███████████████████████████████████████████████████████

███████████████████████████████████████████████████████

███████████████████████████████████████████████████████

███████████████████████████████████████████████████████

███████████████████████████████████████████████████████

███████████████████████████████████████████████████████

█████████

- ████████████████████████████████████████████████████████

████████████████████████████████████████████████████████

████████████████████████████████████████████████████████

████████████████████████████████████████████████████████

████████████████████████████████████████████████████████

████████████████████████████████████████████████████████

████████████████████████████████████████████████████████

████████████████████████████████████████████████████████

████████████████████████████████████████████████████████

████████████████████████████████████████████████████████

███████████████████████████████████████████████████
███████████████████████.

- ███████████████████████████████████████████████████
███████████████████████████████████████████████████
███████████████████████████████████████████████████
███████████████████████████████████████████████████
███████████████████████████████████████.

- ███████████████████████████████████████████████████
███████████████████████████████████████████████████
███████████████████████████████████████.

███████████████████████████████████████████████████
███████████████████████████████████████████████████
███████████████████████████████████████████████████
███████████████████████████████████████████████████
███████████████████████████████████████████████████
███████████████████████████████████████.

███████████████████████████████████████████████████
███████████████████████████████████████████████████
███████████████████████████████████████████████████
███████████████████████████████████████████████████
███████████████████████████████████████████████████
█████████████.

# Abbreviations

ACh        Acetylecholine

ACSF       Artificial cerebro spinal fluid

AD         Alzheimer's disease

Akt        Protein kinase B

APV        2-amino-5-phosphonovaleric acid

BDNF       Brain-derived neurotrophic factor

BSA        Bovine serum albumin

CaMK       Ca2+/calmodulin-dependent protein kinase

cAMP       Adenosine 3',5'-cyclic monophosphate

CB         Calbindin

CCI        Controlled cortical impact

CD68       Cluster of Differentiation 68

CNS        Central nervous system

CP         Crossing points

CREB       Response element-binding protein

DAG        Diacylglycerol

DCX        Doublecortin

DG         DG

DMSO       Dimethyl sulfoxide

DNA        Deoxyribonucleic acid

dpi        Day post injury

EC         Entorhinal cortex

EPM        Elevated Plus Maze

fEPSPs     Field excitatory postsynaptic potential

Fig.       Figure

FP         Fluid percussion

GABA       Gamma-aminobutyric acid

GAPDH      Glycerinaldehyd-3-phosphat-Dehydrogenase

GC         Granular cells

| | |
|---|---|
| GCL | Granular cell layer |
| Gd3+ | Adolinium |
| GFAP | Glial fibrillary acidic protein |
| Gly | Glycine |
| GP | Group |
| GTP | Guanosine triphosphate |
| $H_2O$ | Water |
| HEK | Human embryonic kidney |
| IDG. | Immature dentate gyrus |
| IR | Ischemia-reperfusion |
| KI | Knock in |
| KO | Knock out |
| La3+ | Lanthanum |
| LHD | Linker helical domain |
| LPP | Lateral perforant path |
| LTD | Long-term depression |
| LTP | Long-term potentiation |
| MC | Mossy cells |
| MCI | Mild cognitive impairment |
| mEPSCs | Miniature excitatory postsynaptic currents |
| mGlu1a | Metabotropic glutamate receptor type1 |
| MPP | Medial perforant path |
| MRI | Magnetic resonance imaging |
| mRNA | messenger RNA |
| mTBI | Mild traumatic brain injury |
| mTOR | Mammalian target of rapamycin |
| mTOR | Mammalian target of rapamycin |
| NFT | Neurofibrillary tangles |
| NGF | Nerve growth factor |
| NMDA | N-methyl-D-aspartate |
| NMDAR | N-methyl-D-aspartate receptor |

| | |
|---|---|
| NSS | Neurological Severity Score |
| OAG | Oleoyl-2-acetyl-sn-glycerol |
| OFT | Open field test |
| PD | Parkinson's Disease |
| PIP2 | Phosphatidylinositol 4,5-bisphosphate |
| PLC | Phospholipase C |
| PMSF | Phenylmethylsulfonyl fluoride |
| PPIA | Peptidylprolyl Isomerase A |
| PSD95 | postsynaptic density protein 95 |
| PVDF | Polyvinylidene difluoride |
| RIPA | Radioimmunoprecipitation assay |
| RNA | Ribonucleic acid |
| RNase | Ribonuclease |
| RNP | Ribonucleoprotein |
| ROS | Reactive oxygen species |
| RPM | Round per minute |
| RT | Room temprature |
| SEM | Standard error of the mean |
| sEPSCs | Spontaneous excitatory postsynaptic currents |
| SGZ | Subgranular zone |
| siRNA | Stress-induced tRNA halves |
| sTBI | Severe traumatic brain injury |
| STS | Sodium tanshinone IIA sulfonate |
| TARC | Translational animal research center |
| TBI | Traumatic brain injury |
| TBP | TATA-binding protein |
| TBST | Tris-buffered saline with Tween20 |
| TDs | Transmembrane domains |
| TNF | Tumor necrosis factor |
| TPT | Topotecan |
| TrkB | Tropomyosin receptor kinase B |

| | |
|---|---|
| TRP | Transient receptor potential channels |
| TRPA | Transient receptor potential ankyrin channels |
| TRPC | Transient receptor potential canonical channels |
| TRPM | Transient receptor potential melastatin channels |
| TRPP | Transient receptor potential polycystin channels |
| TRPV | Transient receptor potential vanilloid channels |
| TTX | Tetrodotoxin |
| USA | United States of America |
| VDAC | Voltage-dependent anion channel |
| VGLUT | Vesicular glutamate transporter |
| WB | Western Blot |
| WD | Weight drop |
| WHO | World health organization |
| WT | Wildtype |

# Table of Contents

# Chapter 1

## 1  Introduction

The thesis topic deals with the importance of the TRPC6 channel. To understand the topic, an overview of TRP channels will be given with a primary emphasis on TRPC6. The known role of TRPC6 in the hippocampus and disease will be presented.

### 1.1.  Discovery of TRP channels

Transient receptor potential channels (TRP channels) are a group of ion channels located predominantly on the plasma membrane of numerous animal cell types. Many of these channels mediate a variety of sensations, such as pain, temperature, different tastes, pressure, and vision. In the body, some TRP channels are thought to behave like microscopic thermometers and are used in animals to sense hot or cold. The first transient receptor potential (TRP) ion channel identified was a Drosophila locus whose ablation resulted in a phenotype in which the photoreceptor light response decayed to baseline during prolonged illumination [1]. The flies were severely blinded after the decay and needed at least one minute in the dark to regain their complete sensitivity.

The mutant was given the term "**t**ransient **r**eceptor **p**otential" or trp because of the electrophysiological characteristics. [2] The discovery of the TRP fly in 1969 and the molecular identification of the trp gene in 1975 prepared the ground for the subsequent explosion of discoveries. [1] In 1995, the first human homolog was brought to light. Since then, more than 100 TRP channels and roughly 30 trp genes have been located [3], and research for more is still ongoing even today.

So far, there are eight families of TRP have been identified. TRPC (canonical), TRPV (vanilloid), TRPM (melastatin), TRPA (ankyrin), TRPP (polycystin), TRPML (mucolipin), and TRPN (Drosophila NOMPC). In yeast, the eighth TRP family was recently identified and named TRPY, in which Y stands for yeast. The families are classified based on the similarities to the Drosophila TRP. Group 1, which has the most substantial similarities to Drosophila, includes TRPC, TRPV, TRPM, and TRPA. Group 2 TRP channels include TRPP and TRPML, which have distal relevance to Drosophila

TRP (Figure1)[4].[3] While it is challenging to distinguish the function of each family and member-only based on the categorization, the TRP superfamily is categorized based on distinctions in their amino acid sequences and topological structures.[3] TRP channels are constructed from subunits with six membrane-spanning domains that share an evolutionary ancestor with voltage-gated $K^+$ channels (KV). TRP channels presumably form tetramers in which the amino acids connecting the fifth and sixth transmembrane domains line the pore, analogous to the comparatively well-understood KV class. However, these channels are less selective for ions as most of them let the entry of any cation, including $Ca^{2+}$, into the cell.[5] Therefore, functional studies of the various domains that control temperature regulation or ion conduction properties and the interactions between these domains and various ligands will reveal new information about how channels function and aid in the search for more specialized agonist/antagonist molecules.[6]
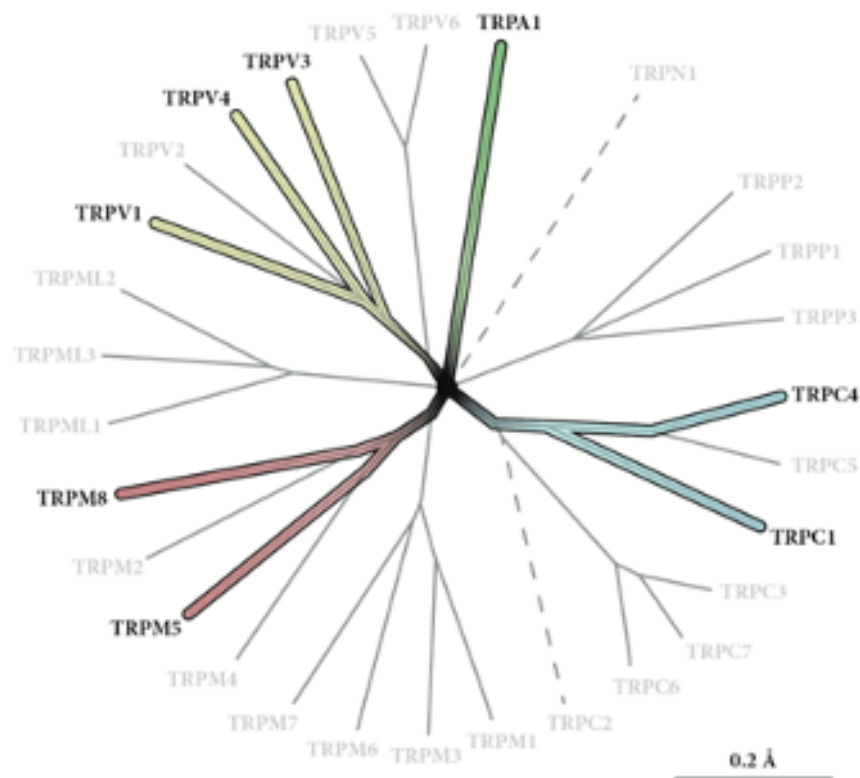


**Figure 1**. The transient receptor potential (TRP) channel family's phylogenetic tree. So far, 28 human TRP channels have been discovered. TRPN1 is expressed in insects and fish but not mammals, while TRPC2 is a human pseudogene. Different colors represent TRP channels that have been reported to be engaged in chemo sensing or impacted by hazardous substances. [7]

## 1.1  Transient receptor potential canonical (TRPC) ion channels

The relevance of store-operated/capacitive $Ca^{2+}$ influx in human immune cells fueled the race to clone Drosophila TRP homologs in mammals. TRPC1, the first mammalian TRP channel homolog, was cloned in 1995, exactly 27 years ago, by two separate groups, Montell and Birnbaumer.[8,9] The other six members of the TRPC subfamily were cloned soon after (TRPC3; TRPC2; TRPC4; TRPC5; TRPC6; TRPC7)[10]. Humans lack the TRPC2 gene in mice and other animals, but they have the genes that code for TRPC1, TRPC3, TRPC4, TRPC5, TRPC6, and TRPC7.[11] The TRPC subfamily contains seven members as mentioned above, TRPC1–7. Which were further classified into four subfamilies based on the proportion of similarity between their sequences: TRPC1, TRPC2, TRPC4/5, and TRPC3/6/7.[12]

The receptor-operated $Ca^{2+}$ signaling and a store-operated calcium entry (SOCE) are two important mechanisms regulating calcium homeostasis. Both are mediated by TRPC ion channels, which are expressed in various cell types and tissues, including the brain, placenta, adrenal gland, retina endothelia, testis, and kidney.[13] High-resolution structures for TRPC were not obtained until 2018. Owing to significant advances in single-particle cryogenic electron microscopy (cryo-EM) technology, high-resolution structures of several previously unattainable unreachable receptor classes, including that of TRPCs, have been resolved to close to 3 Å.[14] The current cryo-EM structures include homomeric TRPC3, TRPC4 (Fig2A), TRPC5, and TRPC6 (Fig2B). The general topologies of these TRPCs are identical, with each subunit having six transmembrane helices and the cytoplasmic N-termini encircling the C-termini. [15]

The first four transmembrane α helices (S1-S4) form a voltage sensor-like domain resembling the voltage sensor domains of voltage-gated $K^+$, $Na^+$, and $Ca^{2+}$ channels, and the final two α helices (S5-S6) form a structurally conserved ion conducting or pore domain shared by all TRP channels, voltage-gated channels, inwardly rectifying $K^+$ channels, and bacterial $K^+$ and $Na^+$ channels[14].
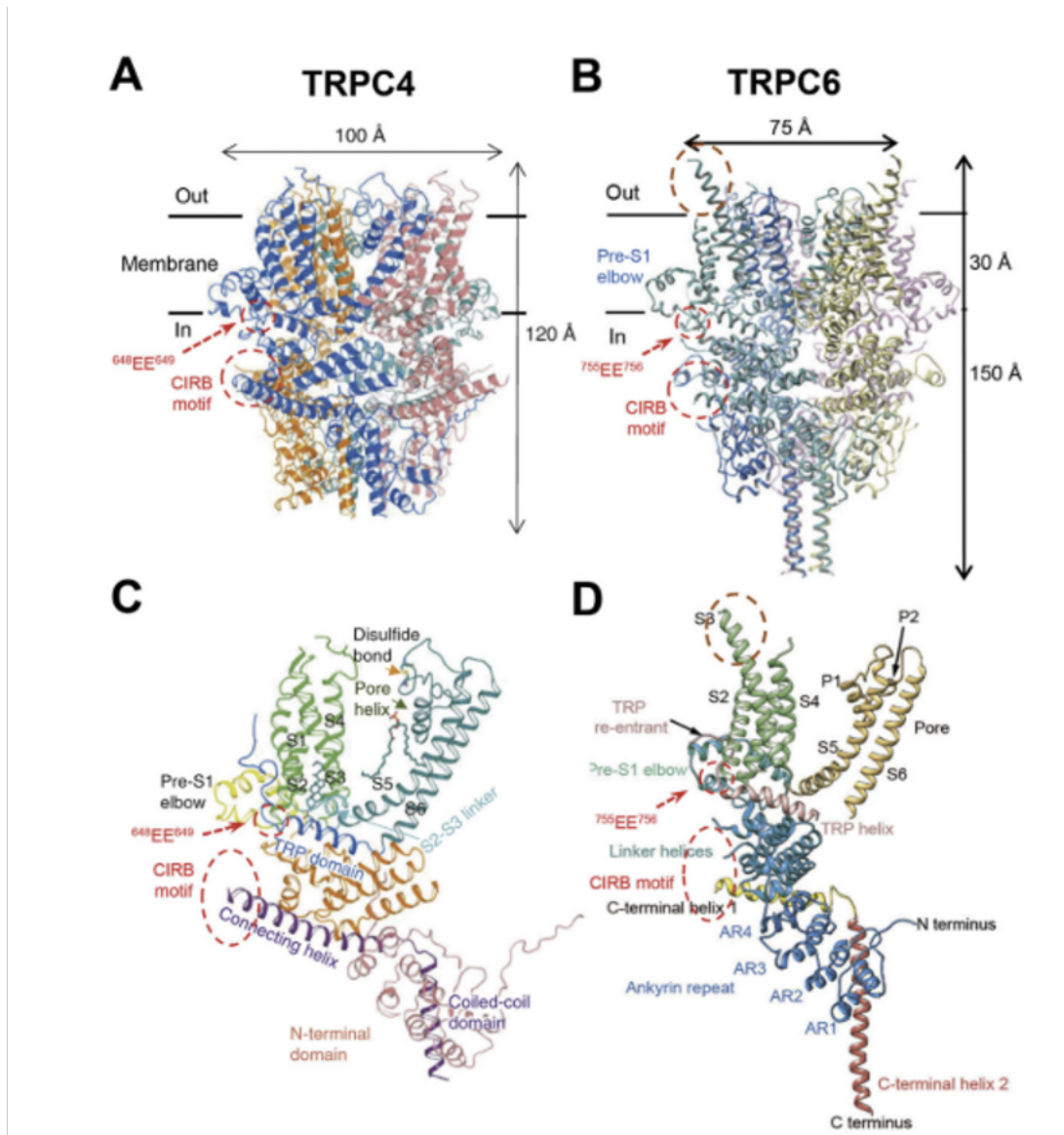
**Figure 2. Structures of TRPC channels**. A & B, cryo-EM structures of C terminus truncated mouse TRPC4 (aa 1–758) (A) and full-length human TRPC6 (aa 1–931) (B), as reported by Duan et al. (2018) and Tang et al. (2018), respectively. The transmembrane regions are defined by the horizontal black lines with a thickness of about 30 Å. Areas of the Calmodulin- and IP3 receptor-binding (CIRB) motifs and the two conserved acidic residues (EE) critical for regulation by STIM1 are indicated by the dashed red circles. The extracellular protrusion of the S3 transmembrane helix in TRPC6 is encircled by a brown dashed line. In both examples, note the missing structures between the TRP re-entrant loop and the CIRB motif. C & D, ribbon diagrams of single subunits of TRPC4 (C) and TRPC6 (D). TRP domain (in C) is equivalent to the TRP helix (in D); Connecting helix and coiled-coil domain (in C) are equivalent to C terminal helices 1 and 2 (in D).

The voltage sensor-like domain of one protomer is domain-swapped to interact with the pore domain of the adjoining protomer in the tetrameric complexes, and the four pore domains combine at the center of the tetrameric complex to create the ion-conducting pore. This configuration is also frequent in TRP channels and voltage-gated ion channels. The S5 and S6 helices and an additional pore (P) loop are arranged symmetrically from all four protomers to create the ion-conducting pore[16].

The resolved TRPC structures have lower gates with radiuses of <1 Å, denoting closed conformations. The conserved glycine, which is three residues away from the glutamate (E630 in TRPC3 and E686 in TRPC6) located in the entrance of the selectivity filter and proven for TRPC3 to be crucial for the $Ca^{2+}$ permeability of the channel, constituted the narrowest region of the selectivity filter.[17]

All TRPC structures have a three-helical region known as the pre-S1 elbow and pre-S1 helix before the transmembrane S1 helix. This region is partly immersed in the membrane, with its N-terminus exposed to the cytoplasmic side to interact with a lengthy stretch of firmly folded linker helices at the proximal N-terminus of each protomer.[14] Immediately before the linker helices are four ankyrin-like repeats that constitute the cytoplasmic architecture, which completely surrounds the four helical bundles formed by the second C-terminal helix (CH2)[18], which is also referred to as coiled-coil or pore helix domains, from the four protomers running in parallel.

The CH1 domain, or the linking helix or rib helix, comes before the CH2 domain through a brief loop that crosses over the neighboring protomer, placing the CH2 domain near the ankyrin repeats of the same protomer[14].The crossover knots and the four helical bundles generated by CH2 may aid in stabilizing the tetrameric structure. On the other hand, the CH1 domain enters a cavity between the linker helices and ankyrin repeats of a nearby protomer, running parallel to the membrane and nearly perpendicular to CH2 (~100–120°). The CH1 domain runs anti-parallelly with the TRP: domain, a well-conserved area in all TRP channels considered crucial for channel gating. A TRP re-entrant helix, half buried in the membrane and often resembles a short open loop rather than a helix, is located between the TRP and CH1 domain and a stretch of unresolved region exposed to the cytoplasm.[16,18]

All TRPC isoforms, including the invertebrate TRP and TRPL, have the distinctive CIRB (Calmodulin and IP3 Receptor Binding) motif, which can be located at the C-terminal end of the unresolved region and the start of CH1.[14,17] It's interesting to note

that this motif also interacts with phosphoinositides and inositol polyphosphates (TRPC6)[19], Gαi/o proteins (TRPC4/5)[20] and SEC14 and Spectrin Domain Containing 1 (SESTD1), a $Ca^{2+}$ dependent phospholipid/ cytoskeleton-binding protein (TRPC4/5)[21]. The CIRB motif is a hub for regulation because it can interact with many partners since it is exposed to the cytoplasmic environment. (Fig. 2C–D)[14].

TRPC channels' activation occurs mostly downstream of the GPCR-Gq/11-PLCβ and receptor tyrosine kinase couples to PLCγ.[10] $Ca^{2+}$ is a crucial regulator of TRPC channels, activating TRPC5 while inhibiting TRPC3 and TRPC6 channels. Calmodulin and other $Ca^{2+}$ binding proteins are frequently involved in this regulation [22]. Several more elements affect how the TRPC channel activity is regulated, in addition to PLC and $Ca^{2+}$. For example, GPCR stimulation might recruit PLC and arrestin-1 to form a complex that directly activates TRPC3 channels in chromaffin cells and increases calcium-dependent acute catecholamine production. According to various studies, PIP2 is necessary to keep TRPCs channels active.[23]

It is still unclear, nevertheless, how exactly PIP2 decrease affects TRPC channel activation.[24] After stimulating the PLC pathway, FRET was utilized to assess PIP2 or DAG dynamics in conjunction with TRPC6/C7 current activation or inactivation. It was proven that the channels' activation linked with the kinetics of PIP2 decreased, and their inactivation was caused by PIP2's dissociation[25]. Open TRPC4 may interact with Gi2 but not Gq, even though TRPC channels are commonly believed to be opened through the Gq-coupled receptors-PLC route (Figure 3). Consequently, the direct protein-protein interaction can mediate how Gi2 modifies TRPC4 function.[26] TRPC6 has intense activity when stimulated by a GPCR agonist, gradually decreasing over time. It was established that the current decay was related to either the phosphorylation of the GPCR at residues Ser448 and Ser768/714 in TRPC6 or to the phosphorylation of the GPCR itself, which was brought about by a DAG-dependent activation of PKC.[27] The expression of the channel protein at the cell membrane is also influenced by TRPC6 phosphorylation.

MAPKs and proline-directed kinases, including cyclin-dependent kinase 5, are known to phosphorylate TRPC6 at Ser14 (Cdk5).[10] TRPC6's Ser14 phosphorylation improves its membrane expression. On the other hand, Chen et al. showed that TRPC6 activity loss might also be partially attributed to the GPCRs being rendered inactive by PKC-dependent phosphorylation.[27]
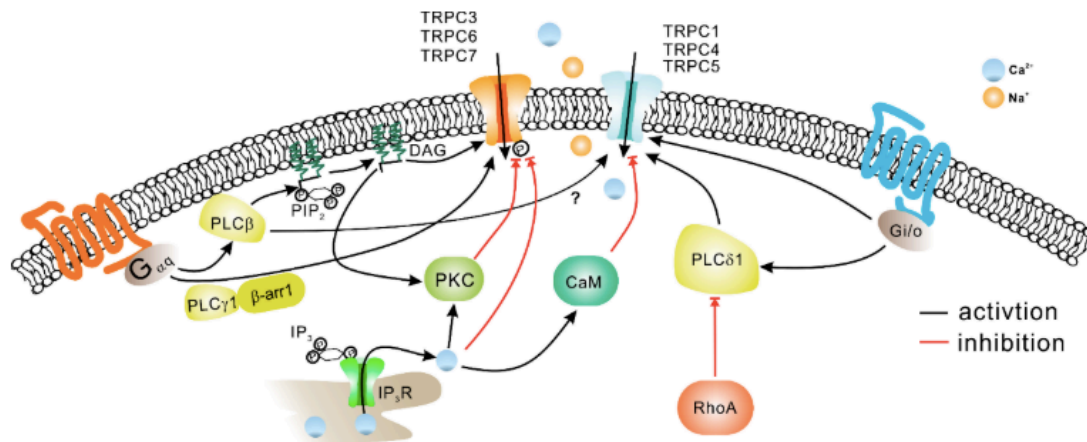
**Figure 3.** [10] **The mechanisms involved in regulating TRPC activity.** When Gq/11-coupled receptors are activated, PLC hydrolyzes phosphatidylinositol 4,5-bisphosphate (PIP2) and produces inositol 1,4,5-triphosphate (IP3) and diacylglycerols (DAG). IP3 activates IP3 receptors (IP3R) in the endoplasmic reticulum, resulting in the release of stored $Ca^{2+}$ and the depletion of $Ca^{2+}$ stores. DAG can directly activate TRPC3, TRPC6, and TRPC7 channels. Furthermore, DAG, in combination with $Ca^{2+}$, may activate PKC, which may phosphorylate TRPC channels. TRPC3/TRPC6 activity is inhibited by PKC phosphorylation. $Ca^{2+}$ may reduce TRPC channel activity directly or indirectly through calmodulin (CaM). It is possible to activate TRPC4 channels upstream of Gq/11 and through protein interactions with Gi/o. In addition to DAG, it has been reported that PLC, IP3, or -arrestin-1 are required to activate TRPC3 and TRPC6 channels. [10]

Numerous mammalian cells express TRPCs, which are involved in various physiological and pathological activities. [28] Their function in the cardiovascular system, skeletal muscle, pancreatic cells, neurons, bone, salivary gland cells, the immunological system, and many other organ systems in animals have been revealed through the gene-knockout (KO)/knock-in (KI) and pharmacological tools [10]. Among TRPCs, I will focus on TRPC6, the object of my thesis.

## 1.2  TRPC6 Channels

### 1.2.1  Discovery of TRPC6

The human TRPC6 gene was found on chromosome 11q21-q22 in 1998 by E'Desposito et al. It consists of 13 exons that code for a full-length TRPC6 protein of 931 amino acids.[29] TRPC6 is abundant in the placenta, heart, lung, pancreas, kidney, and numerous brain regions. It is widely expressed in the nervous system, including extrinsic fibers innervating intrinsic cardiac ganglia olfactory epithelium neurons, retinal ganglion cells, and many brain regions such as the cortex, hippocampus, and substantia nigra. According to Goel et al.,[30] TRPC6 is present in the kidney's glomeruli, particularly tubular cells of the cortex, outer and inner medulla, and podocytes. It is present in the lung's undifferentiated and differentiated bronchial epithelial cells as well as the smooth muscle of human airways.[14] A functioning TRPC6 tetramer is physiologically triggered by the second messenger, DAG, which was broken down by the hydrolysis of phospholipase C (PLC) mediated phosphatidylinositol 4,5-bisphosphate (PIP2) following activation of G protein-coupled receptors. Flufenamate, another well-known agonist, activates TRPC6 while blocking other cation channels. TRPC6, like the rest of TRP channels, is blocked by ions from earth minerals with three valences, such as lanthanum (La3+) or gadolinium (Gd3+).[29] Special insights and more details about TRPC6 will be further explained in the following chapters.

### 1.2.2  Structure and pharmacology of TRPC6 channel

The TRPC6 protein comprises six transmembrane domains (TDs), intracellular NH2-ARDs, and the COOH-terminal TRPC6 domain. TRPC6 weighs around 110 kDa and contains 930 and 931 amino acid residues in mice and humans, respectively. TRPC6 assembly requires both the TD and the intracellular cytoplasmic domain. [31] $Ca^{2+}$, $Na^+$, $K^+$, $Cs^+$, and $Ba^{2+}$ are cations that may pass via the TRPC6. [32] By measuring reversal potentials in whole-cell recordings under various bi-ionic conditions, researchers discovered that TRPC6 was approximately five-fold more permeable to $Ca^{2+}$ than to $Na^+$ at voltages close to the reversal potentials (typically close to 10 mV).[33]

In line with this result, researchers discovered that TRPC6 could direct $Ca^{2+}$ influx into a non-excitable heterologous expression system as evaluated by Fura-2.[34] Another work by Inoue et al. (2001) revealed that $Ca^{2+}$ penetration through TRPC6 was complex, as they found a much lower outward current through TRPC6 (at positive

membrane potentials) when $Ca^{2+}$ was the principal cation in external solution compared to $Na^+$. TRPC6's basic structure predicts that the N-terminal cytoplasmic section comprises four ankyrin repeats (AR1- 4) followed by the helical linker domain (LHD), which includes six extra helices joined by loops. On the other hand, the C-terminal cytoplasmic portion is a shorter polypeptide with two long helices joined by a short linker. In other TRP receptors, the N-terminal and C-terminal parts of the polypeptides are known to fold into a cytoplasmic assembly. Individual polypeptides, secondary structures, and long side chains were resolved well by the cryo-EM density map with a total resolution of 3.8Å. [35] An N-terminally shortened (D2-72) human TRPC6 was produced since TRPC3 lacks the residues corresponding to TRPC6's 2-72, despite their remarkable overall sequence similarity. TRPC6 (D2-72) demonstrated improved biochemical stability and was triggered by oleoyl-2-acetyl-sn-glycerol (OAG), a soluble analog of the natural lipid agonist DAG. [36]

As a result of GPCR signaling, diacylglycerol (DAG) is removed from plasma membrane inositol phospholipids by phospholipase C. Importantly, DAG analogs may activate TRPC6 even in excised inside-out membrane patches, indicating that all components required for TRPC6 activation are membrane-delimited.[37]This further suggests that DAG and its analogs promote activation in part by binding at or near TRPC6 already present in the plasma membrane. In this sense, rigid analogs of DAG exist in several substances that activate TRPC6, such as hyperforin and other acyl phloroglucinol derivatives. It's fascinating that hyperforin was shown to be a selective TRPC6 modulator because secondary plant chemicals can modulate TRP channels other than those implicated in pain and thermos sensitivity. [38]

The finding of hyperforin as a selective TRPC6 modulator was unexpected at first. Because hyperforin is the first naturally occurring modulator of TRPC family channels, there is optimism that further TRPC subfamily modulators may be identified. [39]Hyperforin, a bicyclic poly-prenylated acyl phloroglucinol derivate, is the principal active element in St. John's wort extract, commonly used as an herbal alternative to treat depression. [40] Several clinical studies and Cochrane meta-analyses validate St. John's wort's clinical effectiveness and tolerability for depression. Classical, synthetic antidepressants directly inhibit neuronal uptake of serotonin, dopamine, and norepinephrine via transport proteins. [41]

Neurotransmitter transporters commonly depend on electrochemical gradients, such as $Na^+$ gradients across the plasma membrane, for the neuronal uptake of serotonin, dopamine, and noradrenaline. In contrast to traditional synthetic antidepressants, hyperforin decreases monoamine absorption by increasing intracellular sodium concentration and eliminating the sodium gradient, which is essential for neurotransmitter transporter activity. [42]

TRPC6 activation directly mediates the action. Sodium and calcium infiltrate the pore of TRPC6 via direct hyperforin channel interaction. An increase in intracellular sodium counterbalances the sodium gradient across the plasma membrane, indirectly suppressing neurotransmitter transporters (Figure 4). The initial increase in neurotransmitters in the synaptic cleft is followed by calcium-dependent neuronal differentiation. By specifically activating TRPC6, hyperforin presumably incorporates inhibition of neurotransmitter absorption and neurotrophic properties.[39] The activation of TRPC6 can also be increased by other endogenous lipids like 20-HETE. [43] 20-HETE is made inside cells through phospholipase A2 activation, but it is also present in extracellular space and the bloodstream. Furthermore, TRPC6 activity is redox-sensitive, and reactive oxygen species (ROS) appear to enhance the likelihood of the TRPC6 opening in the plasma membrane.[34]

ROS, on the other hand, significantly boosts the steady-state surface expression of TRPC6. TRPC6 has also been shown to become activated in response to mechanical displacement of the plasma membrane. [44] But the methods by which this occurs are not fully known and most likely depend on the cell type examined TRPC6 mobilization also occurs in response to tyrosine kinase receptor activation, such as that caused by insulin, as well as integrin activation. [45] TRPC6 overactivation causes various disorders; hence blocking the channel might help treat these conditions. From a series of aminoindanol compounds, SAR7334 was recently found as a potent TRPC6 inhibitor (IC50 = 7.9 nM). The drug has an excellent oral pharmacokinetic profile and a decent selectivity for TRPC6 over TRPC3/7 channels (36-29-fold, IC50 = 282 nM for C3 and 226 nM for C7).[14] SH045, produced from an abundant natural product (+)-larixol, has likewise been demonstrated to block TRPC6 expressed in cell lines at low nanomolar doses (IC50 = 5.8-62 nM depending on the tests utilized). The substance showed considerable selectivity for TRPC7 (about 3.5-fold) but more toward TRPC3 (approximately 13-fold). Likewise, Larixyl acetate is one of the main ingredients of larch resin. The compound exhibited 12- and 5-fold selectivity for TRPC6 over TRPC3 and

C7, respectively. Furthermore, numerous marketed medications have been demonstrated to be TRPC6 inhibitors as Sodium tanshinone IIA sulfonate (STS) and Topotecan (TPT).[46]
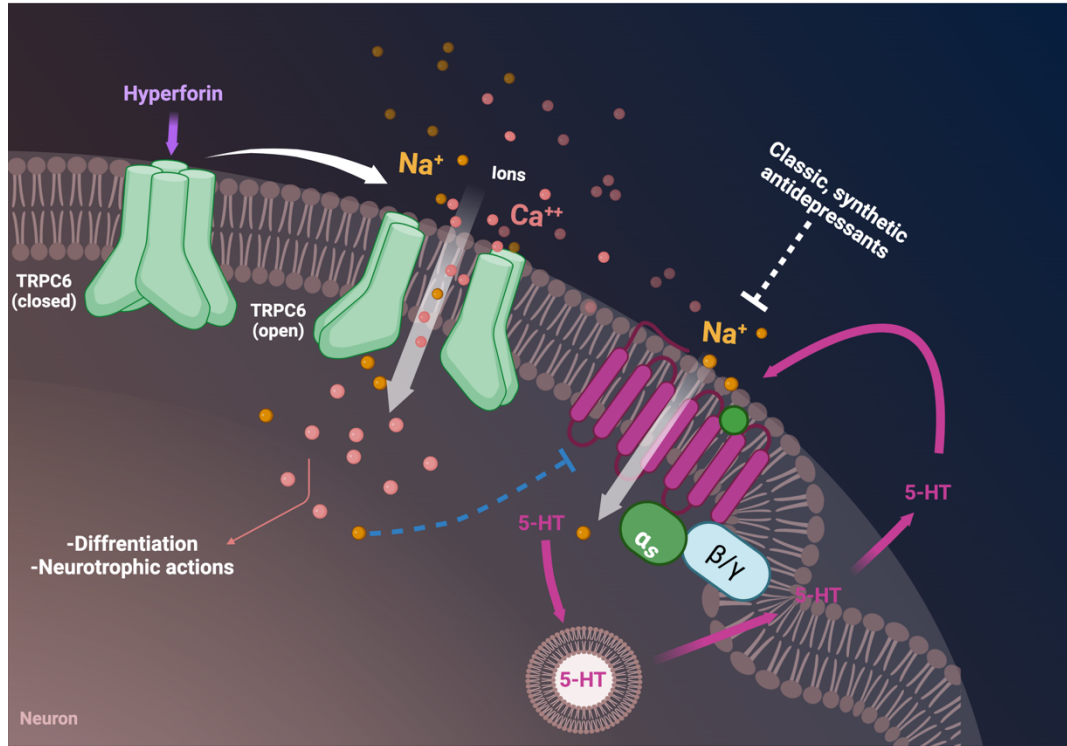


**Figure 4. Neurotransmitter reuptake is indirectly suppressed by hyperforin in a TRPC6-dependent manner.** Upon activation by hyperforin, TRPC6, which is found in the presynaptic membranes, facilitates sodium and calcium entry. The serotonin-sodium symporter (SERT/SLC6A4: solute carrier family 6A4 transporter) is driven by the sodium entry mediated by TRPC6, which negatively affects the sodium gradient across the plasma.

### 1.2.3   Downstream pathways of the TRPC6 channel

$Ca^{2+}$ is a widely distributed second messenger that influences neuron proliferation and survival during brain development. $Ca^{2+}$ signals also impact differentiation, dendrite morphology, and axon guidance via cytoskeletal dynamics and cell adhesion.[47] Each neuron has its own set of $Ca^{2+}$ permeable channels, allowing for the generation of intracellular $Ca^{2+}$ signals with a specific time course, amplitude, and location. TRPC6-mediated $Ca^{2+}$ influx is involved in nerve growth cone guidance, synapse formation, synaptic transmission, neuronal survival, and sensory transduction, and RTKs or GPCRs expressed by neurons mediate it. Brain-derived neurotrophic factor (BDNF) is a neuronal peptide that promotes survival during brain

development [47]. To facilitate survival, BDNF binds to the receptor tropomyosin receptor kinase B (TrkB) and activates the protein kinase B (Akt) and adenosine 3',5'-cyclic monophosphate (cAMP) response element-binding protein (CREB) pathways. TRPC6 downregulation inhibits the protective effect of BDNF on GCs, resulting in apoptosis. $Ca^{2+}$ influx via TRPC6 activates calcium/calmodulin-dependent protein kinase (CaMK) and MAPK, causing CREB, an important transcription factor, to be phosphorylated, resulting in neuronal survival, and enhanced synaptic plasticity (Figure 5).[48]
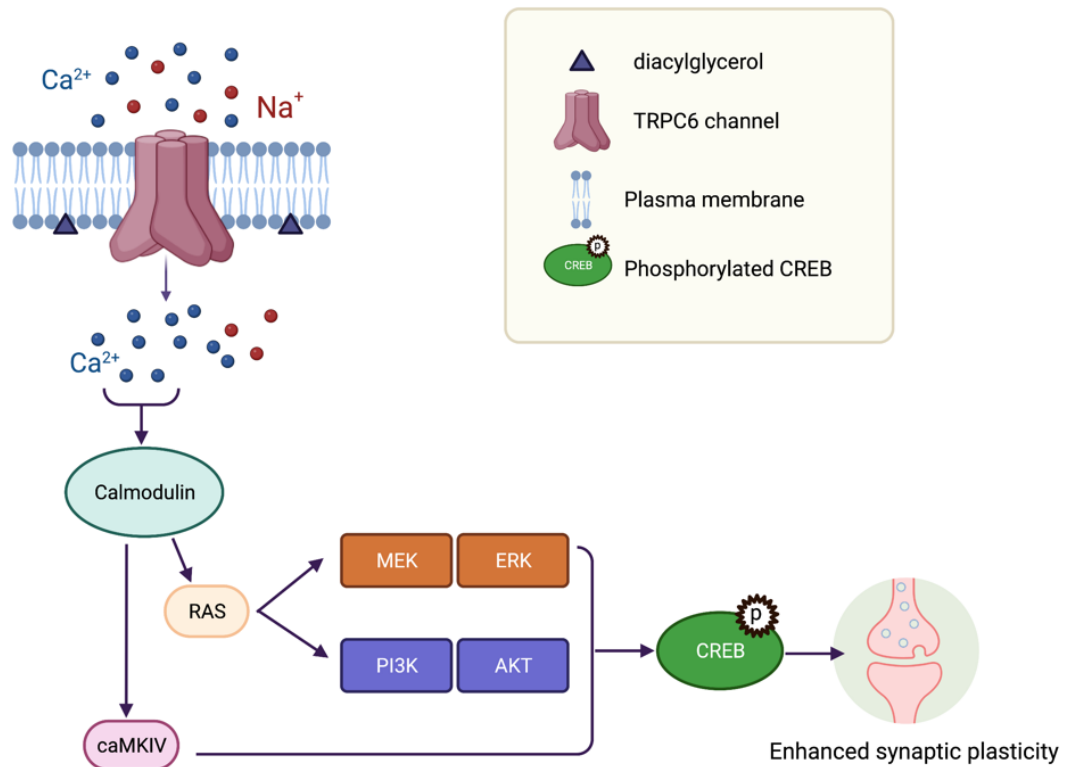


**Figure 5. Downstream signaling of TRPC6** Endogenous DAG activates TRPC6 to cause $Na^+$ and $Ca^{2+}$ influx. $Ca^{2+}$ increases the production of calmodulin, which stimulates various kinases such as CaMK IV via the RAS, PI3K/Akt, and MEK/ERK pathways. In the phosphorylation of CREB, all pathways converge. pCREB dimerizes, binds to the cAMP response element (CRE) and the coactivator CBP (CREB-binding protein), and promotes the expression of neurotrophic genes such as Trk B and TRPC6.

## 1.3  How TRPC6 modulates hippocampal function

The first step is to provide information about hippocampal formation.

### 1.4.1 The hippocampal formation in rodents

#### 1.3.1.1 Description

In rodents (rats or mice), the hippocampal formation is a bilateral and symmetric structure of the telencephalon. This cortical tract bypasses the diencephalon and travels from the septal nuclei rostral-dorsally to the basal forebrain before terminating ventrally (Figure 6). The hippocampus formation's dorso-ventral (or "septotemporal") axis has two poles: a septal/dorsal pole and a temporal/ventral pole. There is also an orthogonal axis of the hippocampal formation, the transverse axis, and an axis perpendicular to it, the radial axis. [49]



**Figure6. Schematic representations of the hippocampal formation in rats.**

A. Location of the hippocampal formation in the rat brain. B. Coronal sections of the hippocampal formation along the anteroposterior axis. Antero-posterior coordinates concerning the bregma are indicated above each section plane. CA1, 2, 3: Ammon's horn fields 1-3; DG: DG, EC: entorhinal cortex, f: fornix; s: the septal pole of the hippocampal formation, t: pole "Temporal" of the hippocampal formation, S: subiculum. (Cheung & Cardinal, 2005), modified figure
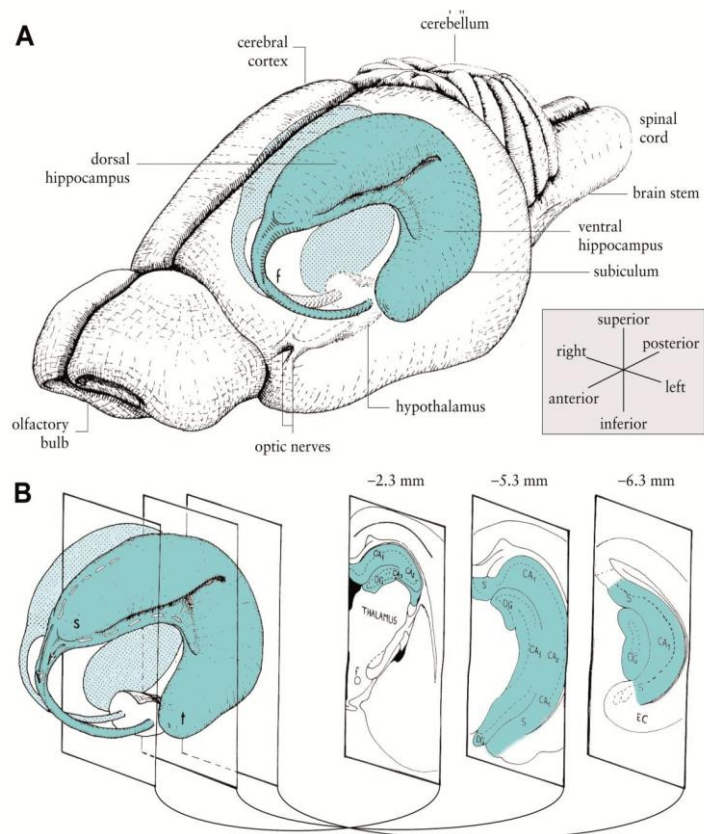
Amaral and Witter (2004) identified two structures in the hippocampus region: The HF and the para-hippocampal region.

The HF is divided into three regions: the subiculum, the hippocampus proper (or Ammon's Horn), and the DG.[50]

### 1.3.1.2  Cytoarchitectonic structure

In the transverse (or coronal) view, the hippocampal formation is made up of two inverted Us that form the principal cell layers of two regions: the Ammon Horn (which is divided into three fields called CA1, CA2, and CA3) and the DG (Figure 7).[51] The hippocampal formation is divided into allocortical layers.

**Figure 7.** **Cytoarchitectonic organization of the mouse dorsal hippocampus**



The coronal section of the dorsal hippocampal is stained with a cresyl violet coloration illustrating the different cell layers. CA1, CA2, CA3: CA1-3 fields of the Ammon Horn; O: stratum oriens; P: pyramidal stratum; R: stratum radiatum; LM: stratum lacunosum moleculare; DG: dentate gyrus; M: molecular layer; G: a layer of granular cells; H: hilus.
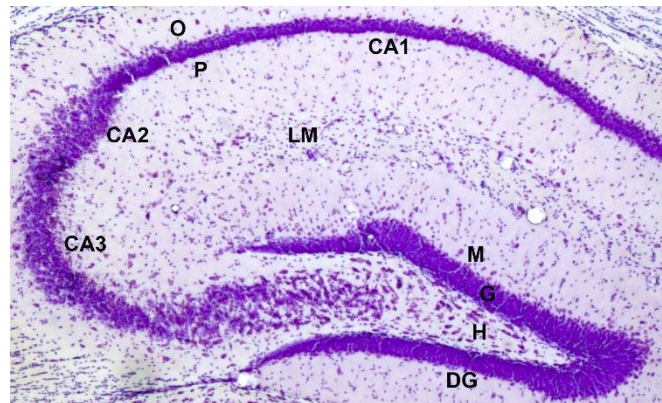
### 1.3.1.2.1 The subiculum

The subiculum is the transition zone between the hippocampus and the parahippocampal cortex regions. It represents, along with CA1, the hippocampal formation's output regions. This region's main histological feature is a broader and less dense pyramidal cell layer than CA1.[52.]

### 1.3.1.2.2  The hippocampus proper

The CA1 field makes up the upper part of the Ammon's Horn in the dorsal hippocampus, while the CA2 and CA3 regions comprise the lower parts. (Figure 8). The CA2 region of the hippocampus is challenging to identify in rats and mice due to its small size. It is often ignored or confused with the distal part of CA3: CA3a and the CA2-CA3a terminology is commonly used in the literature to refer to this region.[53]

The following layers can be distinguished at the level of the CA1-3 fields: the alveus, a fiber layer enclosing the hippocampus's afferent and efferent fibers; the stratum oriens; the pyramidal cell layer, which consists primarily of pyramidal cell bodies; as well as the strata radiatum and lacunosum moleculare. At the level of the CA3 field, there is an additional layer located between the stratum pyramidale and the stratum radiatum: the stratum lucidum, which contains the axons of the GCs known as mossy fibers and their axon terminals innervating the distal dendrites of the CA3 pyramidal cells.[54]

**1.3.1.2.3** The Dentate gyrus

One of the hippocampal formation's distinguishing characteristics is that many of its connections are unidirectional (Figure 8). Thus, the entorhinal cortex sends most of its input to the DG via fibers known as the perforant path.[55]

On the other hand, the DG does not return a projection to the entorhinal cortex. Because the entorhinal cortex is the source of much of the cortical sensory information that the hippocampal formation uses to carry out its functions, and because the DG is the major termination of projections from the entorhinal cortex, it is reasonable to think of the DG as the first step in the information processing that eventually leads to the production of episodic memories.[56]
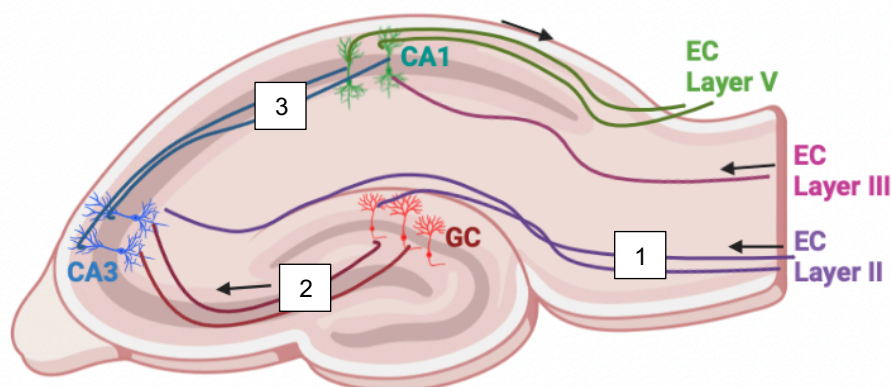


**Figure 8. The mouse hippocampal formation.** The major fields are indicated. Projections (**1**) originate from layer II of the entorhinal cortex (EC) and terminate in the molecular layer of the DG and the stratum lacunosum-moleculare of the CA3 field of the hippocampus. An additional component of the perforant path originates in layer III and terminates in the CA1 field of the hippocampus. GCs of the DG give rise to the mossy fibers (**2**) that terminate both within the polymorphic layer of the DG and within the stratum lucidum of the CA3 field of the

hippocampus. The CA3 field, in turn, gives rise to the Schaffer collaterals (**3**) that innervate the CA1 field of the hippocampus.

Three layers make up the DG (Figs. 1–2). The molecular layer is a largely cell-free layer that, in the rat, measures about 250 m thick and contains, among other things, the dendrites of the dentate GCs. The fibers of the perforant path, which originate in the entorhinal cortex, are the other significant occupants of the molecular layer.[56] Also, a small number of interneurons that reside in the molecular layer and fibers from various extrinsic inputs terminate there. GCs packed closely together comprise most of the primary or granule cell layer. The granule cell layer has a thickness of 4 to 8 neurons or 60 m. While the GCL is mainly made up of GCs, some other neurons are located at the granule's boundary and polymorphic layers.[57] The cell body of the dentate pyramidal basket cell, for example, is often located just within the GCL at its border with the polymorphic layer. The polymorphic layer contains a variety of cell types, the most prominent of which is the mossy cell.[57]

### 1.3.1.2.4 Hippocampal cells

The hippocampal formation contains numerous cell types that can be classified into three large families:

- Non-neuronal glial cells primarily consist of astrocytes, which are found in all layers of the HF, and oligodendrocytes, the cell bodies of which are found mainly in white matter, including the alveus.[58]
- GABAergic inhibitory neurons are found in all layers of the HF; it is a very diverse population of neurons that includes many different cell types that differ in morphology, projection sites, and neurochemical content.[59] Some express metabotropic glutamate receptor type1 (mGlu1a) and the neuropeptide somatostatin. This latter cell type is an archetypal feedback inhibitory cell, as most of their excitatory input comes from the principal cells innervated by these interneurons. However, it has been demonstrated that feed-forward inhibition in the hippocampal formation is mainly carried out by parvalbumin-containing interneurons, whose spiking is effectively fueled by feed-forward excitatory afferents. As a result, multiple types of inhibitory cells are developed in the hippocampal formation to regulate the many computational domains of principal neurons.[60]

- Excitatory Glutamatergic neurons, including the pyramidal cells of the CA1, CA2, and CA3 regions, GCs of the DG; the "giant cells" located in the stratum radiatum layers of CA1 and CA3, and hilar mossy cells.[61]

This manuscript extensively studies the DG with unique insights into the granular cells. Their unusually delayed and heterogeneous maturation distinguishes GCs. Most of them (85%) are formed after birth. Between embryonic days 10 and 14, neural precursors migrate from the primary dentate matrix to the DG, where they differentiate into neurons. [62] Neurogenesis peaks at the end of the first postnatal week and is nearly complete by the end of the first month. [63] Interestingly, the DG retains the ability to generate new neurons throughout life, albeit at a slower rate. [64]

Immature GCs are produced in the subgranular zone and are integrated into pre-existing circuits in adulthood. This enhances a variety of brain functions, including learning and memory.[65] The four stages of adult neurogenesis are the precursor cell phase, early survival phase, postmitotic maturation phase, and late survival phase (Figure 9). Six separate milestones can be distinguished based on cell morphology and a set of marker proteins. However, they still tend to overemphasize the precursor cell phases of adult neurogenesis at this time.[66] Adult neurogenesis develops from a radial glia-like precursor cell through three distinct progenitor phases with intense proliferative activity, a postmitotic maturation phase, and finally, the appearance of a new granule cell.[67]

The purpose of the precursor cell phase is to increase the number of cells that have the potential to become neurons. The cell cycle is terminated at the early survival phase. Within days of birth, most neonatal cells are eliminated.[68] The postmitotic maturation phase is associated with the formation of functional connections, axon and dendrite growth, and synaptogenesis. The late survival phase is a time for fine-tuning. The entire period of adult neurogenesis is estimated to last seven weeks.[68] Characteristic electrophysiological patterns allow functional states to be assigned to morphologically distinct developmental stages.[69]

Identifying a critical period of plasticity that occurs transiently during the maturation of newborn neurons was the most pivotal discovery in the functional study of adult

hippocampal neurogenesis.[70] It has been demonstrated in slice recordings that newborn neurons between the ages of 4 and 8 weeks have a lower induction threshold for long-term potentiation, a higher magnitude of responses, and are preferentially activated by afferent stimulation.[71] Mature GCs, conversely, are less excitable and less malleable (see below), raising questions about their function. Nonetheless, several recent papers suggest that this cell population plays a role in DG learning and memory formation.[72]
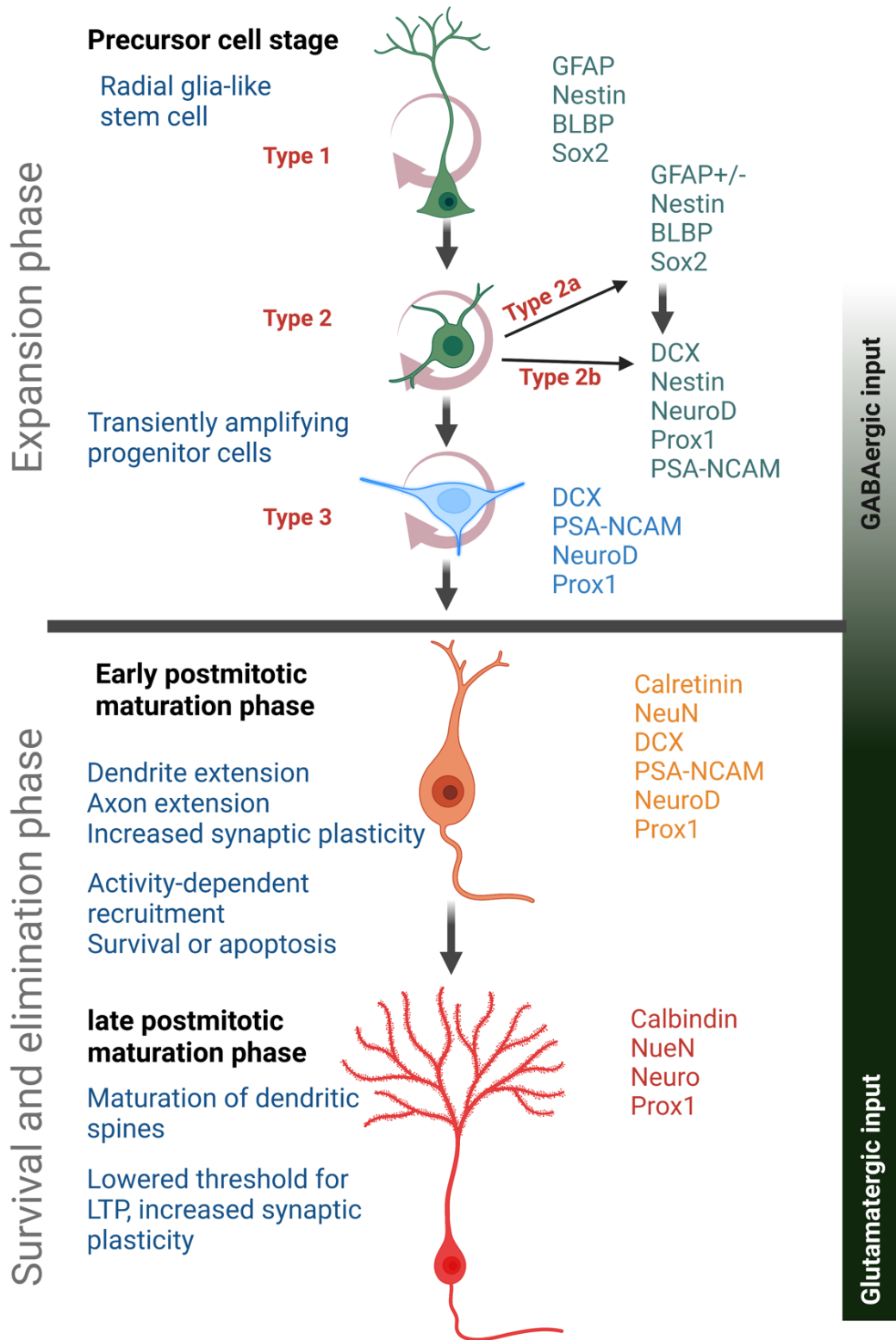
**Figure 9. Developmental stages during adult hippocampal neurogenesis**. GFAP, Glial fibrillary acidic protein; BLBP, brain lipid-binding protein; DCX, PSA-NCAM, polysialilated neural-cell-adhesion molecule; LTP, long-term potentiation.

### 1.3.2  Trpc6 expression in the hippocampus

A study conducted by Nagy et al. 2013 using electron microscopy found TRPC6 to be localized on the plasma membranes of the dendrites, spines, and somata of dentate GCs in the hippocampus. Moreover, the TRPC6 were frequently observed intracellularly, occasionally associated with the membrane cisternae.[73] These data align with another study by Zhou et al. 2008 that showed TRPC6 expression peaked between postnatal days 7 and 28 (P7-28), a period known to be vital for synaptogenesis in vivo. TRPC6 protein was also found in synaptosome and postsynaptic fractions of the P14 hippocampus, with higher levels in the postsynaptic fractions than in the synaptosome fractions.

These data indicated that TRPC6 is found in the postsynaptic sites of hippocampal neurons. Further evidence demonstrating that TRPC6 was mainly confined to excitatory postsynaptic sites came from electron microscopy of the P14 hippocampus, which implies that TRPC6 is found in the postsynaptic locations that are excitatory. TRPC6 could be observed in the dendrites of some interneurons as well. Double immunofluorescent staining showed that TRPC6 was present in the dendrites of hilar interneurons and hippocampal interneurons with horizontal dendrites in the stratum oriens expressing mGlu1a receptors. In contrast, parvalbumin immunoreactivity was revealed in TRPC6-expressing dendrites with a radial appearance in the stratum radiatum. Electron microscopy showed that the immunogold particles depicting TRPC6 were located on the surface membranes of the interneuron dendrites. [73].

### 1.3.3  TRPC6 modulates hippocampal memory and cognition

The development of synapses in the developing brain is a multi-step process that involves several sequential processes, many of which are controlled by $Ca^{2+}$ signaling.[74] They include neurogenesis, neuronal polarity formation, migration, axonal pathfinding, dendritic morphology establishment, and synaptogenesis.[75]. Owing to its different activation characteristics, TRPC6 may function as a cellular sensor for environmental cues during dendritic development because it can translate extracellular cues into intracellular signals. $Ca^{2+}$ influx via TRPC6 is

required for TRPC6-induced dendritic growth via the CaMKIV-CREB-dependent pathway, especially in the early postnatal days when neuronal activity is low.[76] finally, TRPC6 overexpression boosts the number of spines in hippocampal neurons, while the shRNA-TRPC6 treatment reduced the dendritic spines of DG granule neurons; in terms of spine loss, the thin and mushroom types predominated.[77]

TRPC6 seems to play an essential role in spatial learning, working memory, and social recognition memory. Indeed, downregulation of TRPC6 expression using shRNA impaired the social recognition memory of mice in a three-chamber test.[78] Moreover, testing these mice via the Morris water maze, which evaluates long-term spatial learning and memory of mice, revealed that decreased TRPC6 expression altered the cognitive plasticity aspects in mice.[79] [77]

## 1.4 TRPC6 channels in neurological diseases

Given TRPC6 channels' diverse involvement in physiological function, dysfunction of these channels could be equally responsible for a wide range of pathological conditions that I will describe below. One of the primary causes of such dysfunction has been linked to identified defects in the gene encoding the channels. Variations in channel abundance, sensitization, or desensitization, which result in exaggerated or diminished responses to various pathological stimuli, can contribute more subtly to the emergence of several diseases. In turn, abnormal endogenous production of various agents during disease development can affect TRPC6 function in a way that contributes to disease progression. In general, dysregulation of TRPC6 function may cause disease through one or more mechanisms, including (1) $Ca^{2+}$ signaling to mistune, (2) disturbances in $Mg^{2+}$ and $Ca^{2+}$ homeostasis, (3) disruption of cell proliferation and growth, (4) mistargeting of interacting proteins, and (5) changes in excitable cell electrical activity.[80]

### 1.4.1 Depression

Depression is one of the most severe clinical problems associated with mood disorders. It impacts a person's thoughts, behavior, and feelings. Despite decades of research, gaps in the pathophysiology of depression remain, and the disease progression and onset mechanism remain unknown. Several studies have implicated

different brain parts in depression and found that the anterior cingulate cortex is heavily involved. Aside from the anterior cingulate cortex, depressive mood disorder involves the hypothalamus, amygdala, thalamus, cerebellum, and hippocampus. [81] Indeed, hippocampus volume was smaller in depressive patients' brain imaging examinations, and moderate apoptosis and atrophy were found in the CA1 region and the DG during postmortem brain research.

In CNS neurons, TRPC6 functions as neurotrophin signaling's downstream effector, regulating brain-derived neurotrophic factor (BDNF) induced increases in quantal neuronal transmitter release, synapse density, spine shape, and dendritic lengths. In the chronic unpredictable stress model of depression, TRPC6 expression was significantly reduced in the hippocampus,[82,] in addition to changes in the BDNF levels which is thought to play an essential role in the pathogenesis of depression [83]. People have used St. John's wort, Hypericum perforatum, for ages to cure mild to moderate depression.

Hyperforin mimics BDNF or Nerve growth factor (NGF) in hippocampus preparations and regulates neuronal plasticity by activating TRPC6.[39]In organotypic hippocampal slices, hyperforin (0.3 M) stimulates neurite out-growth via TRPC6 and modifies spine shape in CA1 as well as CA3 pyramidal neurons. TRPC6-specific shRNA-mediated knockdown or the production of a mutant TRPC6 with a dead pore prevented these effects. Hyperforin causes an increase in CREB protein levels as well as CREB phosphorylation in the cortex. The physiological effects are mirrored by hyperforin-dependent increases in TRPC6 and TrkB expression in the cortex. Comparable features were detected in the hippocampus without hyperforin-dependent neurogenesis.[82]

### 1.4.2 Epilepsy

Epilepsy is defined by recurrent and spontaneous seizures caused by the synchronized bursting of localized neurons in various brain parts. In 2018, approximately 50 million people had epilepsy.[81] The epileptic hippocampus exhibits increased susceptibility to ictogenic stimuli and neuronal excitability, as well as a high level of synchrony between neurons. The DG is a gateway that regulates seizure activity propagation in hippocampal circuits. The DG functions as a frequency-dependent filter for entorhinal cortex paroxysmal activity.[84] The molecular targets of current epilepsy drugs are mostly ion channels like Ca2+, glutamate, and GABA.

TRPC6, like other disorders, plays a role in epileptogenesis. TRPC6 expression was downregulated in chronic epileptic rats, and TRPC6 genetic ablation increased seizure susceptibility and neuronal vulnerability in the DG but not in the CA1 and CA3 neurons of the hippocampus. Hyperforin, a trpc6 agonist, reduced the neuroinflammatory response (microglial activation, p65-ser276-NFB phosphorylation, and TNF-expression).[81]

### 1.4.3 <u>Alzheimer</u>

Alzheimer's disease (AD) is the most prevalent neurodegenerative condition worldwide. Clinical signs of AD include memory loss, cognitive impairment, emotional lability, language breakdown, and loss of bodily function in the ultimate stage.[85] One of the leading theories for the etiology of AD is the "amyloid hypothesis." Other notable AD characteristics include the buildup of tau protein, impairment of calcium homeostasis, and activation of glial cells. As neuronal survival, learning, and memory are impaired in AD, TRPC6 may contribute to the onset of AD. The experiments that used hyperforin as a TRPC6 agonist provide pharmacological evidence to support the possibility that TRPC6 plays a function in AD. [86]

Several studies have shown that hyperforin can lower Aβ levels and improve behavioral performance in AD models. Hyperforin could reduce amyloid deposit formation in rats injected with amyloid fibrils in the hippocampus, reducing Aβ-induced neurotoxicity, reactive oxidative species, and behavioral impairments. Furthermore, tetrahydro hyperforin, a hyperforin derivative IDN5706, prevents cognitive deficit and synaptic impairment in double transgenic APPswe/PSEN1E9 mice in a dose-dependent manner. Tetrahydrohyperforin inhibits APP proteolytic processing, total fibrillar and oligomeric forms of A, tau hyperphosphorylation, and astrogliosis. According to additional research, TRPC6 appears to be the target of tetrahydrohyperferrin.[87] In this study, tetrahydro hyperforin, the TRPC3/6/7 activator OAG, SKF96365, and Aβ oligomers are incubated with mouse hippocampus slices. OAG and tetrahydro hyperforin both stimulate fEPSPs in a manner that is blocked by SKF96365. [88] The fEPSP reduction brought on by A oligomers can be undone by tetrahydro-hyperforin. Tetrahydro hyperforin improves spatial memory in wild-type mice, but co-administration of SKF96365 reverses this benefit. With other recognized TRPC6 agonists, tetrahydro hyperforin has a significant amount of pharmacophore similarity (IDN5522, OAG, and Hyp). These results highlight the possible protective

effects of TRPC6 in AD and suggest that hyperforin and its derivatives may be viable treatments for the disease [89].

### 1.4.4 <u>Stroke and traumatic brain injury</u>

One of the leading causes of disability and death in both developed and developing nations is brain injury.[90] Brain injuries fall into two major categories: traumatic and non-traumatic brain injuries, depending on the underlying cause. Non-traumatic brain injury primarily results from infections, brain tumors, ischemia, or stroke.[91] In contrast, the damage to the brain in TBI is typically brought on by external forces, either direct or transmitted, brought on by falls, car accidents, sports-related injuries, abuse/assault, or pressure explosions. No matter what the underlying cause, brain damage can induce temporary or permanent dysfunction due to physical, cognitive, and behavioral deficits.[92] Ischemic stroke is caused by the blockage of an artery or arteries leading to the brain.

The normal function of neurons is hampered by focal impairment or occlusion of blood circulation to the brain. Excitotoxicity, oxidative and nitrosative stress, $Ca^{2+}$ overload, inflammation, and apoptosis are among the mechanisms underlying ischemic stroke.[93] Among these mechanisms, intracellular $Ca^{2+}$ overload is essential in neuronal injury caused by an ischemic stroke. Glutamate receptors, such as the N-methyl-D-aspartate receptor (NMDAR), are thought to be major intracellular $Ca^{2+}$ influx pathways in the central nervous system (CNS) following cerebral ischemia-reperfusion (IR) injury.[94] The TRPC6 has recently been linked to $Ca^{2+}$ homeostasis and implicated in the molecular pathogenesis of ischemic stroke, according to mounting evidence. [95]

Both in vitro and in vivo ischemic stroke models have shown TRPC6 to be essential for neuroprotection.[96] Additionally, TRPC6 functions as a negative regulator, blocking the $Ca^{2+}$ currents that NMDA causes in hippocampus neurons.[97] Interestingly, NMDAR has been shown to regulate TRPC6 transcription and degradation in neurons in a bidirectional manner via NR2A or NR2B activation. TRPC6 expression is maintained via CREB-dependent mechanisms, which has a neuroprotective effect and can potentially be used as a protective strategy against ischemic stroke[98]. Resveratrol, neuroprotectin D1, and the main compound in green tea, (-)-epigallocatechin-3-gallate, inhibit calpain-mediated TRPC6 proteolysis and activate MEK/ERK or CaMKIV-dependent CREB pathways in addition, hyperforin inhibits TRPC6 degradation and increasing phosphorylated CREB in CaMKIV and Ras/MEK/ERK-dependent

mechanisms thus improving neurological status in experimental stroke patients[99]. Furthermore, TRPC6 overexpression in BMSCs improves neuronal functions in rats following ischemic stroke, linked to the BDNF/CREB pathway[100]. Another study suggested that TRPC6 may function downstream of IL-17A and that IL-17A may enhance TRPC6 degradation, aggravating cerebral IR injury[101]. When considered collectively, the evidence presented above indicates that TRPC6 has a beneficial role in neuroprotection and that TRPC6 expression is decreased during ischemic stroke[102].

In TBI, the physical injury is what starts the biochemical and pathological effects. Therefore, the type of insult considerably impacts how TBI presents clinically. For instance, a lot of open head injuries result from items like knives or bullets harming the brain as they pass through the skull. Unlike open-head injuries, closed-head injuries are linked to blunt, overpressure, or accelerating forces[103]. The Glasgow Coma Scale is primarily used to classify TBI according to clinical severity (GCS)[104]. The GCS (range 3–15) provides a quick evaluation of the severity of brain damage by summing the results of its three component scales (eye, motor, and verbal). A score of 13 to 15 indicates mild (mTBI), 9 to 12 indicates moderate (mTBI), and 8 indicates severe (sTBI)[104]. The morphological, biochemical, molecular, and behavioral changes connected to brain injury in people have been carefully reflected in a number of animal TBI models established during the last few decades. Injury to the brain has been induced using mouse TBI models in three distinct settings: focal impact, diffuse impact, and non-impact. Animal models for focal impact brain injury are further categorized as follows: weight drop (WD), fluid percussion (FP), and controlled cortical impact (CCI)[105]. CCI provides control over biomechanical factors known to be related to TBI by allowing quantitative control over damage force and velocity as well as the degree of tissue deformation. Between bregma and lambda, a craniotomy is performed. Meanwhile, a rigid impactor is driven by a pneumatic or electromagnetic impact device to apply mechanical force to the dura[106] resulting in deformation in the underlying cortex, leading to BBB malfunction, concussion, contusion, axonal damage, and loss of cortical tissue comparable to those found in patients[106].

Both human and animal models of TBI exhibit the clinical trait of hippocampal and cortical disruption, regions essential to memory function.[107] It is believed that the physiological disruption of the hippocampus's circuitry, including the DG and areas CA3 and CA1, is largely to blame for episodic memory impairment following TBI.[108] It has been demonstrated that TBI alters phasic and tonic inhibitory transmission onto

GCs.[109] Following CCI, the reduced phasic synaptic GABA$_A$ergic transmission onto the GCs remains several months after the injury. Reduced potassium-chloride membrane transporter KCC2 expression correlates with impaired phasic inhibition, which lessens the chloride's driving force through GABA$_A$ receptors.[110] Thus, there appears to be a decrease in phasic GABA$_A$ergic inhibition across TBI models, but the time course of these alterations varies with the degree of the injury. Tonic inhibition, however, is affected differently depending on the cell type. For instance, GCs have increased tonic inhibition, but semilunar GCs, a subgroup of GCs, have decreased tonic inhibition. As a result, inhibition changes cause a complex DG malfunction.[111]

CA1 plays a distinct role in episodic memory encoding and retrieval. In contrast to the DG's hyperexcitable response to injury, activity in the area CA1 circuit becomes hypoexcitable.[112] CA1 showed a decreased net response to afferent fiber stimulation one week after TBI, with a higher threshold to initiate population spikes. As a result, after injury, the output of the CA1 circuit, which is mediated by the firing of CA1 pyramidal neurons, is reduced. Changes in synaptic inputs onto pyramidal cells can explain some of the hypo excitability of the CA1 circuit.[113]

Inflammatory events in the brain following a TBI are well known to contribute to widespread cell death and chronic tissue degeneration. Neuroinflammation is a complex response that involves a variety of cell types both within the CNS and in the peripheral circulation. Astrocytes and microglia, both CNS cells, are thought to be key players in initiating an inflammatory response after injury.[114] Astrogliosis has been defined in terms of neuroprotection as well as neurodegeneration. Specific roles of reactive astrocytes in models of moderate and severe CCI TBI have been investigated. Removing proliferating reactive astrocytes in mice resulted in neuronal degeneration and inflammation, confirming their critical role in preserving neuronal tissue after moderate but not severe TBI [115].

Furthermore, reactive astrocytes were found to play an essential role in preventing the infiltration of inflammatory cells in areas with intact cortical neurons. In contrast, inhibiting astrocytic proliferation with agents that disrupt various cell cycle stages results in less neuronal cell death after fluid percussion injury in rats. Reduced astrocytic proliferation was also associated with decreased glial scar formation, microglial activation, and improved histological and cognitive outcomes following TBI, implying that the presence of reactive astrocytes can create an environment conducive

to degeneration.[116] Microglia play an important role in mounting an immune response following TBI. A study of pathological changes in injured post-mortem human brains discovered that microglia were activated for an extended period, even years after the injury. Neuropathological and inflammatory changes in a mouse CCI model were tracked for a year after the experimental TBI.[117] Compared to controls, microglia were chronically activated, with higher levels of Iba-1, CD68, and the MHC Class II molecule CR3/43. Morphology was classified as hypertrophic or bushy.[118]

 This was accompanied by lesion expansion, hippocampal neuron loss, white matter damage, and myelin loss. Many significant studies emphasize that the microglial response in injury can be context and injury-severity-dependent (as demonstrated using different injury models). Thus a better understanding of the pleiotropic nature of these responses is required to advance our understanding of the microglial contribution to injury.[116]

# 2 <u>Hypothesis and aim of work</u>

TRPC6's precise physiological function is still a riddle. TRPC6 is an intrinsic component of receptor-operated cation entry, which plays a role in several physiological processes. The role of TRPC6 in the brain is crucial for several reasons.

*First*, it is involved in various physiological processes necessary for regular brain function; TRPC6 is required in synaptic plasticity processes such as dendritic growth, spine morphology, and increased excitatory synapses.[36]

*Second*, the pathophysiology of some illnesses, including stroke, TBI, and depression, may be influenced by TRPC6 channels. Therefore, studying TRPC6 channel function in the brain can provide critical insights into both the normal processes of these channels and their potential role in disease. [119]

This information can be utilized in developing new therapies and treatments for neurological and psychiatric disorders.[102]

In brief, using TRPC6 WT and KO mouse models, the goals of this scientific study are as follows:

To investigate the role of TRPC6 on hippocampal maturation and plasticity.

To examine the role of TRPC6 in the pathophysiology of traumatic brain injury.

# Chapter 3

# 3   Material and Methods

## 3.1   Materials

### 3.1.1   Consumable and Instruments

**Table 1**. *Consumables and Instrument*

| Name | Manufacturer |
| --- | --- |
| 4×objective lens | Plan N, NA 0.1; Olympus, Shinjuku, Japan |
| 40×water-immersion objective | LUMPlan FI/IR, NA 0.8w; Olympus, Shinjuku, Japan |
| ACCU-Jet Pro | Brand |
| AG245 Analytic Balance | Mettler Toledo |
| Autoclave | Fedegari Autoclavi |
| Buffer Tank and Lid | Bio-Rad Laboratories Inc. |
| CCD camera | XM10, Olympus, Shinjuku, Japan |
| Direct-Q® 3UV | Merck Millipore |
| Duran Bottles (2 L, 1 L, 500 mL, 250 mL, 100 mL) | Schott |
| EPC10 amplifier | HEKA, Reutlingen, Germany |
| Eppendorf Research plus 10, 20, 200, 1000µl | Eppendorf, Hamburg, DE |
| Falcon tube 15, 50 ml | Greiner, Bio-One GmbH, Frickenhausen, DE |
| Falcon Tube 50 mL, 15 mL | Greiner bio-one |
| Fiber Pads | Bio-Rad Laboratories Inc. |
| Fom /B50 Autoclave | Fedegari Autoclavi SPA |
| Freezer FORMA 900 Series | Thermo Fisher Scientific |
| Freezing container Nalgene® | Thermo Fisher Scientific |
| Gel blotting sheets GB003 | GE Healthcare |
| Gel Releasers | Bio-Rad Laboratories Inc. |
| Glass capillaries | Hilgenberg, Malsfeld, Germany |
| IKAMAG™ RET | IKA-Werke GmbH |
| Imager FUSION Pulse TS | Vilber |

| | |
|---|---|
| Labofuge 400R Centrifuge | Heraeus Instruments |
| Laminar Airflow Bench HERAsafe | Heraeus Instruments |
| Laminar Airflow Bench Lamin Air | Heraeus Instruments |
| Latex gloves | VWR |
| Liebherr MediLine | Liebherr |
| Liquid nitrogen freezing container LS3000 | Taylor Wharton |
| Magnetic stirrer | Janke & Kunkel GmbH & Co. KG, Staufen, DE |
| MaxQ™ 4000 Benchtop Orbital Shaker | Thermo Fisher Scientific |
| Microm CU 65 Cooling Unit | Thermo Scientific, Waltham, USA |
| Microscopslides, MenzelGläser Superfrost Plus | Thermo Scientific, Braunschweig, DE |
| Microtube (0.5 mL, 1.5 mL, 2 mL) | Sarstedt |
| Miele Professional PG 8583 | Miele |
| Millipore Direct-Q 3UV | Merck Millipore |
| Mini Cell Buffer Dams | Bio-Rad Laboratories Inc. |
| Mini Gel Holder Cassette | Bio-Rad Laboratories Inc. |
| Mini Star Microcentrifuge | VWR |
| Mini Trans-Blot©Cell | Bio-Rad Laboratories Inc. |
| Mini-PROTEAN Casting Stand | Bio-Rad Laboratories Inc. |
| Mini-PROTEAN Clamps | Bio-Rad Laboratories Inc. |
| Mini-PROTEAN Comb, 10-well | Bio-Rad Laboratories Inc. |
| Mini-PROTEAN Comb, 15-well | Bio-Rad Laboratories Inc. |
| Mini-PROTEAN Short Plates | Bio-Rad Laboratories Inc. |
| Mini-PROTEAN Spacer Plates | Bio-Rad Laboratories Inc. |
| Mini-PROTEANTetraElectrode Assembly | Bio-Rad Laboratories Inc. |
| Natural Flat Cap Microcentrifuge Tubes 0,5; 1,5; 2,0 ml | Starlab International GmbH, Hamburg, DE |
| Nitril gloves | VWR |
| Olympus BX51WI upright microscope | Olympus, Shinjuku, Japan |
| Operation-microscope, technoskop OPMI 1-FC 459909 | Carl Zeiss Microscopy GmbH; Oberkochen, DE |

| | |
|---|---|
| Pasteur pipettes Volac | Poulten & Graf GmbH, Wertheim, DE |
| PB3002 Delta Range | Mettler Toledo |
| pH-Electrode Blueline 11 | SI Analytics GmbH; Mainz, DE |
| pH-Meter PB-11 | Heraeus Holding GmbH; Hanau, DE |
| pHenomenal® pH 1100L | VWR |
| Pipet 5, 10,25 ml | Greiner, Bio-One GmbH, Frickenhausen, DE |
| PIPETMAN Classic (P20, P100, P200, P1000) | Gilson |
| Pipette tips 1000 µL, 200 µL, 10 µL | Sarstedt AG & Co. KG; Nümbrecht, DE |
| Pipettes 1000 µL, 200 µL, 20 µL | Gilson, Middleton & Labnet International |
| Pipettes 1000 µL, 200 µL, 20 µL | Eppendorf |
| Potter S | B. Braun Biotech International |
| PowerPac™ HC Power Supply | Bio-Rad Laboratories |
| PVDF membrane | Thermo Fisher Scientific |
| Reaction tubes | Eppendorf AG; Hamburg, DE |
| Refrigerator | Liebherr |
| Rocking Platform | VWR |
| Roller | Bio-Rad Laboratories |
| SafeSeal Tips Premium 1000 µL sterol | Biozym Scientific |
| Scale AG245 | Mettler Toledo |
| Separating Spin column | Qiagen GmbH; Hilden, DE |
| Serological pipette (2 mL, 5 mL, 10 mL, 25 mL) | Sarstedt |
| Serological pipette 25 mL, 10 mL, 5 mL | Sarstedt |
| Shaker Orbit LS | Labnet |
| Shandon Immu-Mount | Thermo Scientific, Braunschweig, DE |
| SM7 remote unit and control box | Luigs and Neumann, Ratingen, Germany |
| Stereomicroscope Stemi 305 | Carl Zeiss Microscopy GmbH; Oberkochen, DE |
| Sterilization tape for autoclaves | A. Hartenstein |
| Super PAP Pen | Daido Sangyo |
| Super Frost™ Microscope Slides | Thermo Fisher Scientific |
| Synergie™ Fusion RP C18 | Phenomenex, Torrance, USA |
| TC-Plate 6 Well | Sarstedt |
| Temperature probe Physitemp BAT-12 | Physitemp; New Jersey, USA |

| | |
|---|---|
| Tetra Cooling Unit | Bio-Rad Laboratories |
| Thermomixer 5436 | Eppendorf, Hamburg, DE |
| Thermomixer Comfort | Eppendorf AG; Hamburg, DE |
| TipOne® Tips (20 µL, 200 µL) steril | Starlab |
| Tissue embedding cassettes | Kartell Spa |
| Tissue slicer | VT1200 S, Leica, Wetzlar, Germany |
| Tissue lyser NM300 | Retsch GmbH; Haan, DE |
| UNIVERSAL 320R centrifuge | Andreas Hettich GmbH |
| Vibrating microtome HM 650 V | Thermo Scientific, Waltham, USA |
| Volumetric flask 100 mL | Simax |
| Vortex-Genie 2 | Scientific Industries |
| Vortexer Vortex Genie 2 | Bender & Hobein |
| Water bath 1086 | GFL mbH; Burgwedel, DE |
| Water bath type 3044 | Koettermann |
| Water Bath WNB 22 | Memmert |
| Zeiss Axioimager M1 microscope | Carl Zeiss, Jena, DE |

### 3.1.2  Computer Software

**Table 2**. *Computer Software*

| Name | Description |
|---|---|
| Clampfit software | Molecular Devices, San José, CA, USA |
| FIJI 2.3.0/1.53f | Open Source |
| Igor Pro 9. | Wave Metrix, Lake Oswego, OR, USA |
| LSM Image browser | Carl Zeiss, Jena, DE |
| Microsoft Excel 16.57 | Microsoft |
| Microsoft PowerPoint 16.57 | Microsoft |
| Microsoft Word 16.57 | Microsoft |
| Molecular Devices Flex Software | Wokingham, Berkshire, United Kingdom |
| Patchmaster software | HEKA, Reutlingen, Germany |
| PRISM Graph Pad 9.2.0. | Graph Pad Software |
| Stereomicroscope Stemi 305 | Carl Zeiss Microscopy GmbH; Oberkochen, DE |
| confocal laser scanning microscope | LSM5 Exciter; Zeiss |

### 3.1.3 Chemicals, Reagents & kits

**Table 3**. *Chemicals, reagents, and kit*

| Product name | Manufacturer |
| --- | --- |
| 0.05% Trypsin EDTA | Thermo Fisher Scientific |
| 2-Mercaptoethanol | Sigma-Aldrich |
| 2-Propanol ROTISOLV® HPLC | Carl Roth |
| 30% Acrylamid Mix | Carl Roth |
| Acetic acid | Carl Roth |
| Amersham™ ECL™ Prime Western Blotting Detection Reagent | GE Healthcare |
| Ammonium persulfate | Thermo Fisher Scientific |
| Ammonium acetate | Thermo Fisher Scientific |
| Bio-Rad Protein Assay Dye Reagent Concentrate | Bio-Rad Laboratories Inc. |
| Calcium chloride dihydrate ≥ 99%, Ph. Eur., USP | Carl Roth |
| Chloroform ≥99.5% | Sigma-Aldrich |
| Dihydro Ethidium bromide (DHE) | Thermo Fisher Scientific |
| Ethanol ≥99.5%, Ph.Eur., extra pure | Carl Roth |
| Ethanol ≥99% | Fisher Chemical |
| Ethanol 99.5% Ph. Eur. | Carl Roth |
| Ethylenediaminetetraaceticacid(EDTA) disodium salt dihydrate ≥99% | Carl Roth |
| Isoflurane-Piramal | Piramal Critical Care Deutschland GmbH |
| Magnesium chloride hexahydrate ≥99% | Carl Roth |
| Methanol ≥99.9% | Fisher Chemical |
| Mini Protease Inhibitor Cocktail | Roche |
| Sodiumdeoxycholate | Merck |
| Sodiumpyruvate | Thermo Fisher Scientific |
| Novex® TBE-Urea Sample Buffer | Invitrogen |
| PAGERuler™ Prestained Protein Ladder | Thermo Fisher Scientific |

| | |
|---|---|
| Polyethylene glycol alkylphenyl ether (Triton-X 100) | Carl Roth |
| Polysorbate 20 (TWEEN® 20) | Carl Roth |
| Potassium chloride ≥99.5% | Carl Roth |
| Potassium dihydrogen phosphate | Merck |
| Sodium chloride | VWR Chemicals |
| Sodium dihydrogen phosphate monohydrate ≥98% | Carl Roth |
| Sodium Dodecyl Sulfate | Thermo Fisher Scientific |
| Sodium hydroxide pellets | Carl Roth |
| Sodium Pyruvate (100 mM) | Thermo Fisher Scientific |
| TEMED ≥99% | Carl Roth |
| Tris hydrochloride | SERVA Electrophoresis |
| Tris-(hydroxymethyl)-aminomethane ≥99.9% (Tris) | Carl Roth |
| Absolute Blue qPCR Sybrgreen Mix | Thermo Fisher Scientific Inc., Waltham, USA |
| Ammonium persulfate | Carl Roth GmbH, Karlsruhe, DE |
| Bepanthen® eye ointment | Bayer Vital, Leverkusen, DE |
| Bovine Serum Albumin | Carl Roth GmbH, Karlsruhe, DE |
| LightCycler®480 Probes Master | F. Hoffmann-La Roche A, Basel, CH |
| Maxima Probe qPCR Master Mix | Thermo Fisher Scientific, Schwerte, DE |
| Mercaptoethanol | Sigma-Aldrich GmbH; Steinheim, DE |
| Methanol ≥ 99.8 % | Honeywell International Inc.; Muskegon, MI &Sigma-Aldrich, St. Louis, USA |
| Microscope slide Superfrost® Plus | Thermo Scientific; Braunschweig, DE |
| Microtome blade C35 | Feather; Köln, DE |
| Normal goat serum | BioRad Laboratories, Hercules, USA |
| PBS Dulbeccos's | Bio&SELL GmbH; Nürnberg, DE |
| Phosphate buffered saline + TX100 (PBST) | PBS + 0,1 % Triton X-100 |
| Prolene 6-0 | Ethicon, San Lorenzo/USA |

| | |
|---|---|
| Qiazol Lysis reagent | Qiagen GmbH; Hilden, DE |
| QuantiTect Reverse Transcription Kit | Qiagen N.V., Venlo, NL |
| RIPA lysis buffer + protease inhibitor | 1 M Tris (pH 7.4), 1 M NaCl, 0.5 M EDTA, 10 % NP40 + 1 pill of protease inhibitor |
| Roti®Histo kitt | Carl Roth GmbH & Co. KG; Karlsruhe, DE |
| Xylol | PanReac/AppliChem GmbH; Darmstadt, DE |
| TTX (Tetrodotoxin citrate) | Biotrend |
| Gabazine (SR 95531 hydrobromide) | Biotrend |

### 3.1.4  <u>Antibodies</u>

**Table 4**. *Antibodies and dilutions*

| Antibody | Dilution | Manufacturer |
|---|---|---|
| Guinea pig anti- doublecortin | 1:500 | EMD MILLIPORE, Cat. #AB2253 |
| Rabbit anti- VGLUT-2 | 1:1,500 | Synaptic systems, Cat. #135402 |
| Guinea pig anti- calbindin | 1:500 | Synaptic systems RRID: AB_2619902 |
| Rabbit anti- parvalbumin | 1:500 | Synaptic systems, RRID: AB_2156474 |
| Goat anti- rabbit al488 | 1:1000 | RRID: AB_2576217 Thermo Fisher |
| Goat anti- guinea pig al568 | 1:1000 | RRID: AB_2534119 Thermo Fisher |
| Goat anti- mouse al647 | 1:1000 | Invitrogen/Thermo Fisher |
| DAPI | 1:10.000 | Sigma-Aldrich |
| TRPC3 antibody | 1:1000 | Cell Signaling, Frankfurt am Main, Germany; #77934S |
| ß-actin | 1:2000 | Sigma Aldrich, Taufkirchen, Germany; #A1978 |
| AKT antibody | 1:500 | Cell Signaling, Frankfurt am Main, Germany; #9272S |
| Phospho-AKT antibody | 1:500 | Cell Signaling, Frankfurt am Main, Germany; #4060S |
| mTOR antibody | 1:500 | Cell Signaling, Frankfurt am Main, Germany; #2983S |
| Phospho- mTOR antibody | 1:1000 | Cell Signaling, Frankfurt am Main, Germany; #2971S |

| CREB antibody | 1:1000 | Cell Signaling, Frankfurt am Main, Germany; #91975S |
|---|---|---|
| phospho-CREB antibody | 1:1000 | Cell Signaling, Frankfurt am Main, Germany; #9198S |

### 3.1.5  Primers

**Table 5** *Primers*

| Primers | Base sequence 5' -> 3' | Gene Bank number |
|---|---|---|
| PPIA | F- gCgTCTSCTTCgAgCTgTT<br>R- RAAgTCACCACCCTggCA | NM_008907 |
| VGLUT2 | F-GCCATCGTGGACATGGTCAA<br>R-ATAACTCCACCATAGTGGAC | NM_020346 |
| VGLUT1 | F-GCAAGTACATCGAGGACGCCAT<br>R-GCCACGATGATGGCATAGACTG | NM_020309 |
| TRPC3 | F-ATTCCTCGCCATCGGCTATTGG<br>R-GAGGCGTTGAATACAAGCAGACC | NM_019510.3 |
| TRPC6 KO | F-ACTACATTGGCGCAAAACAGA<br>R-CGTCCGCATCATCCTCAATTT | NM_013838 |
| TRPC6 | F-TGGCAGTGAAGTTCCTCGTGGT<br>R-GGAAAATGGTGAAGGAGGCTGC | NM_001282086 |
| cFos | F-GGGAATGGTGAAGACCGTGTCA<br>R-GCAGCCATCTTATTCCGTTCCC | NM_010234.3 |
| ARC | F-GCTGGAAGAAGTCCATCAAGGC<br>R-ACCTCTCCAGACGGTAGAAGAC | NM_001276684.1 |
| Bdnf | F-GGCTGACACTTTTGAGCACGTC<br>R-CTCCAAAGGCACTTGACTGCTG | NM_007540 |
| Akt1 | F-GGACTACTTGCACTCCGAGAAG | NM_009652 |

| | | |
|---|---|---|
| | R-CATAGTGGCACCGTCCTTGATC | |
| Creb1 | F-CACAGACCACTGATGGACAGCA<br>R-CACAGACCACTGATGGACAGCA | NM_009952 |
| mTOR | F-AGAAGGGTCTCCAAGGACGACT<br>R-GCAGGACACAAAGGCAGCATTG | NM_020009 |
| CD68 | F-GGCGGTGGAATACAATGTGTCC<br>R-AGCAGGTCAAGGTGAACAGCTG | NM_009853 |
| GFAP | F- CGGAGACGCATCACCTCTG<br>R- TGGAGGAGTCATTCGAGACAA | NM_001131020 |

### 3.1.6  Buffers and solutions

0.5M EDTA

EDTA x 2 $H_2O$              23.26 g

Purified $H_2O$              100 mL

Adjust pH 8.0 using NaOH.

0.1% TWEEN® 20/PBS-CMF

TWEEN® 20              50 µL

PBS-CMF              ad 50 µL

0.5% Triton X 100/PBS

Triton X              250 µL

PBS-CMF              49.750 mL

1.5M Tris pH 6.8

| | |
|---|---|
| Tris | 121.1 g |
| Purified $H_2O$ | 800 mL |

1M Tris-HCl pH 7.4

| | |
|---|---|
| Tris | 121.1 g |
| Purified $H_2O$ | 800 mL |
| HCl 37% | adjust to pH 7.4 |
| Purified $H_2O$ | ad 1 L |

Control pH and autoclave.

1.5M Tris pH 8.8

| | |
|---|---|
| Tris | 121.1 g |
| Purified $H_2O$ | 800 mL |
| HCl 37% | adjust to pH 8.8 |
| Purified $H_2O$ | ad 1 L |

Control pH and autoclave.

10% Ammonium persulfate (APS) solution

| | |
|---|---|
| APS | 100 mg |
| 2-Propanol | 1 mL |

10% Urea solution

| | |
|---|---|
| Urea | 20 g |
| Purified $H_2O$ | 200 mL |

Heat until Urea is completely dissolved.

10X Running buffer pH 8.45 for Western Blotting

| | |
|---|---|
| Tris | 30.2 g |
| Glycine | 144 g |
| 20% SDS | 50 mL |
| Purified $H_2O$ | ad 1 L |

10X Transfer buffer for Western Blotting

| | |
|---|---|
| Tris | 30.3 g |
| Glycine | 144 g |
| Purified $H_2O$ | ad 1 L |

Autoclave.

10X Tris Borate EDTA (TBE) buffer

| | |
|---|---|
| Tris | 108 g |
| Boric acid | 55 g |
| 0.5M EDTA | 20 mL |
| Purified $H_2O$ | ad 1 L |

10X Tris Buffered Saline (TBS) buffer

| | |
|---|---|
| Tris | 24.2 g |
| NaCl | 87.8 g |
| Purified $H_2O$ | ad 1 L |

1M NaCl

| | |
|---|---|
| NaCl | 292 mg |

Purified $H_2O$          5 mL

### 1M NaOH

NaOH          40 g

Purified $H_2O$          ad 1 L

### 1X Running buffer for Western Blotting

10X Running buffer          100 mL

Purified $H_2O$          900 mL

### 1X TBE Running buffer

10X TBE buffer          100 mL

Purified $H_2O$          900 mL

### 1X Transfer buffer for Western Blotting

10X Transfer buffer          100 mL

Methanol          200 mL

Purified $H_2O$          700 mL

### 20% SDS solution

SDS          20 g

Purified $H_2O$          ad 100 mL

Adjust pH 7.2 using HCl 37%.

<u>5% Bovine serum albumin (BSA) Blocking solution for Western Blotting</u>

BSA                          25 g

0.1 TBST buffer              500 mL


<u>5% Bovine serum albumin (BSA) antibody dilution buffer for Western Blotting</u>

BSA                          25 g

0.1 TBST buffer              500 mL

<u>Phosphate buffered saline without $Ca^{2+}$ and $Mg^{2+}$ (PBS-CMF)</u>

NaCl                         8 g

KCl                          0.2 g

$Na_2HPO_4$                  1.5 g

$K_2HPO_4$                   0.2 g

Purified $H_2O$              ad 1 L

Autoclave.

<u>Phenylmethylsulfonyl fluoride (PMSF) 100 mM</u>

PMSF                         175 mg

2-Propanol                   10 mL


<u>Protease Inhibitor solution</u>

Mini Protease Inhibitor      1 tablet

Purified $H_2O$              1 mL


<u>Radioimmunoprecipitation assay (RIPA) buffer</u>

1M Tris-HCl, pH 7.4          1.25 mL

1M NaCl                      3.75 mL

Triton-X100            250 μL

Sodium deoxycholate    125 mg

20% SDS                125 μL

0.5M EDTA              250 μL


Stripping solution for antibody removal

20% SDS                10 mL

0.5M Tris (pH 6.8)     12.5 mL

2-Mercaptoethanol      0.8 mL

Purified $H_2O$        77.5 mL


TBST 0.1%

10X TBS                100 mL

TWEEN® 20              1 mL

Purified $H_2O$        ad 1 L


TBST 0.5%

10X TBS                100 mL

TWEEN® 20              5 mL

Purified $H_2O$        ad 1 L


Tris-EDTA buffer

Tris                   1.21 mg

EDTA                   370 mg

Purified $H_2O$        ad 1 L

Blocking solution for immunohistochemistry

5% NGS

0,5% BSA

0,1% Triton X100

PBS (pH 7,4)


Cresyl violet

cresyl violet.              5 g

ethanol (100 %)      100 mL

stir at 50 °C for 30 min, add to 500 mL Aqua *dest*., filter


Cresyl-violet solution

cresyl-violet           0.031 mM

20 % ethanol


DAPI working solution

10 % of DAPI stock solution, Sigma Aldrich, Steinheim, DE

Paraformaldehyde 4 %

70 °C Aqua *dest*              235 ml

 PFA                           18.8 g

10 M NaOH                    0.47 ml

0.2 M phosphate buffer     235 ml

filter solution.

Electrophysiology slicing solution

212 mM sucrose          72,5676 g

26 mM $NaHCO_3$          2,18426 g

1.25 mM $NaH2PO_4$       0,1724875 g

3 mM KCl                0,22365 g

7 mM $MgCl_2$            1,4231 g

10 mM glucose           1,9817 g


Osmolarity: 305-306, pH 7,8-7,9 only adjusted by fumigation to 7,2. It should be Ice cold and oxygenated (95% O2/5% CO2) for at least 20 minutes before use.


Whole-cell Patch-clamp Intracellular solution

105 mM K-gluconate           1,2298125 g

10 mM HEPES                  0,119155 g

10 mM phosphocreatine-Na     0,12754 g

0.3 mM GTP                   0,0078477 g

4 mM Mg-ATP salt             0,101436 g


(pH 7.3, adjusted with KOH, 293 mOsm)


Active and passive membrane properties of intracellular solution

130mM K-gluconate

10mM HEPES

10mM phosphocreatine-Na

10mM Na-gluconate

0.3mM GTP

4mM MgATP

4mM NaCl

(pH 7.2, adjusted with KOH)

Extracellular Ringer

| | |
|---|---|
| 125 mM NaCl | 7,305 g |
| 25 mM NaHCO3 | 2,10025 g |
| 1.25 mM NaH2PO$_4$ | 0,1724875 g |
| 2.5 mM KCl | 0,186375 g |
| 2 mM CaCl$_2$ | 0,29402 g |
| 1 mM MgCl$_2$ | 0,2033 g |
| 25 mM glucose | 4,95425 g |
| Gabazine | 1:1000 dilution |

It should be oxygenated (95% $O^2$/5% $CO^2$) during the whole experiment.

### 3.1.7 Animals' Approval of animal experiments, strain, and the number of animals used.

All animal experiments were performed in compliance with institutional guidelines of the Johannes Gutenberg-University Mainz, Germany, and approved by the Animal Ethics Committee of the Landesuntersuchungsamt Rheinland-Pfalz (protocol numbers G 19-1-027).

For this study, we used a total of 70 Male and female *B6J;129S8 wild-type* (WT) and *B6J;129S8 -Trpc6tm1Lb1* (MMRRC stock NO 37345-Jax; TRPC6 KO) aged between 3-20 weeks. Obtained by mating male and female heterozygous (Trpc6tm1Lb1). All mice were bred and housed in the translational animal research center (TARC) in Mainz, Germany. And transferred to the laboratory facility on the day of the experiment. Animals were maintained in standard cages, with food and water ad libitum, in a temperature and humidity-controlled room under a 12 h light/12 h dark cycle.

## 3.2 Methods used in Chapter 4
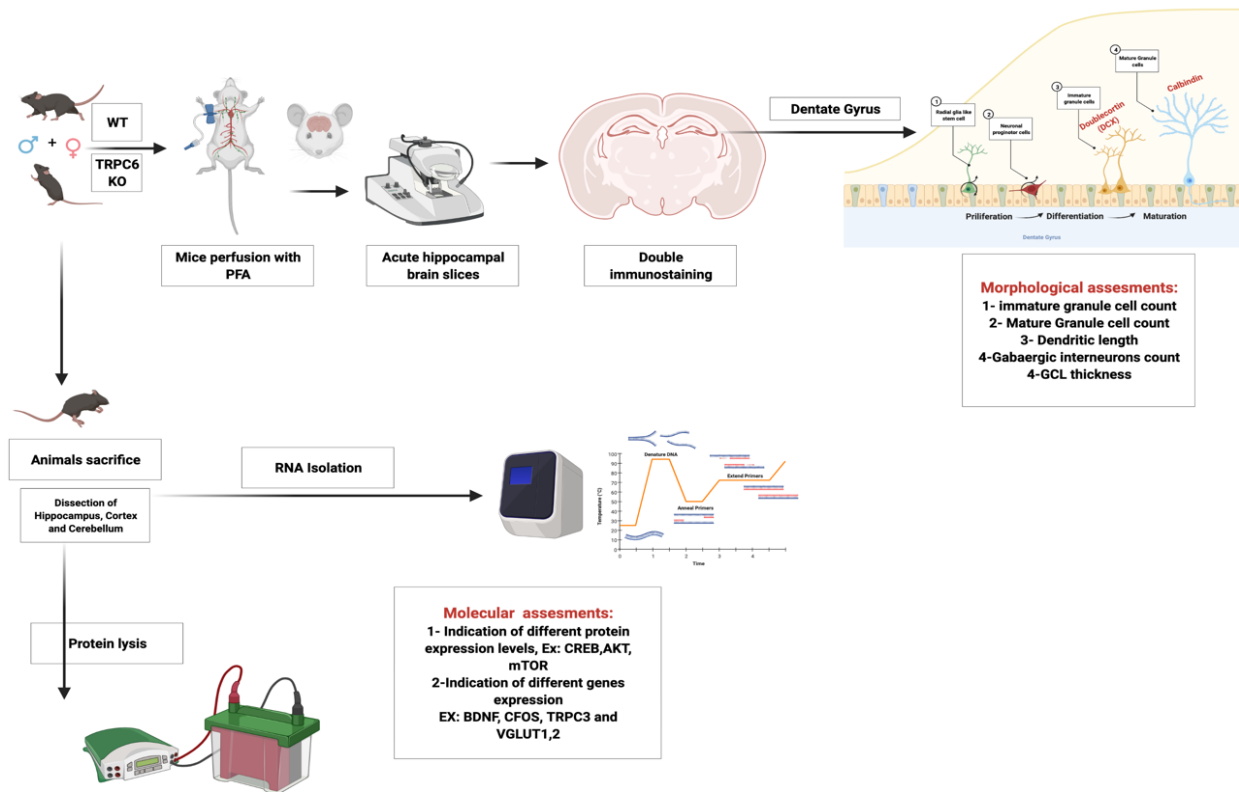


*Figure 10*. **showing the workflow of chapter 4**

### 3.2.1 <u>Immunohistochemistry</u>

For immunohistochemistry, adult mice *(12-15 weeks old; six males, six females)* were deeply anesthetized with isoflurane at 4 Vol% for 90 seconds then transcardially perfused with 40ml PBS followed by 40ml 4% paraformaldehyde (PFA). Subsequently, the brains were removed from the skull and postfixed overnight in 4%PFA. The next day brains were washed with PBS and placed in a low melting point agarose 4% before cutting. Vibratome 50 μm thick slices (from bregma levels -1.22mm to -2.8mm) were obtained with the help of the slicer, then fixed in 4% PFA for 1 day. For blocking, slices were incubated for 2 hr. at room temperature in PBS, pH 7.4, containing 5% goat serum, 0.5% bovine serum albumin, and 0.3% Triton X- 100.

Primary antibodies were diluted in blocking solution and incubated on sections overnight at 4°C. After 3x washing steps with PBST, secondary antibodies were diluted in a blocking solution, and sections were incubated 2hr. with gentle shaking at room temperature. All sections were counterstained with DAP and mounted in Immu- Mount

and coverslips. Finally, the sections were stored darkened at 4 °C (Antibodies were listed in table 4).

With a confocal laser scanning microscope, 40X images and Z-stacks of individual immunostainings were taken using the same filter and acquisition parameters to ensure comparability regardless of experimental conditions. Being blinded to the group or genotype, The number of DCX+ neurons, CB+, and parvalbumin cells were counted by visual inspection of the hippocampal area, including CA1, CA3, and DG (sub-granular layer of the upper blade). The dendritic length of DCX+ cells and cell dispersion between CB+ neurons and VGLUT-2 particles were analyzed using ImageJ (NIH Image). Images were analyzed with appropriate threshold settings for background subtraction.[120]

### 3.2.2   Western Blotting

For western blot, (*12-15 weeks old; six males, six females*) were sacrificed by cervical dislocation. Three different brain areas (cortex, cerebellum, and hippocampus) were dissected and snap-frozen in liquid nitrogen. Samples were then stored at -80°C until the day of the experiment.

Protein extraction

On the day of extraction, brain tissue was placed on ice for a short time. Then were washed with ice-cold PBS-CMF. Depending on the tissue size, 200-1000 µL of RIPA was used. After additional incubation of 30 min on ice, tubes were centrifuged (10,000 g, 10 min. at 4°C), the supernatant was withdrawn, and the pellet was discarded. From this supernatant, 20 µL were collected for the Bradford assay, and the remainder was mixed with protease inhibitor at a ratio of 10:1.1 and aliquoted for later use.

Bradford Protein Assay

The Bradford assay was used to quantify unknown protein concentrations from protein extracts. Coomassie G-250 is the dye used for this assay. Through binding to proteins, a color shift of Coomassie G-250 was detected. Unbound Coomassie G-250 has an absorbance maximum of 470 nm, while the absorbance of bound Coomassie G-250 shifts to a maximum of 595 nm. This change in absorbance is determined photometrically. Since the amount of Coomassie G-250 is proportional to that of

proteins, the exact concentration can be calculated from this. According to Bradford, a calibration grade was first performed using 1000 µg/mL BSA solution to determine standard protein concentration. For this purpose, 125 mg BSA was dissolved in 100 mL purified $H_2O$ ad diluted in a series of dilutions. This is shown in the following table.

**Table 6. Preparation for Bradford calibration curve**

| Stock | Composition | Concentration [µg/mL] |
|-------|-------------|-----------------------|
| 0 | 125 mg BSA add100 mL $H_2O$ | 1000 |
| A | 32 µL stock 0 + 1598 µL $H_2O$ | 20 |
| B | 800 µL stock A + 800 µL $H_2O$ | 10 |
| C | 800 µL stock B + 800 µL $H_2O$ | 5 |
| D | 800 µL stock C + 800 µL $H_2O$ | 2.5 |
| E | 800 µL stock D + 800 µL $H_2O$ | 1.25 |

Protein extracts were prepared as follows: 20 µL of protein extract was collected from the supernatant of samples, and 1980 µL of $H_2O$ was added to each preparation (1:100). 80 µL of 1:100 solution was added to 720 µL into a new Eppendorf tube (1:1000). Finally, 200 µL of Biorad dye was added to each solution and incubated for 5 minutes in the dark. In addition, a blank (1000 µL $H_2O$) and a zero reference (800 µL $H_2O$ + 200 µL Biorad dye) were prepared. The absorbance was determined photometrically at 595 nm and 470 nm.

SDS Page and Western Blotting

Whole tissue extracts were fractionated by 12% SDS-Polyacrylamide gel electrophoresis. The gel consisted of a running and a stacking gel.

Running gel

$H_2O$                              1625 µL

30% acrylamide mix            2000 µL

1.5M Tris (pH 8.8)            1300 µL

20% SDS solution               25 µL

10% APS solution               50 µL

TEMED                          2 µL

Stacking gel

H$_2$O                          1370 µL

30% acrylamide mix             340 µL

1.5M Tris (pH 8.8)             260 µL

20% SDS solution               10 µL

10% APS solution               20 µL

TEMED                          2 µL


Before casting the gels, the glass plates first had to be cleaned with ethanol to remove any troublesome fatty stains. They were then assembled in a special apparatus. First, the running gel was prepared. For this purpose, 4 mL of the corresponding mixture was pipetted between each glass plate and covered with approximately 1 mL of isopropanol. This served to remove excess air bubbles. After polymerizing the gel, the isopropanol was discarded and rewashed with purified H$_2$O. The components of the stacking gel were then pipetted together, 2 mL of each was poured over the existing running gel, and the comb was inserted. After about 30 min, the gel was polymerized and wrapped in wet wipes for storage at 4°C. The samples were prepared by thawing and vortexing them shortly. Extracted proteins were dissolved in 18 µL of water and 6 µL of 4X Roti®Load 1. Incubation was performed for 5 min at 85°C. Meanwhile, the running chamber was prepared, and the gel comb was removed. 60 µL of the protein solution was added to each gel pocket. A 6 µL PageRuler$^{TM}$ pre-stained protein ladder was used as a marker. Electrophoresis was performed at 80V until proteins reached the end of the separating gel. The voltage was then increased to 120V.

Electrophoresis was stopped before the PageRuler$^{TM}$ pre-stained protein ladder reached the running gel's end. After protein extracts were fractionated by 12% SDS-Page, they were transferred to a polyvinylidene difluoride (PVDF) membrane at 4°C for 1h using a transfer apparatus. For this, the PVDF membrane was first activated in methanol and then rehydrated in H$_2$O. The transfer sandwich was assembled in a special holder consisting of (in order from bottom to top): fiber pad, filter paper,

membrane, gel, filter paper, fiber pad. The transfer was performed at 4°C for 1h at 100 V. Membranes were incubated for 1h at room temperature with 5% BSA to block non-specific binding. Afterward, membranes were washed three times with 0.5% TBST (1st 15 min., 2nd 10 min., 3rd 5 min.).

This was followed by overnight incubation at 4°C with a primary antibody that binds specifically to a sequence at the target protein. Antibodies are listed in table 5. The primary antibody was diluted to desired concentration in 5% BSA solution. After overnight incubation, membranes were washed thrice for 10 min using 0.5% TBST and incubated with a horseradish peroxidase-conjugated secondary anti-mouse or anti-rabbit antibody for 1h. After three additional washing steps with 0.5% TBST, membranes were developed with Amersham™ ECL™ Prime Western Blotting Detection Reagent according to the manufacturer's protocols.

Amersham™ ECL™ Prime Western Blotting Detection Reagent

Solution A and B were mixed in equal parts to develop the Western blot membranes. Depending on the size of the membranes, 200-1000 µL of the mixture was added to each membrane. After an incubation period of 5 minutes, the membranes were analyzed using the Vilber Fusion TS FX imager. The following settings were chosen as setup:

**Table 7** *Set up for Fusion FX Imager.*

| Variable | Set up |
|----------|--------|
| Lightning | Prime |
| Time | Auto |
| Tray | 4 |

The amount of protein could be quantified by determining the band intensity using a peroxidase reaction with resulting luminescence.

<u>Stripping the membrane</u>

Stripping was performed to remove the antibodies from the membrane. The stripping solution was preheated to 50°C, and the membrane was incubated with the stripping solution at 50°C for 30 min. After incubation, the membranes were washed twice with 0.5% TBST. An image was developed using the Amersham™ ECL™ Prime Western Blotting Detection Reagent and the Vilber Fusion TS FX Imager to determine complete antibody removal.

<u>Analysis of the membranes</u>

The images obtained from the Vilber Fusion TS FX imager were analyzed using Fiji ImageJ. Each individual band was marked, and the intensity of each was determined. The obtained intensity values were set to the standard B-Actin and converted to percent. The final plots were made using Graph Pad Prism 9.2.0.

### 3.2.3 **Gene expression analysis**

For gene expression analysis (*12 male and female mice of the same age, 12-15 weeks old)* were used. After being sacrificed by cervical dislocation, the brains were extracted and dissected into 3 different regions (hippocampus, cerebellum, and cortex), then snap-frozen in liquid nitrogen and stored at -80°C until the day of the experiment.

<u>RNA extraction and determination of RNA concentration</u>

The RNA required for the molecular genetic studies was extracted from the dissected areas using the Rneasy® Plus Universal Mini Kit (Qiagen, USA). To lyse and homogenize the tissue, it was mixed with 0.9 ml of Qiazol reagent and a metal ball, which comminuted the tissue in the following two-minute step in the Mastermill at 20 Hertz (Hz). After incubation of the mixture for 5 min at RT 100 µl, genomic DNA (gDNA) eliminator and 180 µl chloroform were added, whereby a 15s vortex step after every adding followed. The chloroform and the phenol contained in the Qiazol reagent provided a solution for the proteins. After a further incubation of 2 min, a centrifugation step of 15 min at 4 °C and 12000 x g followed, which served as the phase separation of the mixture. There were three phases, with only the upper colorless, aqueous phase containing RNA. This phase was pipetted off and added to 600 µl of 70 % ethanol.

The DNA-containing white interphase, as well as the proteinaceous, red, organic phase, was discarded. By centrifuging the sample/ ethanol mixtures, they were driven through the membrane of the column, where the RNA bound to the membrane. After washing with 700 μl RWT and 500 μl RPE buffer, followed by centrifugation after each addition, impurities were removed. After adding 500 μl of RPE buffer and centrifugation at 8000 x g for 2 min, the column was transferred to a new tube and centrifuged for 1 min at maximum speed to dry the membrane and remove any remaining ethanol. This is important because ethanol causes the binding of the RNA to the silica membrane. After transferring the columns into new collection tubes, the RNA present on the membrane was eluted with 30 μl of RNA-free water by centrifugation for 1 min at 8000 x g.

By spectrophotometric measurement, it was possible to determine the nucleic acid content and the purity of a sample. For this purpose, the molecule-specific absorption maxima of DNA at 280 nanometers (nm), RNA at 260 nm, and organic impurities at 230 nm were measured. An optical density (OD) value of 1 equals 40 μg RNA per ml. The quotient of $OD_{260}/OD_{280}$ should be between 1.7 and 2.0.

The following formula can calculate the nucleic acid concentration:

$$40 \times OD260 \times \text{dilution factor} = \mu g \text{ RNA/ ml}$$

cDNA-synthesis

Since double-stranded nucleic acids are required for carrying out the qRT-PCR, the extracted, single-stranded RNA must first be rewritten into complementary DNA (cDNA). This was done using the QuantiTect Reverse Transcription Kit.

To eliminate residual gDNA, 0.5 μg RNA from each sample was spiked with 2 μl gDNA wipeout buffer. The samples were made up to 14 μl with RNase-free water and incubated for 8 min at 42 °C. Subsequently, a master mix was created containing the reverse transcriptase (rt), rt buffer, and rt primer mix. Of these, 6 μl were added to each sample, followed by incubation at 42 °C for 30 min. In this step, reverse transcription took place. After a subsequent inactivation of the rt for 3 min at 95 °C, the samples were diluted in the ratio 1:2 with $H_2O$ and stored at -80 °C.

qRT-PCR

The qRT-PCR and the subsequent calculations of the cDNA concentration were carried out with the LightCycler®480 and the corresponding software. The qRT-PCR is based on the principle of classical PCR, which was supplemented by additional quantification of the amplified amount of DNA in real-time. Classical PCR is a method for enzyme-dependent amplification of desired gene sequences. This is divided into three steps, which are repeated in a fixed number. During the denaturation phase, the hydrogen bonds of the DNA double-strand are split, whereby the DNA is now single-stranded. In the subsequent annealing phase, the primers are used to bind to the 3' end of the gene sequence. From these primers, the polymerase synthesizes a complementary strand during elongation in the 5'-3' direction. In the case of the qRT-PCR, an inactive fluorescent dye (e.g., SYBR Green) or a hybridization probe is added to the used cDNA molecules. The fluorescent dye binds un-specifically to DNA and gets activated by DNA production and stimulated by a light source. The hybridization probe is an oligonucleotide that binds specifically to the complementary DNA section and starts to fluoresce upon successful binding.

The resulting signal is quantitatively directly related to the number of amplified DNA. By plotting the intensity of the fluorescence signal against the number of PCR cycles, this can be graphed. The result is a characteristic sigmoidal curve subdivided into three main phases. In the initial phase, a low fluorescence signal occurs. The low number of templates in this stadium can explain this. In the following phase, there is an exponential increase in fluorescence since here, DNA, polymerase, and primer are optimally distributed. In the final plateau phase, the signal intensity stagnates because most of the substrates are consumed, and the heat slowly destroys nucleotides and polymerases. In the phase of exponential growth, which is vital for quantification, crossing points (CP) are defined. These describe the cycle in which the fluorescence for the first time significantly exceeds the background fluorescence. The amount of contained DNA was determined using the Light cycler software since the CP depends on the number of PCR products. Therefore, it was necessary to generate a standard curve, with the aid of which the DNA concentration could be determined for each CP value.

For this purpose, at the same time as the samples, a standard solution was run whose DNA concentration was known. Finally, the normalization followed with the help of the housekeeping gene Peptidylprolyl Isomerase A (PPIA), also known as

cyclophilin A, which corrects RNA measurement errors and different RT efficiencies. PPIA was chosen because it is continuously expressed, and there is no regulation according to CCI[121]. For each target to be examined, a separate master mix had to be created. The individual reagents used for the SYBR-Green method and the hybridization probe method are listed in table 8. Each sample was analyzed in duplicate. The resulting mean was then normalized against the mean of the housekeeping gene, also analyzed in duplicate.

**Table 8***: Ingredients of the SYBR-Green and the hybridization probe master*

| SYBR-Green | | Hybridization probe | |
|---|---|---|---|
| **Reagent** | **Amount per sample** | **Reagent** | **Amount per sample** |
| SYBR-Green | 5 µl | Probes Assay Mix | 5 µl |
| Forward-/ Reverse Primer | each 0.25 µl | Forward-/ Reverse Primer | each 0.25 µl |
| $H_2O$ | 3.5 µl | Hybridization probes | Each 0.5 µl |
| - | - | $H_2O$ | 2.5 µl |

### 3.2.4 **Electrophysiology**
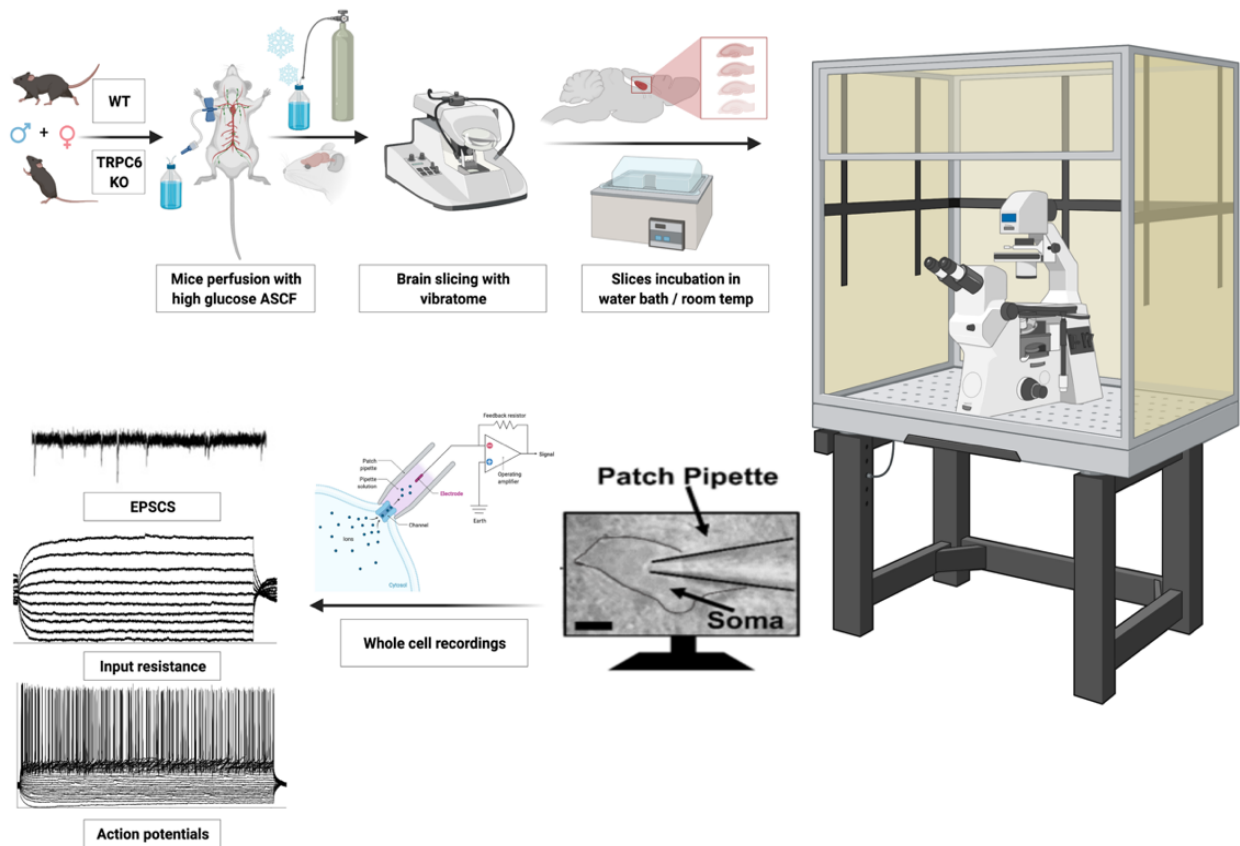


***Figure 11.*** **A diagram showing the steps of the electrophysiology experiment**

Preparation of acute hippocampal slices

Cardiac Perfusion of adult mice

Deeply anesthetized mice (aged 15-20 weeks, n=16 of equal sexes) with 3% isoflurane after checking for the absence of reflex upon tail or paw. The mice were transcardially perfused with ice-cold oxygenated (95% $O_2$/5% $CO_2$) slicing solution (see buffers section) for 2-3 minutes.

Quick extraction of the brain

After the perfusion, the head was quickly decapitated using large scissors then the skull was exposed with a large incision through the skin down the midline. The skin was pulled toward the nose of the animal to fully expose the skull, which provides

a better grip on the head. Following this step, the head was placed in the ice-cold oxygenated slicing ACSF for a few seconds. Keeping the head fully submerged in the solution, the back of the skull was opened with fine scissors by a long-cut caudal to the cerebellum, followed by another cut along the middle from the caudal end, working way up to the olfactory pulps. Using fine forceps, the edges of the skull were gripped to the sides to expose the brain. Reaching under the brain with a curved spatula and being remarkably gentle, the brain was scooped out to the ice-cold slicing solution, which was kept fully submerged. With a razor blade, the brain was cut in half, separating the two hemispheres, which were then placed on the freshly cut medial sides. The brain's dorsal part (5%-10%) was removed from each hemisphere with a parallel cut to the dorsal top, and then both hemispheres were placed on the freshly cut side, with the ventral part of the brain facing upwards. On the specimen plate of the slicer, a drop of super glue was spread properly with a pipette tip to accommodate both hemispheres. Using a filter paper strap, the hemispheres were picked one after another and placed with the dorsal side down on top of the glue in the specimen plate. (Figure12 )
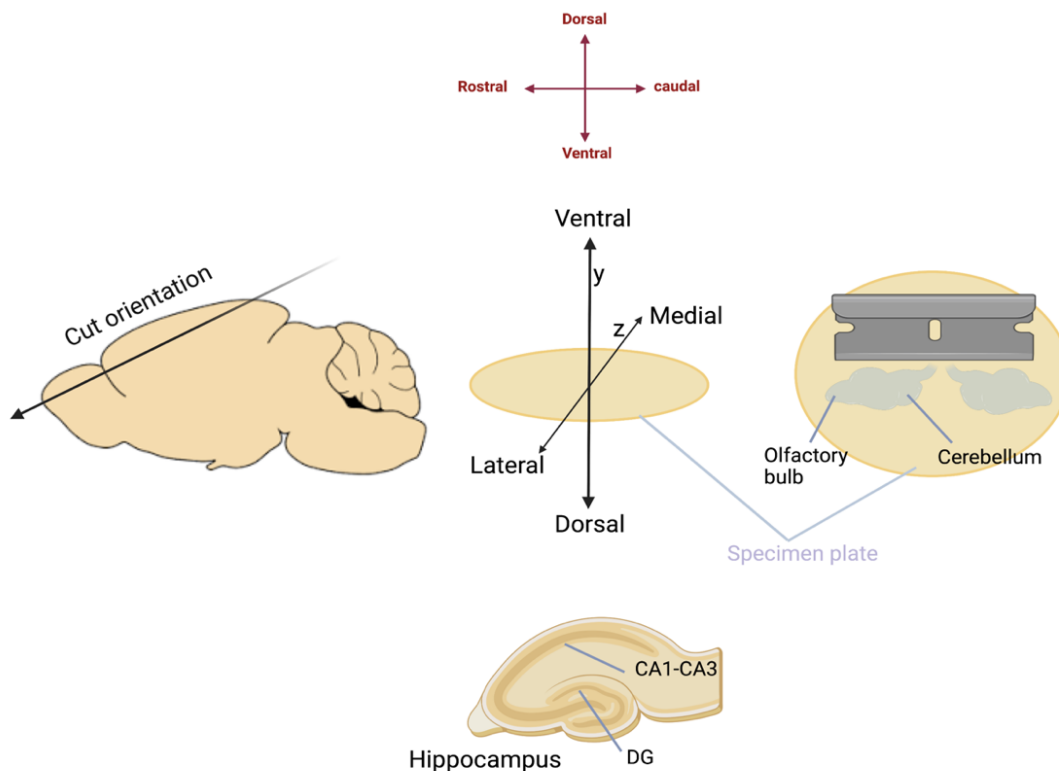


**Figure 12*: Cartoon illustrating the orientation of the cut of the dorsal side of one hemisphere to prepare the brain for horizontal slicing and the isometric projection of the brain orientation on the specimen plate of the vibratome.**

Horizontal slicing of the brain

The vibratome blade was positioned in front of the medial side of the hemispheres and lowered to the same height as the ventral sides facing upwards. The blade was reduced with the help of the vibratome control to 600 µm further in the dorsal direction, and slicing started. The blade should hit the tissue.

250-µm-thick slices of the hippocampus were collected with a winded plastic Pasteur pipette and transferred to the recovery chambers, filled with ACSF in the water bath at 32 °C for 15 mins. The chambers were out of the water path and kept in RT for the whole recording time. The slices were recovered in RT for at least 30 mins before the measurements started.

The same preparation method was applied for acute slices from young mice (3-4 weeks, n=18 of both sexes) except for the cardiac perfusion step, and in this case, the slicing solution was iced with liquid nitrogen. During recording, slices were constantly perfused with oxygenated ACSF containing Gabazine. Neurons were visualized with an Olympus upright microscope fitted with a 4×objective and 40×water-immersion objective and a CCD camera.

The patch-clamp technique

The patch-clamp technique was historically based on the work of Alan Hodgkin and Andrew Huxley, who conducted a series of elegant voltage-clamp experiments in the 1950s that allowed the recording of macroscopic currents in the squid giant axon by controlling the membrane voltage. One limitation of Hodgkin and Huxley's technique was that it needed the resolution to measure the current through a single channel. This was made possible by Neher and Sackman, who invented the patch-clamp technique in 1976. Using this new technique, they could record the first acetylcholine (ACh)-activated single channel from a tiny area (a patch) of the plasma membrane of frog skeletal muscle. This technique and its subsequent improvements represent a significant advancement in monitoring cell membrane function. Recording ionic currents through single channels contained in small patches of cell membranes is possible by sealing a small pipette tip to a clean cell membrane. In conjunction with

whole-cell recording, patch-clamp techniques enable the investigation of ion channel conductance and kinetic behavior.[122]

Conventional patch clamping is accomplished by sealing the tiny tip of a pipette to the surface of the cell membrane in such a way that a tiny membrane area (patch) can be isolated from the rest of the membrane and its voltage controlled while simultaneously recording currents through the ion channels in the patch. A typical electrophysiology rig includes a Faraday cage (to isolate the equipment from electrical noise), a vibration isolation table, a microscope for imaging cells, micromanipulators for moving and positioning the electrodes, low-noise amplifiers, a computer (for generating the stimulus waveform and data acquisition), and a perfusion line. The patch-clamp technique requires a stable platform with minimal vibrations to maintain stable contact between the pipette and the cell.

Patch-clamp recordings are typically used to assess the electrical properties of the membrane (or portions of it) attached to the pipette. The sequence of events that led to the patch-clamp recording of channel activity is as follows. Isolated cells are immersed in the recording solution in the perfusion chamber (Figure 12). A low-voltage square pulse is then applied to the patch pipette as it is moved toward the cell surface. The current amplitude of this pulse is measured to track the formation of the seal.

As soon as the pipette touches the membrane, resistance increases, resulting in a decrease in current according to Ohm's law (I ¼ V/R where I ¼ current, V ¼ voltage, and R ¼ resistance). A tight seal is formed by gentle suction, allowing very high-resolution current recording through the channels in the patch. The tight seal formed between the membrane and the pipette is known as a "Giga seal" because it has a resistance more significant than one giga-ohm ($10^9\Omega$). This high-resistance seal reduces background noise and enables high-resolution recordings of single-channel currents less than one pA. Successful Giga seal completion depends on several factors, including enzymatic cleaning of the cell membrane, pipette configuration, and solution composition.

The tight Giga seal keeps the pipette-to-membrane connection mechanically stable and malleable, allowing for the establishment of various recording configurations. *The cell-attached recording configuration* is obtained at this point. While it measures single channels in their most physiological setting, it is also the starting point for other recording configurations. When a cell-attached mode is established, the tight seal

between the membrane and the pipette forms a powerful bond, and the patch of membrane attached to the pipette can be excised from the cell using various methods.

A vesicle is detached by mechanically pulling the pipette away from the cell. When exposed to air, the vesicle ruptures, leaving a patch of membrane within the pipette (estimated area of the patch 1e10 mm2). The patch is separated from the rest of the cell, and the intracellular side of the membrane encounters the bath solution. This is referred to as *the inside-out configuration*. A second excised patch configuration, *the outside-out configuration*, can be obtained from the cell-attached configuration. The Giga seal is first broken by applying suction through the glass pipette, resulting in the whole-cell configuration. The outside-in configuration is achieved by slowly withdrawing the pipette from the cell from this position. The membrane stretches, breaks and folds back in on itself. As a result, the electrode includes a portion of the membrane with the outside surface facing the bath.

This configuration enables single-channel recordings with easy manipulation of the extracellular milieu while controlling the intracellular environment (with a pipette solution of known composition). Finally, the whole-cell configuration is achieved by breaking the patch with suction from a cell-attached configuration. During cell dialysis, this allows for continuity between the pipette solution and the cytoplasm.[122]
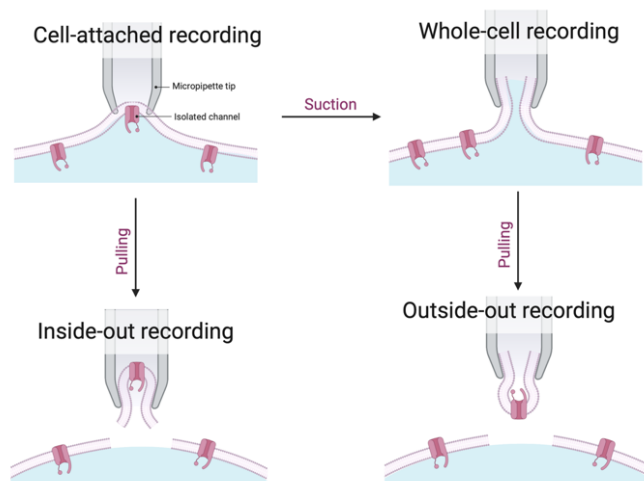


**Figure 13***: **Patch-clamp recording configurations**. The schematic depicts the patch-clamping recording configurations and the maneuvers required to achieve them. Each configuration is described in detail in the text above.

Active and passive properties of granular cells in the upper blade of the DG

Using this method, we can assess the granular cell's passive and active properties. The cell's passive properties include its resting membrane potential, input resistance, and capacitance. The cell's active properties have the action potential threshold, firing rate, and afterhyperpolarization. We can learn more about the electrical activity of these cells and the underlying ion channels and membrane proteins that underlie this activity by analyzing the active and passive characteristics of these cells.

Researchers can use this knowledge to understand better the DG's functionality and how various types of brain trauma or neurological conditions influence it. With an EPC-10 USB Double amplifier, current or voltage clamp recordings were made (HEKA Electronic). Series resistance was 8-20 M in current-clamp recordings. Signals were low pass filtered at 3 or 10 kHz (Bessel), digitized (sampling rate: 20 kHz), and stored using Patch master software on Windows 10. RMP (resting membrane potential) was measured immediately following patch break-in. The steady-state voltage difference caused by a hyperpolarizing current step was used to calculate input resistance (Rin) (-20 pA, 500 ms). All experiments were performed on visually identified mature Granular cells based on relatively large and round-shamed somata. GCs located on the upper blade of the DG were targeted.

Spontaneous (sEPSC) and Miniature excitatory postsynaptic currents (mEPSC)

Spontaneous excitatory postsynaptic currents (sEPSCs) and miniature excitatory postsynaptic currents (mEPSCs) are small electrical currents that flow through a neuron's cell membrane in response to other neurons in the brain, releasing the neurotransmitter glutamate. Patch clamp techniques are commonly used to measure these currents, which involve sealing a small patch of the cell membrane to a micropipette and measuring the currents flowing through the patch.

The main distinction between sEPSCs and mEPSCs is the source of the glutamate that triggers the currents. In the case of sEPSCs, glutamate is released spontaneously from other neurons in the brain without any external stimulation or action potentials in the neuron being measured. mEPSCs, on the other hand, is activated by the release of glutamate in response to a specific stimulus or action potential. The amplitude and frequency of sEPSCs and mEPSCs can reveal important details about the neuron's function and role in learning and memory.

For measuring the sEPSCs, the whole cell recording was obtained from granular cells of the upper blade of the DG by the method mentioned above using electrodes with tip resistance between 3-5 Mohm filled with intracellular solution (mentioned in the buffers section) in a voltage clamp mode at a holding of -70mV. Capacitance and serious resistance were compensated routinely. mEPSCs were recorded the same way but with applying TTX and APV in the extracellular solution (mentioned in the buffers section) for blocking action potentials and NMDA currents. Finally, sEPSCs and mEPSCs were filtered at 2.9 kHz and sampled at 10 kHz using PATCH MASTER software HEKA Instruments, Lambrecht, DE) and a HEKA EPC10 amplifier.

<u>Whole-cell LTP</u>

In the context of long-term potentiation (LTP), the medial and lateral perforant paths are two pathways that carry information from the entorhinal cortex to the hippocampus. The medial perforant path carries information from the medial entorhinal cortex, while the lateral perforant path carries information from the lateral entorhinal cortex. To perform single-cell LTP, we would isolate a single neuron (granular cell) in the DG and then stimulate the medial or lateral perforant path with an electrode or other electrical stimulation method. After that, the perforant path would be stimulated at a high frequency for an extended period.

This is the experimental condition, and LTP is expected to occur in the stimulated pathway. The opposite pathway (i.e., the lateral perforant path if the medial perforant path was stimulated, or vice versa) would not be stimulated as a control. This would allow us to compare the effects of high-frequency stimulation on the stimulated versus non-stimulated pathways and determine whether LTP had occurred. This can provide essential insights into the mechanisms underlying LTP and its role in learning and memory.

In my experiments, to stimulate the MPP, stimulating patch-type pipettes were placed in the DG's middle third of the medial molecular layer and the distal part of the outer molecular layer, respectively. To elicit synaptic responses, monopolar square-wave voltage or current pulses (100-200 s pulse width, 4-25 V or 20-100 A) were delivered via a stimulus isolator (Isoflex, AMPI, or Digitimer DS2A-MKII) connected to a broken tip (10-20 m) stimulating patch-type micropipette filled with ACSF.

## 3.3 Methods used in Chapter 5
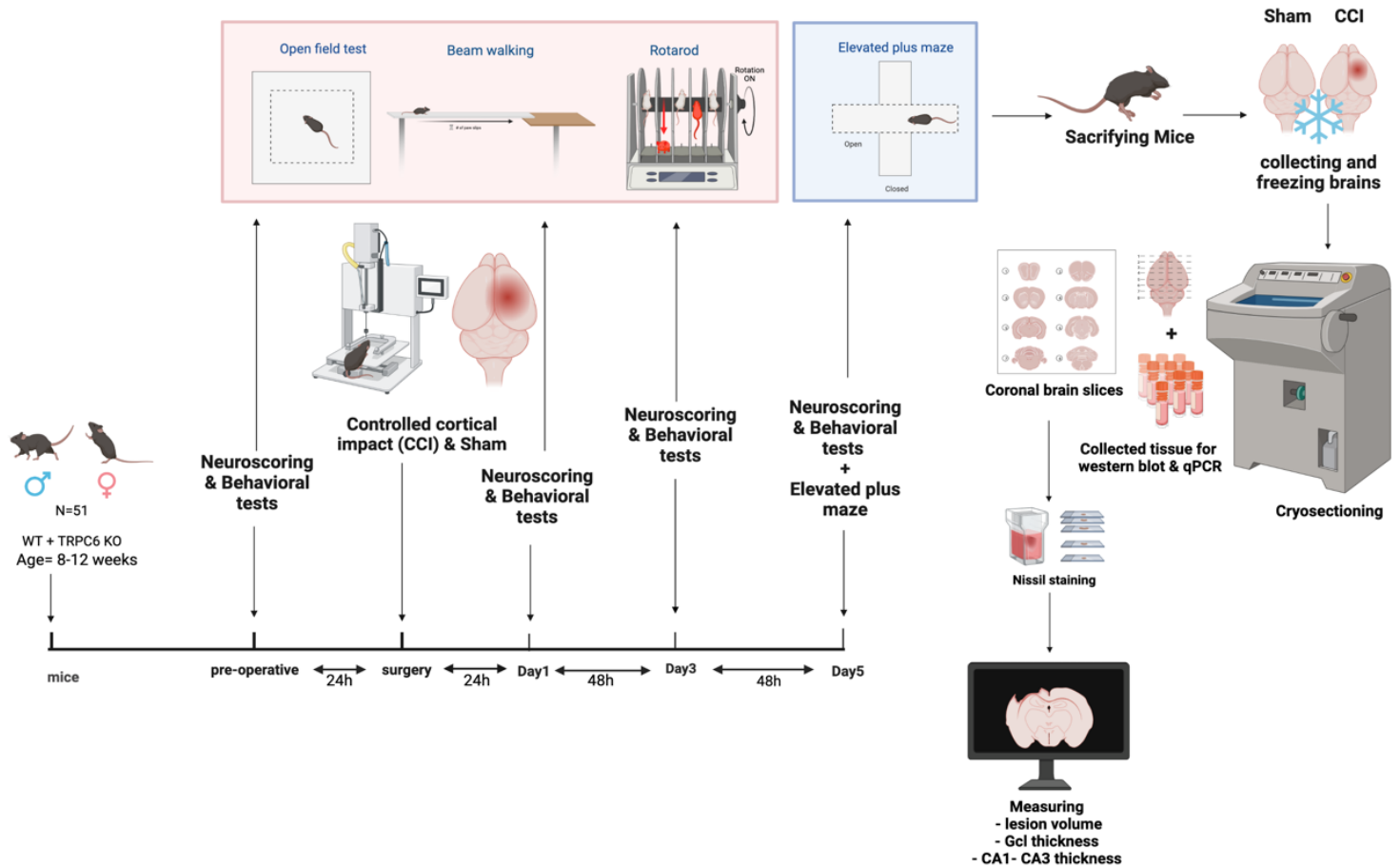


*Figure 14*: **Cartoon illustration showing the workflow in chapter 5**

### 3.3.1 Animals number and randomization

A total of 51 animals of both sexes aged between 8 and 12 weeks were used for the study. Mice were randomized, and the experimenter was blinded to the data analysis and acquisition. The animals were divided into four groups. Gp 1: CCI/WT n=16, Gp 2: CCI/TRPC6 KO n=13, Gp 3: Sham/WT n=12 and Gp 4: Sham/TRPC6 KO n=9. The animals were to be housed alone in filter-top type II cages during the study to reduce the danger of wound infection. All cages included embedding material, nesting tissue, and plastic cylinder for enrichment. In addition, the cages were kept in an airflow cabinet (Uniprotect, zoonlab, USA) under a 12/12 h light/dark cycle at 22+/-2°C, with 55% humidity. Animals had unlimited access to food and water.

### 3.3.2  **Surgery.** narcosis, induction, and anesthesia

To induce narcosis, mice are placed in an acrylic plastic container. In this rectangular container, one end was connected to a device with an anesthetic gas evaporation tank, and the other end was connected to an exhaust gas recovery system. After inhalation of 4 Vol% isoflurane for 1 minute, the mice were observed to become unconscious and then immediately pulled onto a stereotaxic stand. Subsequently, anesthesia was maintained with 2 Vol% isoflurane at a flow rate of 1.0 L/min of oxygen and 0.5 L/min of fresh air through a face mask. The body temperature of the mice was checked by rectal thermometry over the course of approximately half an hour of surgery. To maintain a constant body temperature of 36.5°C, mice were operated on a hot plate. To avoid drying the eyes, an ointment was used.

### 3.3.3  **Controlled cortical impact**

CCI is one of the most utilized and best-characterized models of the experimental TBI[106]. To expose the skull, a 1.5 cm long median incision was made. This was limited by the coronal and the lambdoidal suture.  After the periosteum was removed with cotton swabs, a window of 4 × 4mm was milled with the help of a micro drill. The window was bounded by the bregma, the zygomatic arch, the lambdoidal, and the sagittal suture and was placed in the right hemisphere. However, one side remained closed, which served as a hinge. To perform the TBI, the bolt of the electric-operated CCI impactor was placed on the intact dura mater. The cortical impact was applied using a Benchmark™ Stereotaxic Impactor (Leica Biosystems, Wetzlar, Germany) impactor tip diameter: 3mm, impact velocity: 6 m/s, impact duration: 200 ms, displacement: 1.5 mm). After hemostasis, the cranial bone piece was folded back, and the craniotomy was sealed with tissue glue (Histoacryl, Braun). 2-3 stitches were stitched up the skin incision. Following the operation, the mice were kept in an incubator at 37 °C and 50 % humidity for 1.5 h before they were returned to their original cages.

### 3.3.4  **Sham-operation**

In the case of sham-operated animals, a craniotomy was dispensed with. The craniotomy is considered part of the TBI. [123]Sham animals were handled identically in terms of anesthesia and skin incision. As craniotomy contributes to brain damage in the TBI model[124], only slight drilling on the exposed skull surface instead of craniotomy was performed to allow comparisons between non-injured and injured brains.

Craniotomy alone leads to increased cerebral expression of inflammatory cytokines, and exposure of the brain to the atmosphere causes vascular alterations[125] and leakiness within minutes. To achieve the best possible comparison, the sham animals were subjected to anesthesia, stereotactic fixation, skin incision, periosteal removal, and stitching.

### 3.3.5  Euthanasia and brain removal

Mice were sacrificed by decapitation while blood was collected in 50 ml falcon tubes, pre-rinsed with 80 µl heparin, and immediately centrifuged at 8000 rpm for 10 min; after that, the supernatant was collected in 5 µl tubes and quickly frozen on dry ice. The animal is anesthetized in advance with isoflurane (2 min, 4 Vol%). To remove the brain, the head is separated, and the skin is opened medially if this has not already been done. After incising the occipital region medially, the skull cap is moved away to the right while preserving the brain. Next, the cranial nerves are cut with a scraper, and the brain is removed from the skull. To further process the brain using a cryostat, the brain is frozen in dry ice powder and stored at -20°C.

### 3.3.6  Behavioral tests

Rotarod test

The Rotarod test is sensitive and commonly used to assess mice's motor coordination, endurance, and strength. [126] In this thesis, the test was used to compare the different groups; Gp 1: CCI/WT n=16, Gp 2: CCI/TRPC6 KO n=13, Gp 3: Sham/WT n=12 and Gp 4: Sham/TRPC6 KO n=9. The animals were placed on a rotating rod at a height of approximately 15 cm with a diameter of 3 cm, which accelerated over a period of 5 min continuous from 4 cycles per min to 40 rounds per minute (rpm). The time the mice can keep on the rotating rod with increasing speed was measured. Two days before surgery, the mice were trained in a total of 2x2 passes. The tests were carried out at different time points:  pre-surgery, 1dpi, 3dpi, and 5dpi after surgery.

Neurological severity score

The Neurological Severity Score (NSS) was used to test the neurological motor function of the mice. The test was performed the day before surgery to determine the status quo (pre-test) and a few days after surgery (pre-surgery, 1dpi, 3dpi, and 5dpi) to detect the results of changes with TBI. Based on 5 neurological parameters, conclusions can be drawn on the mice's coordination, balance, and general behavior. A point system was used to characterize the neurological motor function, which reached from 0 to 13 points. The more points are reached, the more severe the neurological impairment (Figure 15). The following parameters were tested:

By clapping hands, the startle reflex of the animal was tested. In addition, the mouse's seeking behavior and running behavior were assessed. Here it was to be observed whether the mouse was running straight or tending to a particular side.

The "Beam walking test" was used to test the coordination skills of the mice. The mouse had to run over bars with a width of 3, 2, and 1 cm. Points were awarded when the mouse stepped beside the bar or sat down/stopped moving on the beam.

The balance of the animal was determined using a square and a round stick. If the mouse could hold with all 4 paws for 10 s, it got 0 points. A point was entered if this was not achieved or the mouse fell off the bar.

Finally, it was assessed whether paresis or hemiparesis was present based on the previous tests. *Figure 4*: **Point scale of the NSS for 5 days Survival cohort**


Open field test and Elevated plus maze test with Ethovision system

The open field test (OFT) is a standard measure used to determine general activity levels, gross locomotor activity, and exploration habits in rodent models of CNS disorders in mice, where both the quality and quantity of the activity can be measured. Based on the natural flight instinct of the mouse in an open area is tested by the "exit from circle" test. The locomotor activity of mice was examined using a video tracking system (EthovisionXT, Noldus, Wageningen, Netherlands) in an open area consisting of a 40x40x40 cm light grey board under 330-350 lux of light. Mice are placed in the arena and allowed to move about freely for 3 minutes while being recorded by an overhead camera. The footage is then analyzed by an automated tracking system for the following parameters: distance moved, velocity, and time spent in pre-defined

zones. Tests are performed the day before surgery to determine the baseline condition (pre-test) and days post-surgery (pre-OP, 1dpi, 3dpi, and 5dpi) to detect changes in the outcome of traumatic brain injury.

The Elevated Plus Maze (EPM) test is used to evaluate the relative anxiety status of mice. Tests were performed on the 5th after surgery to detect changes in traumatic brain injury and cellular therapy outcomes. The EPM is a plus-shaped apparatus consisting of four elevated arms and two opposing arms open to the surroundings (open arms), whereas the two closed opposite arms (closed arms) are equipped with walls. After treatment, if increased time is spent on the open arms and/or an increased number of open arm entries compared to control (untreated), animals are detected on the EPM; this indicates an anxiolytic effect.

The most robust avoidance response has been demonstrated in the first 5 min after the start (placement of the rodent animal in the intersection of the four arms of the EPM) of the EPM assay[127.] [Therefore], any behavior after treatment is commonly recorded for 5 min on the EPM. As an additional measure of anxiety, the number of head drops backward movements (the rodent stands vertically on its two hind legs), and the full range of arm movements (spontaneous motor activity) and different postures (extension or freezing), all recorded with an overhead camera in the room under indirect lighting of 2800 lumens. Thus, multiple behavioral parameters can be compiled to comprehensively assess anxiety-related behavior with the video tracking and analysis system (EthovisionXT, Noldus, Wageningen, Netherlands).

### 3.3.7  **Histology**
Preparation of cryostat sections

Frozen tissue sections were prepared at the coronal plane for the volumetric damage measurement and immunohistochemical studies. For this purpose, the deep-frozen brain was fixed and covered with an embedding medium on a sample plat. For each brain, 16 microscope slides were prepared, divided into rows A and B, with row A containing brain planes 1-10 and B brain planes 11-16. From a brain, this resulted in 6 series of sections. Furthermore, cryotubes were prepared, and the later-made trimming cuts were transferred. These served for further investigations on the regulation of mRNA and protein expression levels. The first sections were taken at bregma +3.14 mm. The brain was then cut frontally in 16 levels, with the individual

levels at 500 µm. Between levels 6 to 13, trimming cuts were made per each level. Here every 6 sections were collected with a thickness of 40 µm and layered on top of each other. The ventral third was discarded, and the dorsal part was divided into two hemispheres. These were transferred separately from each other in cryotubes. The brain sections were stored at -20°C, and the trim sections at -80°C.

<u>Cresyl violet staining</u>

The cresyl violet or Nissl staining is based on the principle that the dye binds to basophilic structures such as RNA and DNA. 5 g of cresyl violet was dissolved in 100 ml of 100 % ethanol at 50 °C for 30 min on the magnetic stirrer to prepare the staining solution. After filling the solution to 500 ml with distilled water, the solution was filtered using a pleated filter. The frozen sections were air-dried for 1 h. The sections were then immersed in different chemicals in the order and duration shown in table 6. This happened in previously prepared dipping baths. Finally, the sections were embedded with Roti®-Histokitt and sealed with coverslips. **Table 9: Cresyl-violet staining protocol**

<u>Determination of the total damage volume</u>

The stained cresyl-violet sections were magnified with a light microscope and recorded and measured by the ZEN® software. For this purpose, the left (contralateral) and the right (ipsilateral) hemispheres were measured separately, as well as the area of the healthy tissue on the ipsilateral side. The area of damage resulted by subtracting the area of the healthy hemisphere from the surface of the entire hemisphere. To determine the total damage volume, the surface area (a) of the individual levels 1-16 was added together and multiplied by the distance between the levels (500µm).

<u>Granular cell layer Thickness</u>   $V = \sum_1^{16} a \times 500\mu m$

In addition to measuring the lesion volume, the Nissl-stained slides were also used to measure the thickness of the granular cell layer (GCL). The GCL lies in the supra-pyramidal blade of the DG as part of the hippocampus Field.[56] Differences in thickness can be used as an additional marker for structural loss. The measurement was taken approximately between Bregma -1.2 mm and -2.1 mm of two sections per animal. Every section was measured in three positions in the contra- and the ipsilesional hemispheres. These positions consist of the inner, middle, and end parts

of the DG. In addition to the GCL thickness, I estimated the thickness of the hippocampus's CA1 and CA3 layers. As in many cases of CCI, these layers are either totally lost or disrupted (Figure 15).



**Figure 5**: Assessment positions for the GCL thickness measurement marked by red arrows. At the same time, the yellow arrows indicate the positions of the CA1 and CA3 layer assessment. The figure shows an example section at Bregma – 1.64 mm (modified mbl.org).

Immunostaining of the cryostat sections

First, the cryosections were air dried at RT for 30 min. Afterward, the sections were bordered with Daco Pen and fixed with 4 % PFA for 5 min in a container. After two 5 min washes on an orbital shaker with PBS, the sections were blocked in a humid chamber for one hr. at RT. After discarding the blocking solution, the primary antibodies diluted in the blocking solution were pipetted on the sections and incubated overnight at 4 °C in the humid chamber. The next day, the slides were washed thrice for 15 minutes with PBS on an orbital shaker. Following the secondary antibodies diluted in blocking solution were applied to the sections (300 µl per well). After incubation for one hr. at RT in a darkened humid chamber, the sections were washed 3-fold for each 15 min and protected from light with PBS. A 5-min incubation followed this with DAPI/ PBS (1:10000) and two times washings with PBS under the exclusion of light. The microscope slides were mounted using the embedding medium Shandon Immu-Mount and coverslips and sealed with nail polish. Finally, the sections were stored darkened at 4 °C. The antibodies used are listed in table 4.

Investigations of histological staining

Images were taken by Leica THUNDER microscopy, an Opto-digital technology that uses the new Computational Clearing method to generate high-resolution and high-contrast images. Computational Clearing removes the typical haze inherent to all widefield images of thick samples. Images were taken as a whole scan (Overview) of each brain slice, followed by more detailed tile scans at the hippocampus region in both the Ipsilateral and contralateral hemispheres.

### 3.3.8  Gene expression analysis

The RNA required for the molecular genetic studies was extracted from the prepared trim sections using the Rneasy® Plus Universal Mini Kit (Qiagen, USA). The following steps of the qRT-PCR are the same as mentioned above in methods of chapter 1. The primers used are mentioned in table 5.

## 3.4  Statistical analysis

Microsoft Office Excel (Microsoft, USA) and GraphPad Prism (Versions 9.2.0. RRID: SCR_002798) were used for the data processing and statistical analysis. All datasets were tested for normal distribution using the Shapiro– Wilk test and QQ- plots. Datasets were tested for statistical significance with Student's t-test (for normally distributed data), or Mann–Whitney U test (MW; for not-normally distributed data), for pairwise comparisons between multiple groups, one-way ANOVA or Kruskal– Wallis tests with adequate post hoc analyses (Holm– Sidak or Dunn's correction, respectively) were used. Data are shown individually and as mean ± SEM. Tests were considered statistically significant at multiplicity-adjusted p-value   < 0.05. Significance levels are indicated by asterisks (*p <.05, **p <.01, ***p <.001, ****p <.0001).

# Chapter 4

# 4 Role of the TRPC6 channel in the hippocampal plasticity

## 4.1 Results

### 4.1.1 TRPC6 deficiency induces maturation and morphological abnormalities in the neurons of the dentate gyrus

The DG is the first region where all sensory modalities merge to form unique representations and memories that bind stimuli together. Thus, it plays a critical role in learning and memory. DG neurons and hippocampus pyramidal cells primarily express TRPC6. TRPC6 actively supports the formation of synapses and dendritic spines, enhances spatial memory, and promotes learning through its effect on the CaMKIV-CREB pathway [128]. To verify the hypothesis that TRPC6 influences neuronal maturation in the DG, immunohistochemistry was performed using brains from TRPC6 WT and KO mice. The hippocampal slices were labeled with anti-DCX (**Fig 16 a, b**), a marker for immature neurons. The data revealed that the TRPC6 KO mice have a significantly higher number of DCX+ cells in the DG GCL than the WT animals (**Fig 16 e**). Interestingly, the morphological analysis showed a significantly increased dendritic length in KO mice compared to WT mice. TRPC6 actively participates in the formation of excitatory synapses and manifests its expression on GABAergic interneurons.[129] The hypothesis being tested in this experiment is likely related to the role of TRPC6 in the formation or maintenance of glutamatergic axon terminals (as indicated by the use of the anti-VGLUT2 marker) and GABAergic interneurons (as characterized by the use of the anti-parvalbumin marker) (**Fig 16 a, k**). The results show a trend towards a decreased number of glutamatergic synapses reaching out to the dendrites of DCX+ cells of the KO mice compared to the WT. However, this difference did not reach a statistically significant level. Moreover, The number of Parvalbumin+ interneurons was not distinguishable between the different genotypes (**Fig 16 g, s**). Nevertheless, this data suggests that the immature granular cells of the KO may have less excitatory input. To confirm the immature phenotype of the DG in the TRPC6 KO mice, the slices were labeled with anti-CB, a marker of mature neurons (**Fig 16 h, l**). Counts of CB+ neurons in the GCL resulted in a significantly decreased number of KO compared to WT (**Fig 16 m**). A substantial dispersion of mature cells was noted along with the low

cell count (**Fig 17 j, n**). A noteworthy reduction of cells in the CA1 region was observed, accompanied by a similar trend of cell loss in the CA3 region. (**Fig 17 t, u**). The combined results indicate an abnormal maturation of the hippocampus in TRPC6 KO mice, a phenomenon that resembles the immature hippocampus seen in several neurodegenerative and psychiatric disorders.[130]
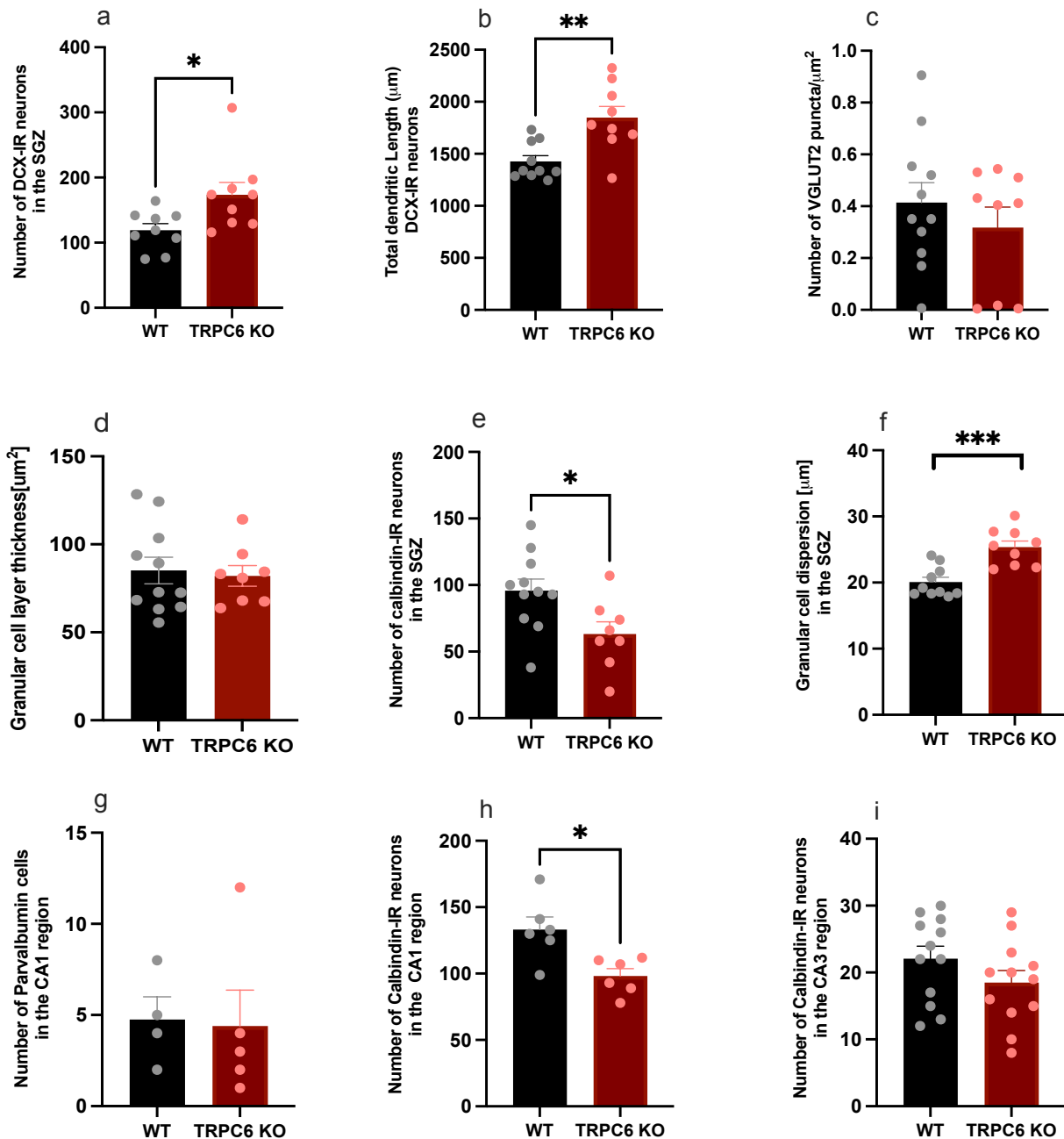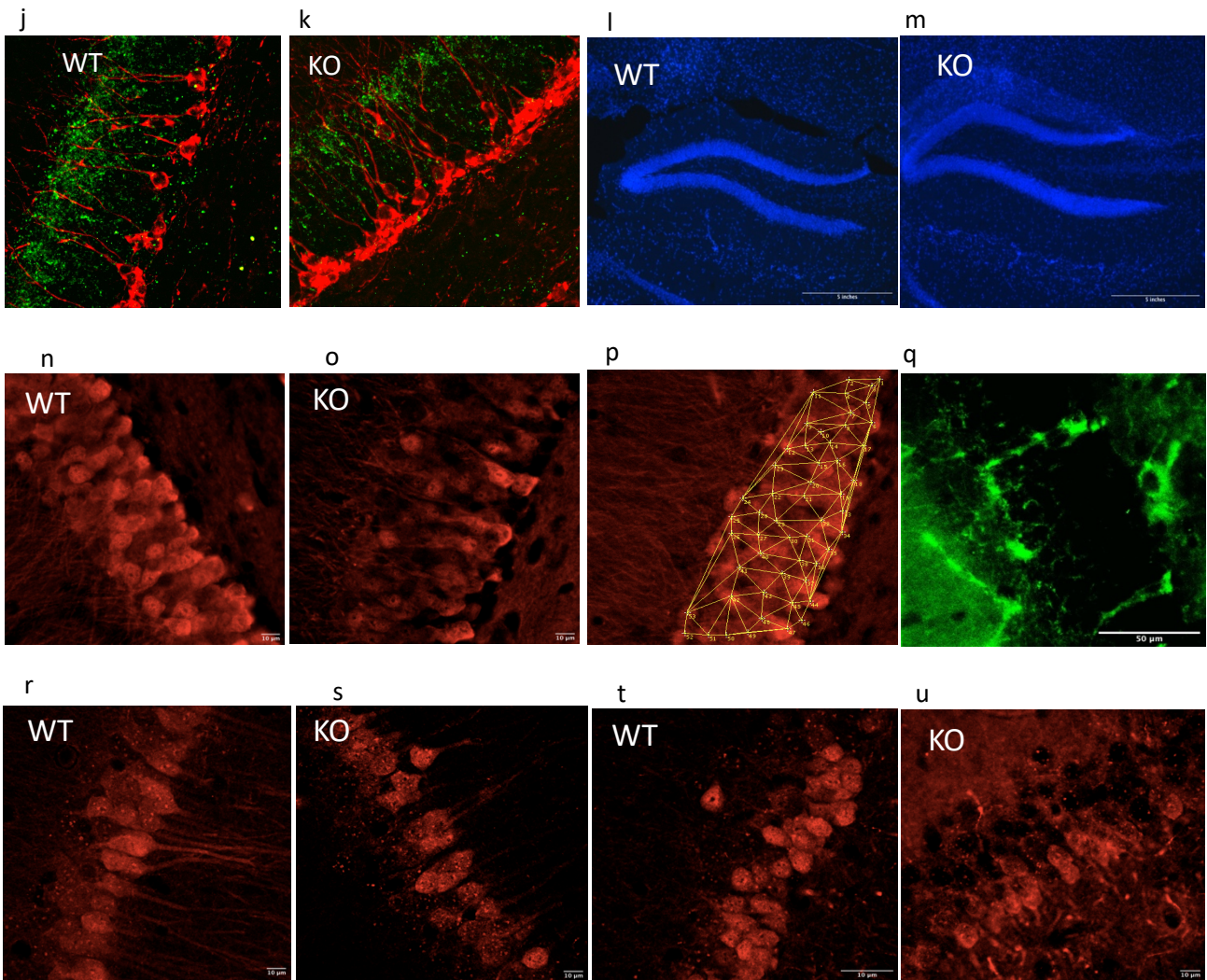
**Figure 6. TRPC6 deficiency induces maturation and morphological abnormalities in the neurons of the DG**. (**a, b**) (DCX, red) labeled immature neurons positioned in the SGZ, showing an increased number of DCX+ neurons with longer dendritic branches in the mutant mice compared to their WT counterparts. VGLUT 2 (green) labeling shows no difference in the amount of the VGLUT 2 puncta on the dendrites of the DCX+ neurons between mutants and WTs. (**e, f, g**) quantitative representations for the number of DCX+ cells, dendritic length, and VGLUT 2 revealed a significant increase in the number of immature granular cells and their dendritic length in the TRPC6 KO compared to the WT mice. (**c, d**) representative images of the DG of WT and TRPC6 KO taken by fluorescent microscope showing no difference in the thickness of the GCL of the mutants compared to WT. The quantification of thickness measurements is represented in graph (**l**). (**h, i**) Immunohistochemical illustration of CB labeling mature granular cells in the DG, showing less labeling in the mutant's GCL compared to the WT counterparts with observed dispersion using the Delaunay Voronoi method of analysis(**j**), the quantification of the number of CB+ neurons reveal a significantly low number in KO with high dispersion (**m, n**). (**k**) anti-Parvalbumin (green), labeled GABAergic

interneurons in the DG region of the TRPC6 KO, the visual counting failed to show a significant difference between the two genotypes, represented in a graph (**s**). (**o, p**) Confocal images showing mature pyramidal cells CB+, in the WT and KO, a significantly lower number of pyramidal cells in the mutants compared to the WT was detected after quantification in the graph (**t**). (**k, l**) shows the CB+ neurons In the CA3 region of WT and KO. Quantification indicates no significant difference between mutants and WTs in graph (**u**).12 adult mice with equal sex (12-15 weeks old) / group. A total of 3 images per slice and 3 slices per animal were analyzed for quantification. Data are shown individually and as mean ± SEM. Student t-test was used for calculating significance, adjusted p-value < 0.05. Significance levels are indicated by asterisks (*p <.05, **p <.01, ***p <.001, ****p <.0001).

### 4.1.2  TRPC6 deficiency altered the expression of genes responsible for cell survival and neuronal plasticity.

Next, The gene expression and protein phosphorylation of essential molecules for neuronal proliferation, survival, and plasticity were examined. It has been shown that TRPC6 activation by hyperforin leads to the activation of the PI3K/Akt pathway, which is a crucial regulator for neuritic outgrowth in hippocampal neurons[131]. The expression of the AKT gene was evaluated in the hippocampus and cortex of the TRPC6 KO mouse model (**Fig 17 a**). The data showed no difference in the gene expression of AKT between the KO and WT mice. Western blot assays were performed to assess the phosphorylation of the protein (**Fig 17 b, g**), which revealed that it was much lower in the hippocampus and slightly more likely in the cortex of the mutant mice compared to WTs.

Further, The mRNA expression levels of the CREB gene, a cAMP-response-element binding protein, and transcription factor that regulates development and plasticity were characterized.[132] In hippocampal cultures, it was shown that overexpressing TRPC6 increased the phosphorylation of $Ca^{2+}$/calmodulin-dependent kinase IV (CaMKIV) and (CREB) and accelerated dendritic development and vice versa. [133] In our KO mouse model, the data reveals that the mRNA levels and protein phosphorylation of CREB were significantly reduced in the hippocampus (**Fig 17 c**). In line with these findings, there was a significant reduction in CREB protein phosphorylation in the hippocampus compared to WT. At the same time, surprisingly, the cortex showed a considerable rise in its phosphorylation (**Fig 17 d, h**). Then it was necessary to check for mTOR gene expression and phosphorylation levels. The

TRPC6 gene is crucial in starting the mTOR signaling process. [134] Our study found that deleting the TRPC6 gene in mice (TRPC6 KO) resulted in a noticeable decrease in mTOR expression and a reduction of its phosphorylation levels in the hippocampus compared to normal mice (WT). (**Fig 17 e, f, i**). In conclusion, deleting the TRPC6 gene in mice decreased expression and phosphorylation levels of key molecules involved in neuronal proliferation, survival, and plasticity, including mTOR, CREB, and AKT. These findings suggest that TRPC6 plays a vital role in regulating these processes.
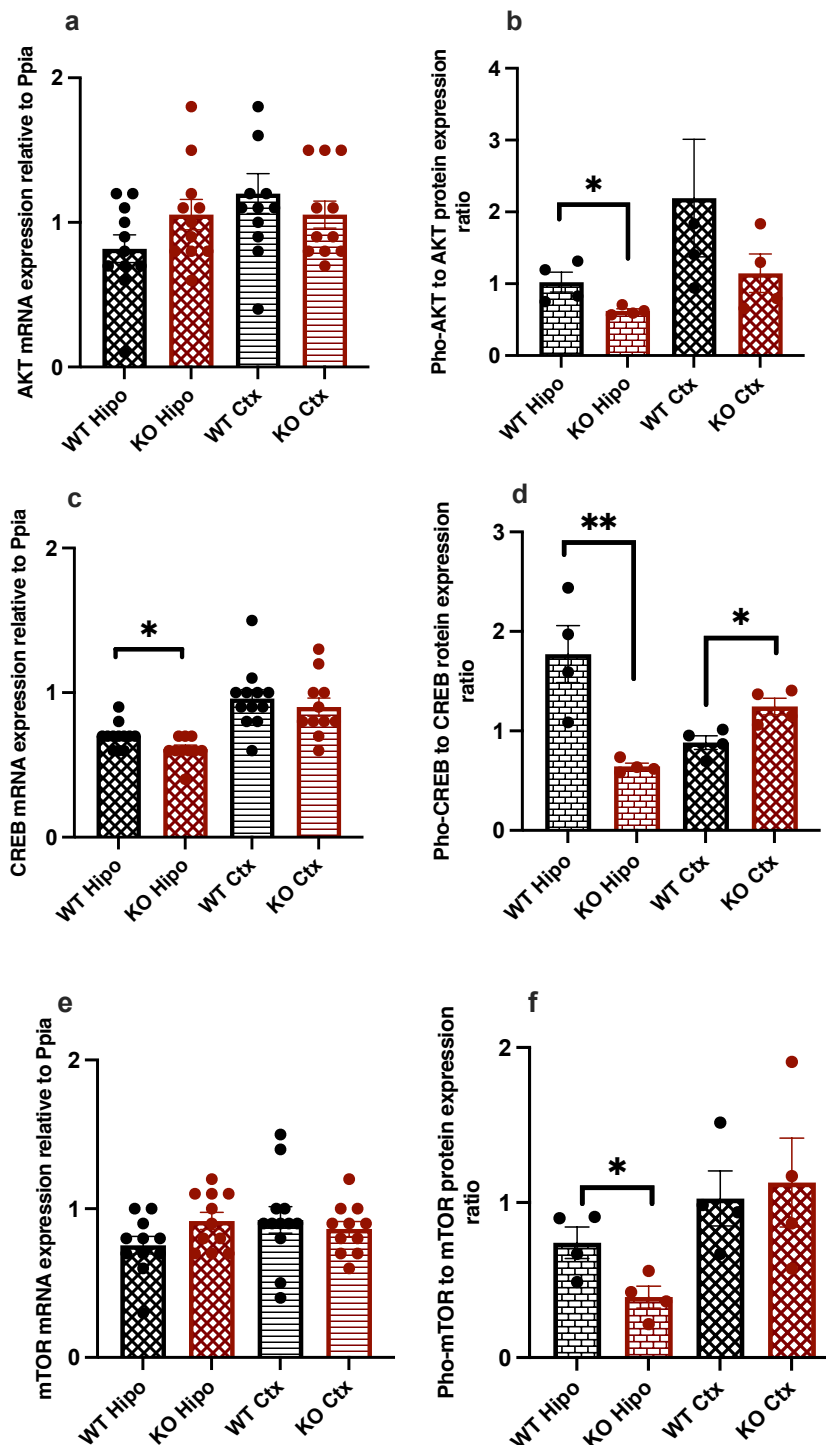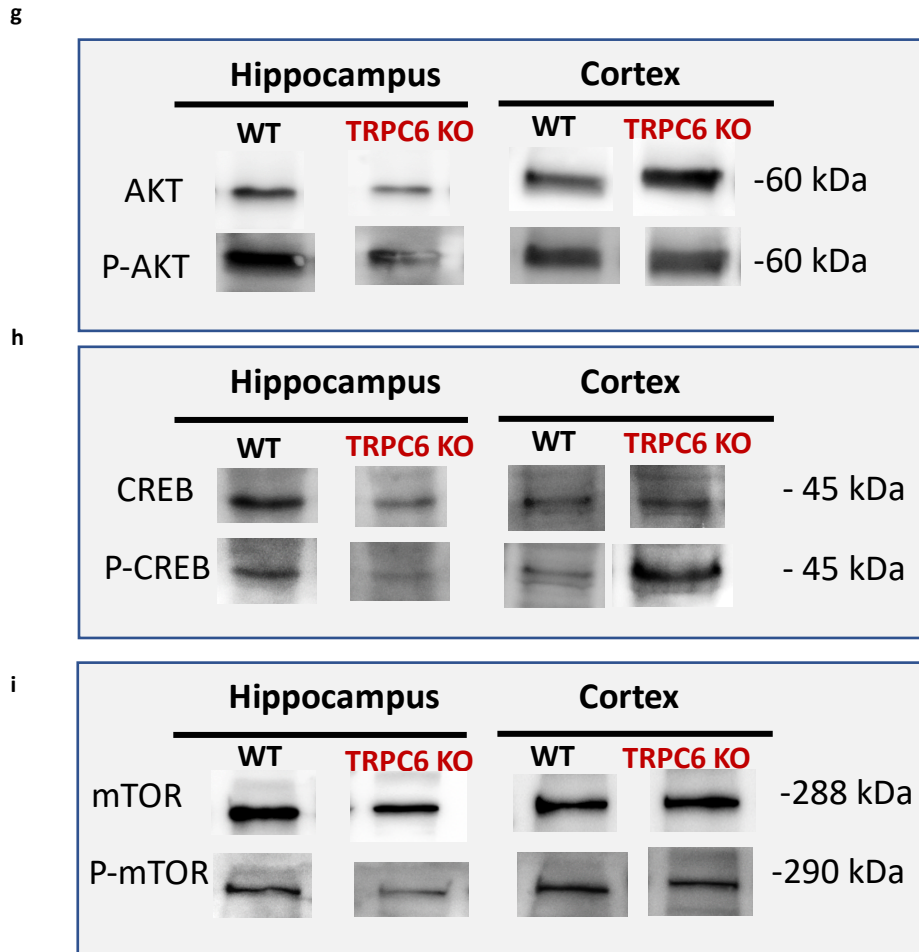
**Figure 7. TRPC6 deficiency altered the expression of genes responsible for cell survival and neuronal plasticity**. Gene expression and protein phosphorylation analyses in the hippocampus and cortex of the TRPC6 knockout mice normalized to Ppia and WT (n=12/group). (**a**) AKT (protein kinase B or Pkb) shows no gene expression differences in the hippocampus and cortex of TRPC6 KO or WT mice. (**b**) Quantification of its phosphorylated protein shows a significant decrease in the hippocampus of the mutant mice but not in the cortex compared to WT. (**c**) Gene expression of CREB was significantly decreased in the hippocampus of TRPC6 KO mice compared to the WT counterparts. (**d**) Similar results were obtained for the phosphorylation of its protein in the hippocampus of the KO mice; however, the phosphorylation was significantly increased in their cortex. (**e**) Gene expression of mTOR shows no significant difference between the different genotypes, (**f**) quantification of phosphorylated mTOR in the hippocampus shows. Significant decrease in the KO mice compared to the WT. (**g, h, i**) The total lysates of both hippocampus and cortex of TRPC6 KO and WT animals (n=4 per group) were blotted with antibodies to phosphorylated AKT, CREB, and mTOR or total CREB, AKT, and mTOR. Using B-actin as a reference protein. Values

represent mean ± SEM; pairwise comparisons were done using one-way ANOVA (*p<0.05, **P<0.00).

### 4.1.3  <u>TRPC6 knockout results in hippocampal hypo-excitability</u>

Coding and retrieving information and spatial navigation are critical cognitive processes that depend on hippocampus formation.[135] TRPC6 expression in the hippocampus aids in developing excitatory synapses.[128] This electrophysiology experiment aims to gain a deeper understanding of the potential role of TRPC6 in neuronal function and connectivity by examining the electrophysiological characteristics of GCs in the upper blade of the DG. This examination utilized the whole cell in the current clamp mode to evaluate the excitability of neurons in acute hippocampal slices from adult TRPC6 KO and WT mice (aged > 15 weeks). The input resistance was similar in both genotypes (WT, n=26; KO, n=17, mean= 240 + s.e.m 20,07 - 28,88). The range between 100-300 MΩ indicates that all the cells investigated were mature, as the input resistance is known to be related to cell maturation (**Fig 18 b**). [136] The cellular firing properties were examined by inducing action potentials by injecting hyper- and depolarizing currents of varying magnitudes, resulting in the generation of trains of action potentials. The example voltage traces in (**Fig 18 a**) indicate that genetic loss of TRPC6 decreased the firing propensity, which resulted in a significantly smaller number of AP firing per stimulus (**Fig 18 c**) and an aberrant firing frequency (**Fig 18 d**) relative to the WT neurons.  The same protocol was conducted on hippocampal slices from developing mice with an age range of 3 to 4 weeks to determine whether the changes in firing properties are related to genotype or age. The input resistance results indicated that the granular cells patched at the upper blade of the DG displayed a mature phenotype (**Fig 18 e**). Nevertheless, an impaired firing rate of action potentials and a reduction in the number of spikes were observed in the KO neurons compared to WT (**Fig 18 f, g**). Finally, a phase blot analysis used to determine the maturity of action potential revealed no difference in action potential maturation between WT and KOs (**Fig 18 h**). In conclusion, the results indicate that TRPC6 deletion leads to a state of hypoexcitability of GCs in adult and developing KO mice.
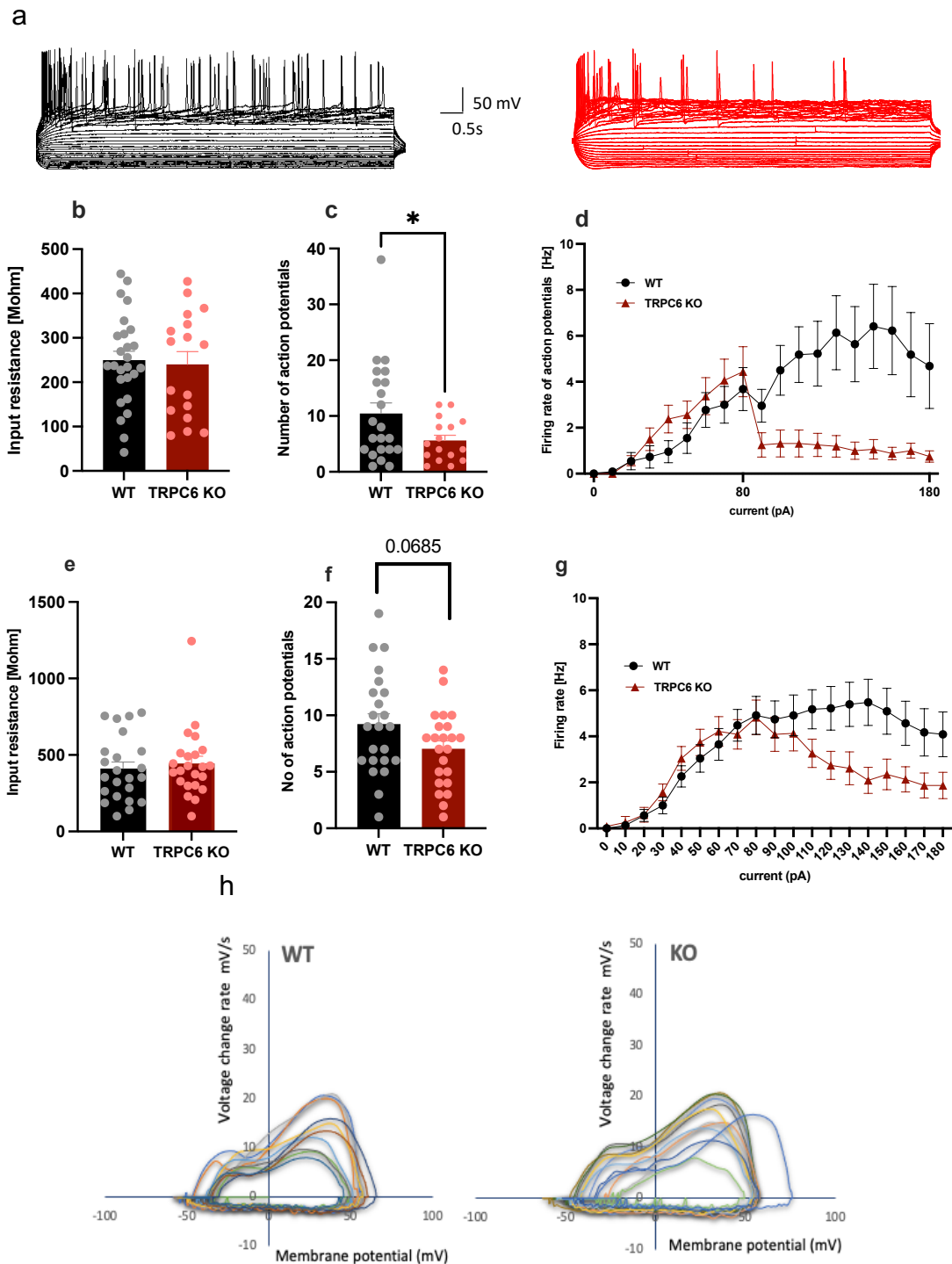
**Figure *8*. TRPC6 knockout resulted in hippocampal hypo-excitability in adult mice**. (**a**) Representative voltage responses of granular cells to 300ms stepwise current injections, WT represented in black, KO in red. (**b**) bar graph of Rinput in the granular cells of both WT(n=26) and TRPC6 KO (n=17) mice (age 15-20 W), the Rinput ranges between 100-300 megaohm in both genotypes. (**c**) bar graph representing the number of action potentials evoked, indicating significantly less number in the KO mice than WT. (**d**) graphs showing decreased KO mice

firing rate (frequency). (**e**) bar graph of Rinput in the granular cells of both WT(n=22) and TRPC6 KO (n=23) mice (age 3-4 Weeks), the Rinput ranges below 1000 megaohm in both genotypes, indicating mature phenotype of cells (**f**) bar graph representing the number of action potentials evoked, indicating less number in the KO mice compared to WT with P value=0.0685. (**g**) graph showing decreased firing rate (frequency) of KO mice. Values represent mean ± SEM; pairwise comparisons were done using students' t-tests (**h**) phase plots of action potentials of cells in the examined groups; each trace represents one cell. Values represent mean ± SEM; pairwise comparisons were done using students' t-tests (*p<0.05, **P<0.001).

### 4.1.4  Characterization of the spontaneous synaptic transmission in the dentate gyrus of TRPC6 KO mice

The synaptic excitatory drive of these granular cells was next examined. To this end, we measured spontaneous excitatory postsynaptic currents (sEPSC) in adult mice in voltage-clamp mode to assess the excitatory synaptic inputs. sEPSC amplitude was significantly lower in KO mice, while the inter-event interval remained unaltered in both genotypes (**Fig 19b, c).** The experiment continued by measuring synaptic excitatory drive in developing mice by examining sEPSCs and mEPSCs. The results showed that the amplitude of sEPSCs and the time between events was lower in neurons from mice without TRPC6 (**Fig 19b, c**). In addition to altered postsynaptic receptors, kinetics was represented by changes in the rise and decay time (**Fig 19d, e**). To isolate miniature EPSCs, TTX and GABAzine were bath-applied to block voltage-dependent sodium channels and GABA A receptors, respectively. Further, D-APV was added to the bath perfusate to blockade the contribution of NMDA receptors, allowing the isolation of AMPA receptor-mediated mEPSC. The responsiveness of the postsynaptic cells was measured by analyzing the peak amplitude of mEPSCs. It was found to be significantly lower in KO compared to WT mice (**Fig 20f**), which can be an indication of fewer AMPA receptors expression on the postsynaptic membrane. The miniature interevent intervals (frequency) (**Fig 20g**) were significantly increased in the TRPC6 mutant mice, possibly due to reduced numbers of synapses or a reduced release probability. The rise and decay time of mEPSC was unchanged between genotypes (**Fig 20i, j**). Taken together, reduced excitability of the DG GCs at both ages with changes in the postsynaptic receptors' kinetics indicates that TRPC6 is essential for obtaining a normal synaptic function during and after development.
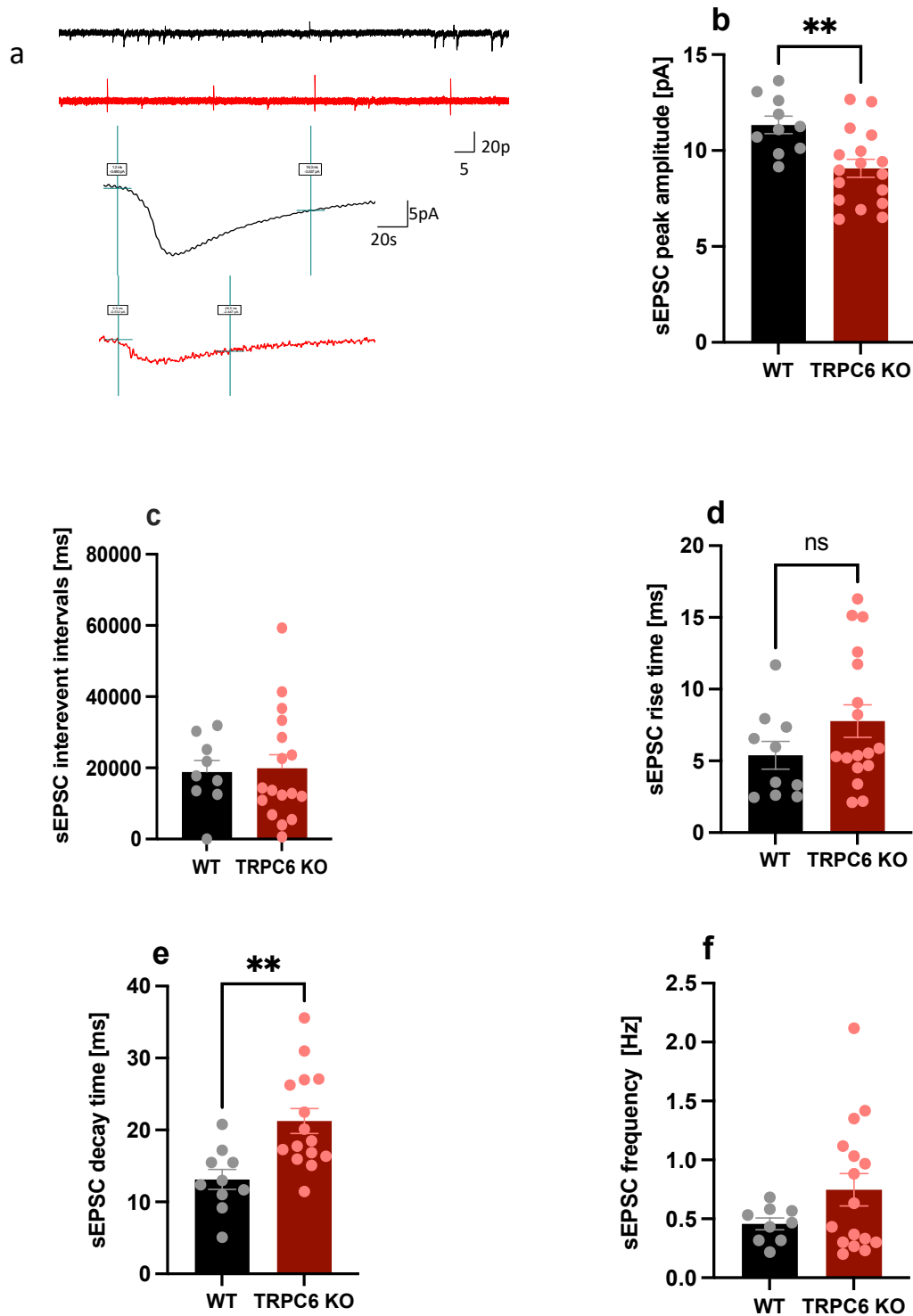
**Figure *9*. TRPC6 depletion changed the synaptic excitatory drive of granular cells of adult mice**. WT(n=26) and TRPC6 KO (n=17) mice (age15-20 W),n representing the number of cells (**a**) Representative traces of sEPSC input (recorded at -70 mV) on to GCs and the average of events traces of both genotypes. WT in black and KO in red. (**b**) bar graph

representing sEPSC peak amplitude bar graph showing significant reduction in peak amplitude of KO events compared to WT. (**c**) bar graph of Interevent intervals. (**d, e**) rise and decay time of peaks. Values represent mean ± SEM; pairwise comparisons were done using students' t-tests (*p<0.05, **P<0.001).
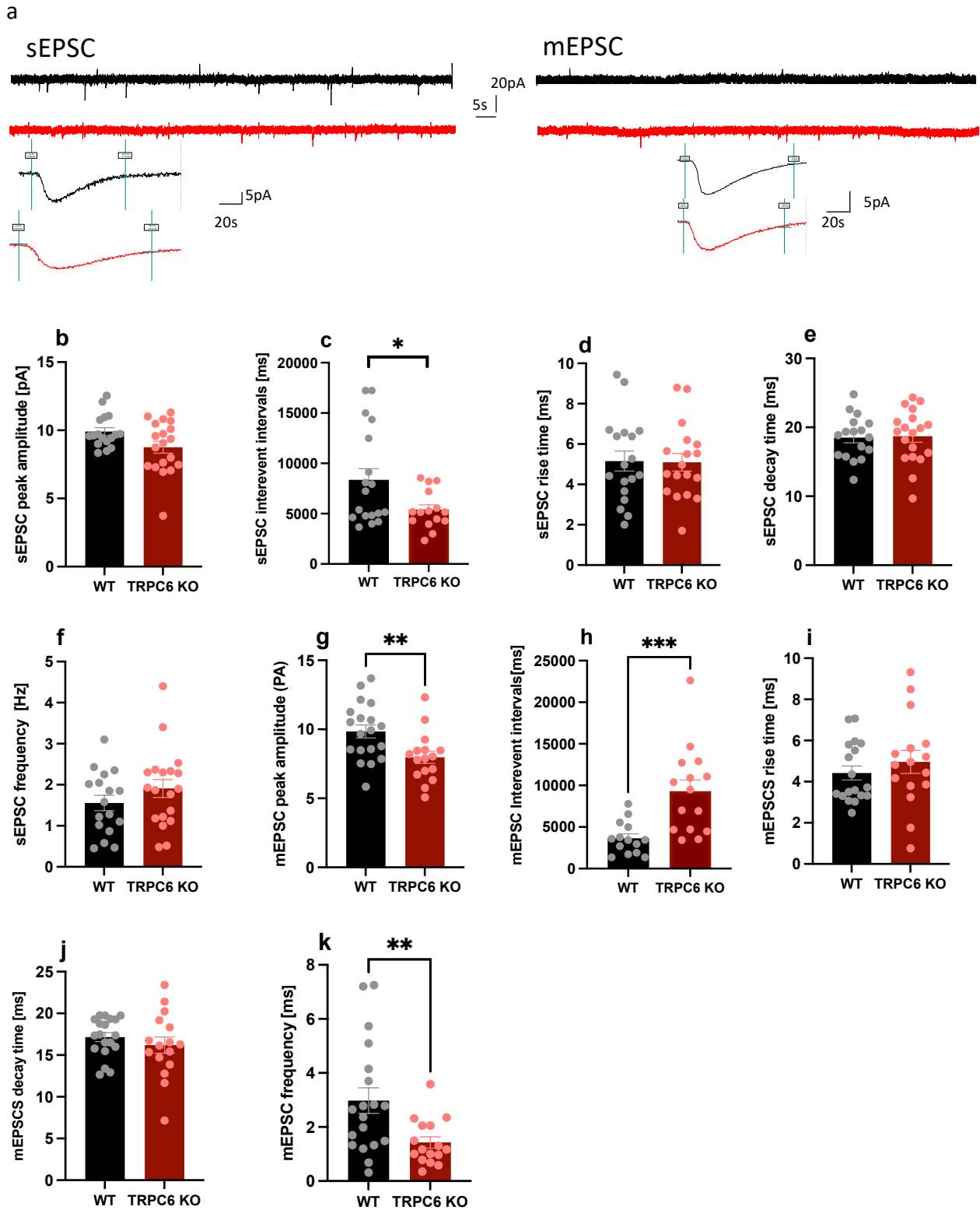
**Figure *10*. TRPC6 depletion changed the synaptic excitatory drive of granular cells of developing mice**. (**a**) Representative traces of sEPSC input (recorded at -70 mV) onto GCs and the average of events traces of both genotypes. WT in black and KO in red. WT(n=20), KO( n=18). (**b**) bar graph representing sEPSC peak amplitude showing significant reduction in KO mice. (**c**) bar graph showing a significant reduction in interevent intervals of KO events compared to WT. (**d**) bar graph representing the reduction in the rise time of KO neurons compared to WT with a p-value of 0.0656. (**e**) bar graph showing a significant increase in the decay time of KO compared to WT. (**f**) bar graph of miniatures peak amplitude representing a significant reduction in the KO. (**g**) bar graph of miniatures interevent intervals showing a significant increase of events of KO neurons compared to WT. (**h, i**) bar graphs of miniatures' rise and decay time with a significant reduction of both in the KO neurons.

### 4.1.5  TRPC6 knockout mice failed to induce long-term potentiation

For the hippocampal memory to work, synaptic responses must undergo LTP. Associative memories, regarded as the neuronal correlates of memory engrams, are formed partly via the PP synapses on hippocampal GCs. Two excitatory input pathways, the MPP and the LPP synapse onto the dendrites of dentate GCs. LTP of the MPP input to DG cells can be explained by an increase in the postsynaptic response to the transmitter; it is blocked by NMDA receptor antagonists or by injecting $Ca^{2+}$ chelating agents into the postsynaptic cell.[137]

Upon stimulating MPP (**Fig 21a**), the LTP induction was abolished in the TRPC6 KO compared to WT (**Fig 21b**). The induction of LTP in MPP synapses led to LTD  in synapses of the non-induced LPP pathway of the WT but not in the KO. A recent study that examined morphological changes within the middle third of the molecular layer reported an increase in spine frequency after delta burst stimulation (400 Hz patterned stimulation) that also induced robust LTP. [138] Interestingly, this effect was counterbalanced by a shrinking of other spines, such that the net synaptic area of the granule cell dendrites was unchanged.[138] This could be mediated by heterosynaptic plasticity. However, another possibility is that LPP-mediated effects promoted synaptic depression and shrinking in a population of synapses, while MPP activity promoted synaptic expansion. Since synapses may initially change and become dysfunctional because of TRPC6 depletion, the synapses in the KO mice were already severely impacted and could not deteriorate further. [139]

a



b
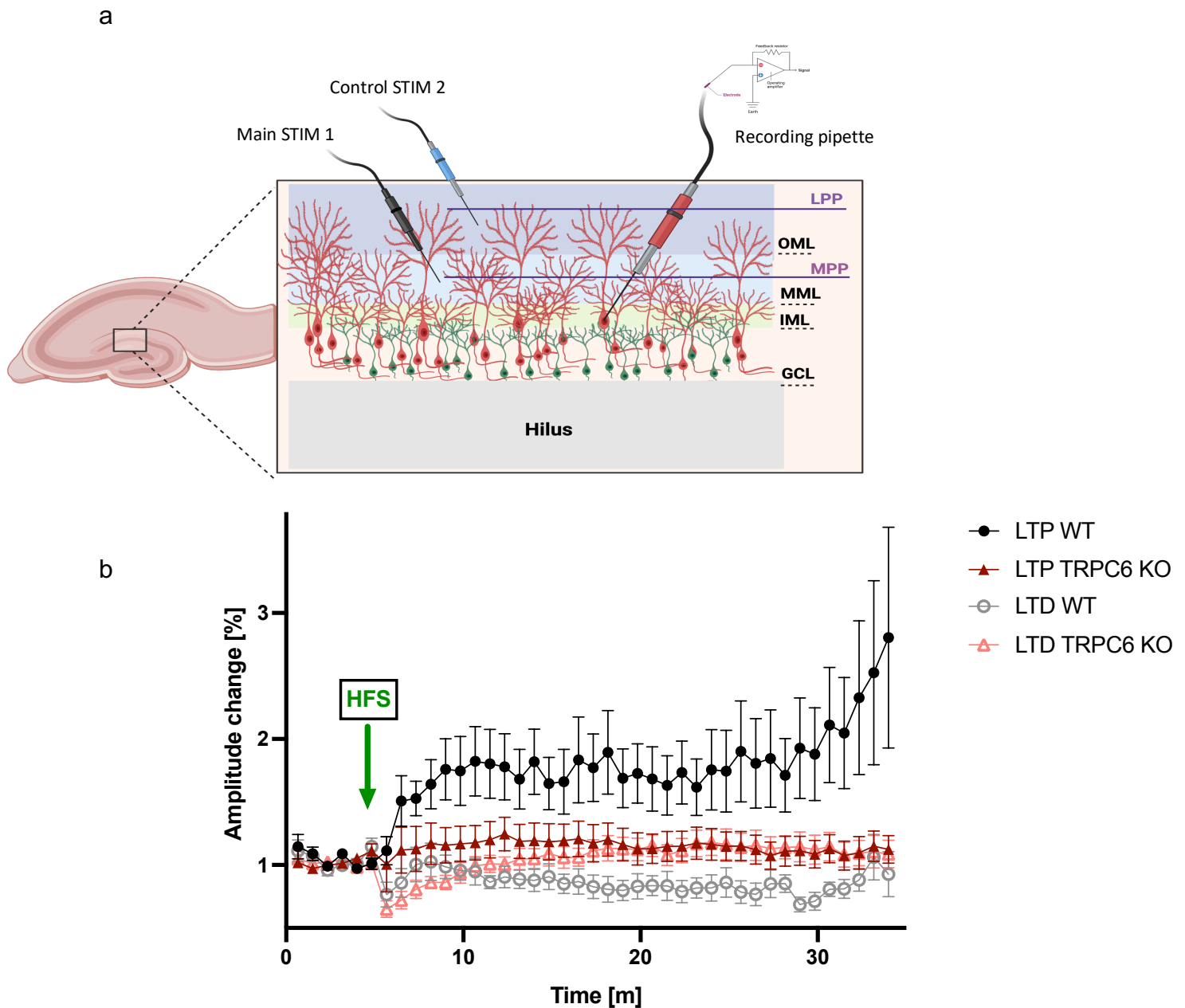


**Figure 11***: **TRPC6 knockout mice failed to induce long-term potentiation.** (**a**) Schematic overview that illustrates the recording situation with stimulation and recording pipettes. LTP of synaptic currents is abolished in TRPC6 KO mice compared to WT. (**b**) LTP was induced in MPP synapses with a low-frequency pairing protocol together with Heterosynaptic LTD of the noninduced LPP pathway in WT and TRPC6 KO.

## 4.2 Discussion

This compelling research project explored the impact of TRPC6 on the development and plasticity of the hippocampus. The results revealed some surprising discoveries about the importance of TRPC6 in the brain. My study reports that when TRPC6 is deleted in mice, several significant changes are observed in the hippocampus, including a decrease in mature neurons, an upsurge in immature granule cells, and a trend toward a decreased number of glutamatergic synapses. One likely mechanism is the observed decrease in gene expression and phosphorylation of AKT, CREB, and mTOR in the hippocampus, which are crucial for normal neuronal function and connectivity, indicating that TRPC6 regulates signaling pathways critical for neuronal survival and plasticity. Furthermore, TRPC6 KO mice showed a decrease in the excitability of mature granular cells, with fewer action potentials firing per stimulus and a reduced firing frequency besides alterations in synaptic function, including a lower sEPSC amplitude and altered kinetics of postsynaptic receptors. Finally, the study demonstrated that the induction of long-term potentiation in the medial perforant path synapses was abolished after TRPC6 deletion. These findings prove that TRPC6 plays a crucial role in the proper maturation and function of the hippocampus.

In the literature, the direct relation between TRPC6 and hippocampal neurogenesis and neuronal maturation was not investigated in the TRPC6 KO mice. However, TRPC6 downregulation was a common factor in many neurodegenerative diseases where neurogenesis and neuronal maturation impairment is a hallmark. These neurodegenerative diseases include AD and epilepsy. [140]

A thorough examination of the hippocampus of these diseases' mouse models revealed a common, conserved motif within each, now known as an 'immature dentate gyrus' (iDG). Animals with an iDG have higher levels of immature neuronal markers (such as doublecortin and calretinin) and lower levels of mature neuronal markers, most notably calbindin. Elevated neurogenesis is a secondary feature of iDG mice present in most iDG mouse lines. [141]

My study revealed that TRPC6 KO mice share the same characteristics as the models mentioned above; TRPC6 KO DG had remarkably high doublecortin and low calbindin expression, manifested by high and low cell counts.

One exciting explanation for the iDG was published by Hagihara et al. in 2019. In this article, mature neurons re-express the molecular markers of neural progenitor cells and immature neurons after differentiating to a pseudo-immature state. The indicators for neural progenitor cells and immature neurons may not always function as markers for adult hippocampal neurogenesis since a variety of circumstances, such as inflammation and hyper-excitation of neurons, can easily cause dematuration.[142]

Another explanation published by Mendez-David et al. found that DCX expression is regulated non-linearly compared to adult hippocampal neurogenesis levels. They demonstrated in this study that fluoxetine, an antidepressant, accelerates the maturation of young neurons by hastening the transition from the DCX positive stage to the NeuN/mature, positive stage via B-arrestin 2 (which operates downstream of many G-protein coupled receptors).[143] And in B-arrestin knockout mice, this transition did not occur, resulting in an accumulation of DCX in the young neurons.

TRPC6 KO mice may have increased neurogenesis compared to WT, or their newly emerged neurons are trapped in an immature state. However, the limitations of my study should be reported. First, after remarking the increase in DCX and decrease in CB-expressing granule cells, a marker for neurogenesis as BrdU+ (which is incorporated into the newly synthesized DNA strand of proliferating cells and can be used as a cytogenetic marker during the neonatal period (postnatal days 1–3), should have been used to check if the rate of neurogenesis is consistent with these changes. Second, DCX+ cells' relative position should have been considered if it is shifted from the subgranular zone to the middle or outer GCL, as the shifting of work is proof of the dematuration of neurons.[142]

The present study did not address the link between TRPC6 KO and neurodegenerative diseases. However, examining them in the TRPC6 KO model would be interesting to see whether TRPC6 loss is the reason behind the iDG phenotype.

CB is a primary $Ca^{2+}$ buffer of mature GCs in the hippocampus's DG and a potential eliminator of intracellular calcium when the cell is overloaded, as in neuronal injuries.[144] According to research using CB-deficient animals, CB is crucial for  LTP and synaptic consolidation of hippocampus memory. The expression of CB by GCs and their axons during postnatal development coincides with the functional maturation of the DG and behavioral maturation of rats, providing more evidence for the potential role of CB in memory formation.[145]

Besides low CB immunoreactivity, further analysis for the GCL using the Voronoi method, my data shows significant high dispersion between the mature neurons of the DG of the TRPC6 KO mice compared to wildtypes.

Granular cell dispersion (GCD) is a histological characteristic observed in the dentate gyri of individuals with chronic epilepsy. Animal models of epilepsy showed several types of dispersed GC layers, which are assumed to be replicative of the pathophysiology experienced by epileptic patients and similar to the brains of humans with the condition. There have been several different GCD overlapping patterns identified. Among these are segmental broadening and duplication, often known as "tram-tracking," of the GC layer, as well as localized distributed clusters of GCs that are ectopically present in either the hilus or molecular DG layer. [146]

It would be interesting to conduct additional studies to determine the type of GCD present in our TRPC6 KO model. All data considered, as TRPC6 affects $Ca^{2+}$ signaling-dependent mechanisms and neuronal transcriptional regulation, this may suggest that TRPC6 deletion either results in the death of mature neurons or the lowering of CB expression levels due to impaired calcium homeostasis in the hippocampus.[147]

Because TRPC6 is expressed in GABAergic interneurons and plays a crucial role in forming excitatory synapses. [128] Anti-VGLUT2, a good marker for glutamatergic axon terminals, and anti-parvalbumin, a marker for GABAergic interneurons, were used to check if any changes occurred due to TRPC6 deletion. The data revealed a reduction tendency in the VGLUT2 puncta density, which indicates fewer glutamatergic axons reaching out to the dendrites of DCX+ cells of the KO mice. These observations showed no change in the number of parvalbumin+ interneurons in the hippocampus.

My findings agree with a study from Griesi-Oliveira et al. showing that TRPC6 expression levels can modulate glutamatergic synapse formation in rat neurons and that a reduction of VGLUT-1 puncta density is a phenomenon observed in patients with neuropsychiatric disorders as autism.[148] Since TRPC6 proteins are highly expressed during the dendritic growth phase, they are involved in synaptic plasticity changes ranging from dendritic growth, spine morphology changes, and an increase in excitatory synapses.[133] Further morphological analysis on the dendrites of the immature DCX+ neurons was conducted. Surprisingly, longer dendritic branches were found in the KO compared to WT. This explains that in our TRPC6 KO model, the

longer dendrites of DCX+ cells are a compensatory mechanism for the loss of the spines, which means the dendrites were growing longer, reaching out for synaptic connections.

Numerous data showed that specific TRPC6 silencing reduced dendritic spine densities of mature neurons in hippocampal cultures. Zhou et al. demonstrated that TRPC6 was crucial in forming dendritic spines and excitatory synapses in vitro and in vivo and was mostly confined to excitatory postsynaptic locations. TRPC6 could be a key mediator for detecting the extracellular signals that influence synaptic and behavioral plasticity, as neurotrophic factors are essential for spine development, plasticity, and memory. [149]

Notably, the effect of TRPC6 on spine formation depends on the CaMKIV-CREB-pathway. Moreover, TRPC6 silencing also eliminated BDNF's effect on spine formation. [133.] For that reason, An extensive examination was carried out to delve deeper into the connection between TRPC6 and crucial targets for neuronal proliferation, survival, and plasticity, in the hippocampus. The targets in question were CREB, AKT, and mTOR. The findings revealed a substantial reduction in both the gene expression of CREB and the protein phosphorylation levels of CREB, AKT, and mTOR in the hippocampus of the KO mice compared to the control group of WT mice.

My findings are reinforced by a study by Heiser et al. presenting findings into the signaling cascade of TRPC6-mediated neuritic outgrowth in PC12 cells and primary hippocampal neurons. They revealed that the TRPC6 activator hyperforin activates three signal cascades downstream of calcium that culminate in CREB phosphorylation: Ras/MEK/ERK, PI3K/Akt, and CAMKIV. These pathways are required for TRPC6-mediated changes in synaptic plasticity in PC12 cells and primary hippocampal neurons.[150] It is noteworthy that Phosphorylated CREB was lower in the brains of AD patients and in vitro neurons treated with Aβ. Furthermore, it has been discovered that Aβ's effect on hippocampal synaptic loss, synaptic plasticity impairment, and memory deficit is mediated by changes in cAMP/PKA-dependent CREB signaling.[151]

Another study by A. Fortin et al. suggests that TRPC channels activate mTOR-dependent translation of GluA1 subunits by activating the CaMKK/AKT signaling pathway. And this was the first study to link TRPC channels to mTOR-dependent translation.[152]

Surprisingly, there was a tendency towards high mRNA expression levels of both Akt and mTOR in the hippocampus of the KO mice. mTOR-regulated neuron processes influence higher physiological functions such as neuronal excitability, survival, synaptic plasticity, and cognition. Any disruption in mTOR expression or mutations in genes coding for proteins involved in mTOR pathways results in brain diseases such as depression. [153] A large body of evidence from animal and human studies supports the role of mTOR and mTOR pathways in epilepsy. Following epilepsy, the level of mTOR in the hippocampus increases. Furthermore, a close relationship has been reported between mTOR activation and specific histological and pathological abnormalities in epileptic patients. [154]

This data provides another exciting link between TRPC6 deletion and epilepsy and AD pathogenesis. However, the tendency of higher expression of mTOR in the KO might be a compensatory mechanism for the low phosphorylation of its protein in the hippocampus.

One characteristic of the iDG phenomena is the hyperexcitability of the granule cells.[130] On the contrary, the TRPC6 KO hippocampus exhibits a state of hypoexcitability. My electrophysiological data shows that mature granular cells from TRPC6 KO mice inhibit significantly reduced excitability, which was demonstrated as a reduction in the firing propensity, low number of action potentials, and reduced firing frequency compared with the WT. These changes in active and passive membrane properties indicate complex alterations of functional connectivity and, potentially, morphological properties of these granular cells. The data obtained was regardless of the animal's sex or age, as both the four months old TRPC6 KO mice had the same hypo-excitability as the 1-month-old.

A study by El Hamdaoui et al. supports my findings; hence they reported that TRPC6 knockout mice have significantly reduced cell excitability in DG cells and CA1 pyramidal cells. In this study, hyperforin increased excitability in DG neurons in WT mice. This effect, as well as the hyperforin-induced inward current, was abolished in TRPC6 knockout mice. Because the hyperforin-induced delayed potassium-mediated current persists in TRPC6 KO mice, which could be an independent mechanism of action. [155] Moreover, Griesi- Oliveira et al. obtained similar results using shRNA to downregulate TRPC6 in mouse primary neurons.[148]

Additional data from Jerome Mertens et al. showed that whole-cell recordings of APs revealed that neurons expressing shRNAs against TRPC6 had a significantly lower firing rate than controls. Notably, abnormal AP firing in response to membrane depolarization has also been observed in DG-like neurons derived from iPSCs from bipolar disorder patients.[156]

The axon initial segment (AIS) is a specialized structure that initiates action potentials and maintains neuronal polarity. High-density sodium channels and potassium and calcium channels are required for action potential initiation at the AIS. Neuronal density is reduced in some pathological conditions due to cell loss and altered neuronal activity and neurotransmission. Previous research has shown that neuronal activity plays a vital role in the structural plasticity of the AIS. The activation of calcineurin and the opening of voltage-gated calcium channels play essential roles in relocating or shortening the AIS. And hence causing hypoexcitability of neurons.[157]

There is no established direct relationship between TRPC6 and the AIS. However, TRPC6 activates the calcineurin enzyme.[158] The observed hypoexcitability in the hippocampus of TRPC6 KO mice could be attributed to reduced calcineurin expression, which results from the absence of TRPC6. Further studies are required to fully characterize the expression levels of calcium-binding proteins in TRPC6 KO mice in relation to the AIS and neuronal excitability.

An additional explanation for the reduced excitability in TRPC6 KO mice may be associated with changes in NMDA receptors. The NMDA receptor subunits are expressed in the same brain areas as TRPC6, suggesting possible crosstalk between them. Shen et al. reported that TRPC6 inhibited the NMDA-induced current significantly in cultured hippocampal neurons. Nevertheless, it did not affect the current mediated by other ionotropic glutamate receptor subtypes, such as the AMPA glutamate receptor.[158] The researchers in this study proposed two possible mechanisms by which TRPC6 could inhibit the NMDA current. TRPC6 may directly regulate NMDA receptors through interactions with its subunits, or TRPC6 may affect the phosphorylation state of NMDA receptor subunits. The lack of TRPC6 expression in the KO mice presents a scenario where the NMDA receptors may exhibit heightened excitability. However, it is necessary to note that the hypoexcitability observed in the KO mice is a compensatory mechanism to mitigate potential cytotoxicity. These

findings highlight the complex interplay between ion channels and receptors and the need for further research to understand the underlying mechanisms fully.

Contrary to our findings, other studies have reported opposite results concerning the effect of TRPC6 deletion. These studies have noted that silencing TRPC6 leads to an enhancement of neuronal excitability in the DG.

A study by Kim et al. demonstrated that knocking down TRPC6 with siRNA increased seizure susceptibility. Moreover, TRPC6 knockdown rendered normally resistant DGCs susceptible to excitotoxic cell death induced by SE but reduced SE-induced cell death in the downstream CA3 and CA1 regions.[159]

The effects of TRPC6 activation and inhibition on seizure-induced neuronal cell death in the hippocampus of rats are conflicting. Despite this, studies have revealed increased TRPC6 expression in the human cortex and mouse hippocampus of brain samples from temporal lobe epilepsy (TLE) patients and pilocarpine-treated mice. Interestingly, TRPC6 knockout mice did not exhibit any differences in seizure susceptibility or seizure-induced neuronal cell death across all hippocampus regions (unpublished data. Zheng, F.). [160] These findings emphasize the need for further research to understand the complex interplay between TRPC6 in the neuronal excitation mechanism and epilepsy fully.

TRPC6 deficiency increases GABAergic inhibitory input to DGC. [161]Nevertheless, the inhibitory GABA A currents were blocked during the whole experiment using GABazine, which raises the possibility that TRPC6 deletion may have as well altered the functionality of both sodium and potassium voltage-gated channels.

Eun-Kim et al. showed that the downregulation of TRPC6 resulted in increased excitability and inhibitory transmission of the DGCs and CA1 neurons in response to paired-pulse stimulation. Yet, it was also noted that TRPC6 downregulation had a detrimental effect on GABAergic inhibition in the hippocampus, both during and after high-frequency stimulation. Likewise, the findings indicated a reduction in Kv4.3 clusters in the membrane fractions and dendritic localization of DGC and GABAergic interneurons due to TRPC6 inhibition. Eventually, the study reported a decrease in the phosphorylation of ERK1/2 and a reduction in the efficacy of 4-Ap in neuronal excitability.[162]

Further analysis of these granular cells' synaptic excitatory drive using both sEPSC and mEPSC measurements revealed altered post-, and presynaptic receptor kinetics manifested as events with lower peak amplitudes and frequencies. These findings are consistent with the findings of Zhou et al., which state that downregulation of TRPC6 lowers spine density, lowers the frequency of spontaneous miniature excitatory postsynaptic currents, decreases the expression of postsynaptic density protein 95 (PSD95), and inhibits phosphorylation of calcium-calmodulin-dependent protein kinase II[128].

We wondered whether the electrophysiological function related to synaptic plasticity of the KO mice has changed, so the LTP from PP to the DG region was recorded by measuring the fEPSPs slope.

Neural plasticity refers to the ability of neurons to change in response to experience. It plays a critical role in learning and memory, as it strengthens existing synapses, enabling the formation and retention of memories. LTP and LTD, which are mechanisms of neural plasticity, have been extensively studied in the context of glutamate neurons in the hippocampus. The fate of synaptic plasticity, whether LTP or LTD, is determined by the concentration of calcium ions present in the postsynaptic neuron. LTD occurs when the calcium concentration is moderate but below its threshold level. [163]

The DG is critical in memory formation because it integrates and consolidates redundant, perforant path inputs and converts them into spatiotemporal patterns of sparse activity in the CA3 hippocampal area. These complex and vital processes rely heavily on the functional integrity of DG granule neurons [164]. It was discovered by Hashimotodani et al. that MC - GC LTP induction requires postsynaptic BDNF-TrkB signaling as indicated by several complementary manipulations: Endogenous BDNF molecular inactivation, pharmacological inhibition of TrkB signaling, and TrkB receptor deletion from GCs all reduced MC-GC LTP.[165]

The absence of the TRPC6 gene in KO mice profoundly impacted the formation of long-term memories in the hippocampus. Specifically, the mossy fiber pathway could not undergo the crucial process of LTP, which is critical for forming memories. This contrasts with wild-type mice, where the non-stimulated lateral perforant path demonstrated LTD. The significance of these findings cannot be overstated, as they highlight the vital role that the TRPC6 gene plays in the formation and retention of

memories. The results presented in this thesis have been supported by numerous other studies, strengthening the validity of the proposed theory of iDG.

Reports have surfaced of working memory impairments in mice with the iDG phenotype. Mice with the iDG phenotype frequently exhibit a decreased frequency facilitation at mossy fiber-CA3 synapses, which could impact the CA3 region's ability to process working memory. Frequency facilitation is crucial for quickly encoding new information into the hippocampus, making it a vital memory component.[130]

Studies have revealed that TRPC6 knockout mice exhibit weakened synaptic plasticity, including impaired LTP, decreased dendritic length and spine density, and reduced levels of PSD-95 staining. It has also been reported that TRPC6 knockdown in the DG of mice has a negative impact on cognition and anxiety-like behavior.[155]

Further, behavioral experiments have revealed that mice administered shRNA-TRPC6 demonstrated an augmented level of anxiety-like behavior, as evidenced by the diminished amount of time spent in the central portion of an open-field test. Additionally, these mice displayed poor performance in tasks related to spatial learning and working memory, as seen in their inability to differentiate between unfamiliar and familiar mice in a three-chamber test.[166] Besides, it has been observed that positive regulators of TRPC6 can restore the LTP deficit in brain slices from transgenic mouse models of AD.[167]

TRPC6 was found to be expressed on the presynaptic sites of granular cell synapses, suggesting that TRPC6 deficiency interferes with the postsynaptic glutamate response as well as regulating the excitability of calcium homeostasis at the presynaptic terminals. Dendritic spines, which consist of actin filaments and serve as sites of synaptic connections, are found throughout the nervous system and are primarily associated with convergent neurons. In CNS, over 90% of excitatory synapses are located exclusively on these spines. The size of the dendritic spines plays a role in the strength of the synaptic transmission. More prominent spines have synapses containing more neurotransmitter receptors and a thicker PSD protein, leading to a more robust synaptic transmission than smaller ones.[163]

The decisive link between TRPC6 deletion and the absence of LTP in KO mice is established because the deletion significantly reduces synapses. This firmly

establishes the crucial role of TRPC6 in the LTP process and provides a compelling explanation for the observed outcome.

Considering these previous studies in connection to my results, The significance of exploring the relationship between TRPC6 and the iDG phenotype and working memory is highlighted, as it holds the potential for revealing new therapeutic approaches for cognitive disorders.

# Chapter 5

# 5 Role of TRPC6 in the pathophysiology of traumatic brain injury (TBI)

## 5.1 Results

### 5.1.1 TRPC6 deletion did not result in any short-term changes in neurological outcome

This experiment aimed to study the influence of TRPC6 deletion in acute brain injury. The CCI model of TBI was used to induce highly repeatable and region-specific cortical damage. [168.] Mice were subjected either to the CCI or sham procedure. Body weight, pericranial and rectal temperatures, the duration of the surgery, and the total anesthesia time before and during the process, respectively, were all within the normal range and did not vary across the groups (data not shown). The survival time was set to 5 dpi. A modified 13-point neurological severity score was employed to evaluate neurological deficits and recovery after TBI, assessing motor function, awareness, balance, and general behavior. Rotarod and OFT behavioral tests were used pre and post-surgery, while the EPM test was only applied on 5 dpi. (**Fig 22a**). The NSS results showed a peak at 1 dpi in all TBI groups and a significant reduction from three to 5 dpi, with no genotype-specific distinction (**Fig 22b**). In sham mice, NSS constantly remained low over time (data not shown). There was no difference in the rotarod test between WT and TRPC6 KO TBI mice. However, TBI induces motor deficits in both groups at 1 and 3 dpi with recovery at 5 dpi (**Fig 22c**). The OFT did not reveal differences between the genotypes concerning latency time, center time, or distance moved (**Fig 22d, e, f**). Moreover, the EPM test, done only at 5 dpi, failed to show any significant discrepancy between the different groups regarding time spent in open and closed arms. Overall, CCI resulted in substantial neurological deficits throughout the observation period, which peaked at 1 and declined by 3 and 5  dpi (**Fig 22f, g**).

**a**



**b**



**c**
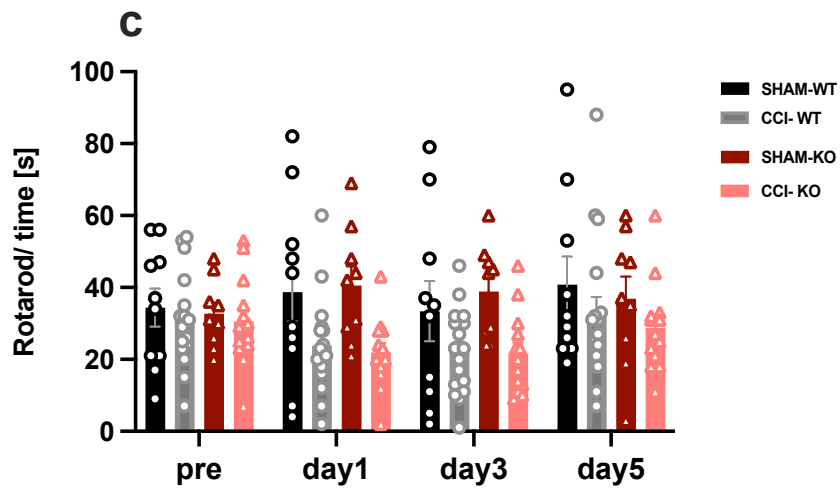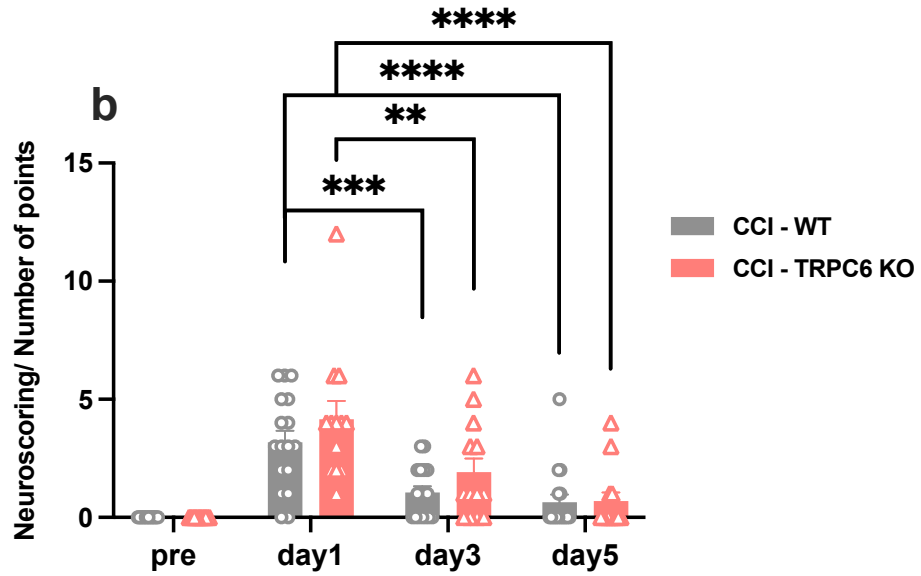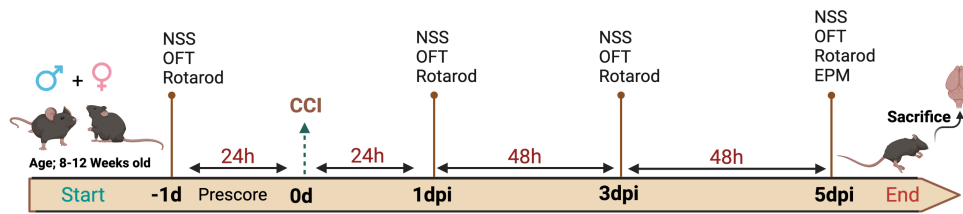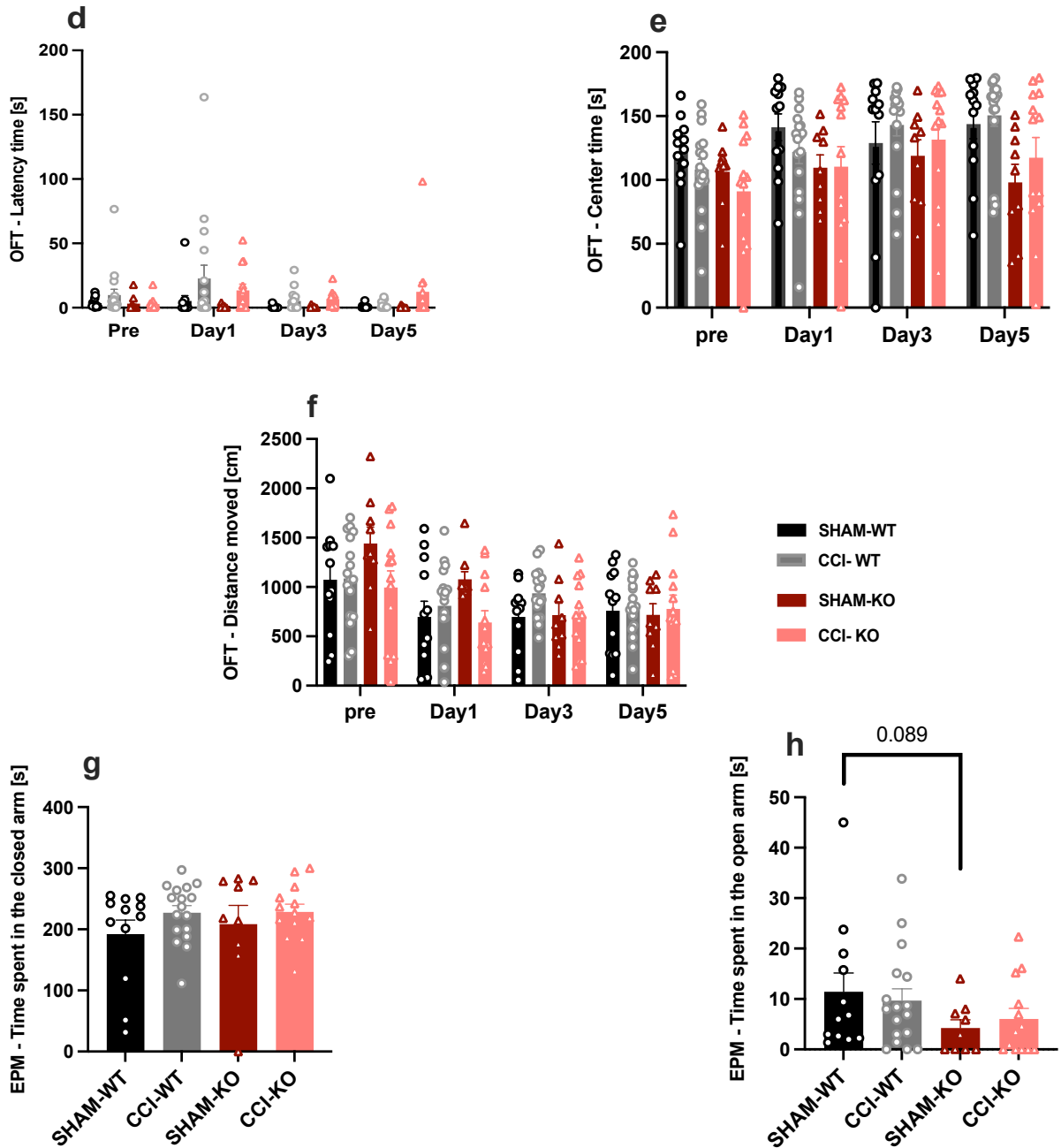
**Figure 12: Nearly no difference existed between the neurological outcomes in behaving mice**. (**a**) 5-day survival groups experimental design (equal sex ratio aged between 8-12 weeks old, n=51). NSS, rotarod performance, and OFT were all performed one day before the TBI, as well as at 1, 3, and 5 dpi. (**b**) NSS was used to assess neurological recovery in wild-type and TRPC6 knockout mice (higher scores indicate increased severity). (**c**) The Rotarod test showed no significant differences in rota-rod latency between the groups on the testing days. (**d, e,f**) OFT, indicating no significant difference between WT and TRPC6 KO mice I latency time, centre time, and distance moved. (**g, h**) EPM, time spent in the closed arm by all groups is more prolonged than time spent in the open arm on the 5th day post-surgery. (**i**) color

coding representing different groups on the graphs. Values represent mean ± SEM; pairwise comparisons were done using one-way ANOVA (*p<0.05, **P<0.001).

### 5.1.2  TRPC6 deletion leads to increased lesion volume after CCI

During the initial days following the primary injury, TBI triggers secondary processes such as edema production, BBB disruption, and $Ca^{2+}$ excitotoxicity that cause a progressive loss of crucial brain tissue[169], which results in the formation of a lesion (**Fig 23a**). Consecutive brain cryosections were stained with cresyl violet to determine the severity of the lesions in the brain five days post-injury (**Fig 23**). The histological examination revealed brain tissue loss and the creation of a lesion cavity in the ipsilesional hemisphere which in some cases extended to the hippocampus and had an atrophic appearance to the GCL, CA1, and CA3 regions when compared to the contralateral hemisphere (**Fig 23 b**). Quantifying the lesion volume showed that TRPC6 deletion generates significant tissue loss as translated by more considerable lesion volume in the KO group than in the WT (**Fig 23c**). This result was not sex-specific, as quantifying the lesion volume based on the gender difference did not show any significant difference (**Fig 23d**).
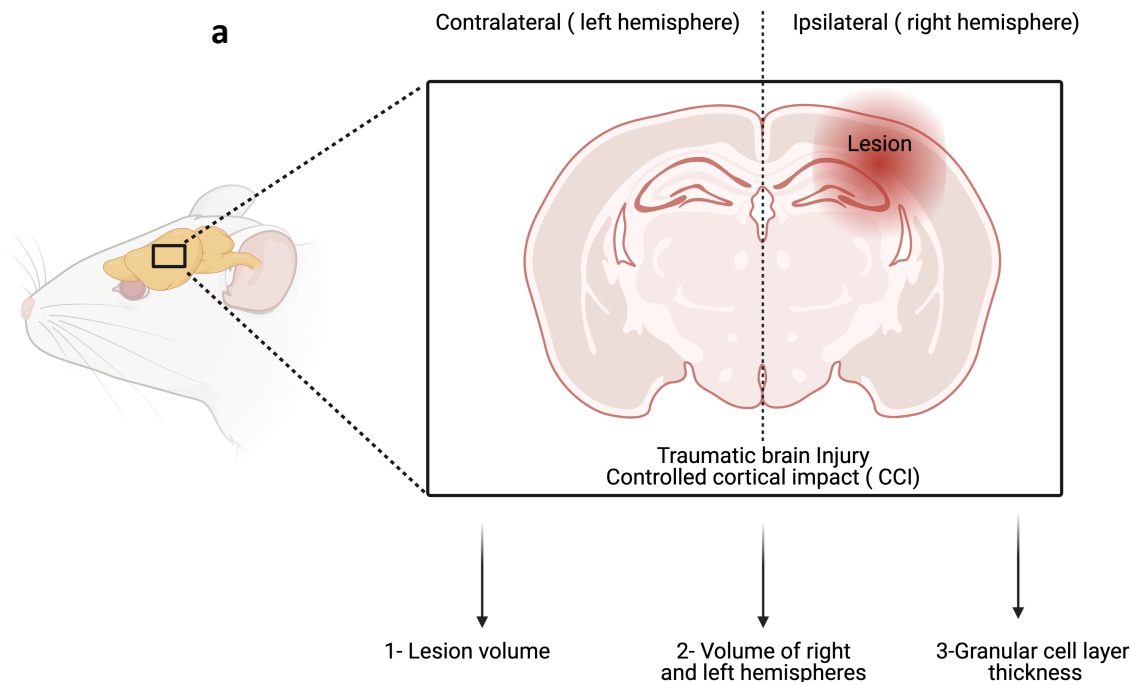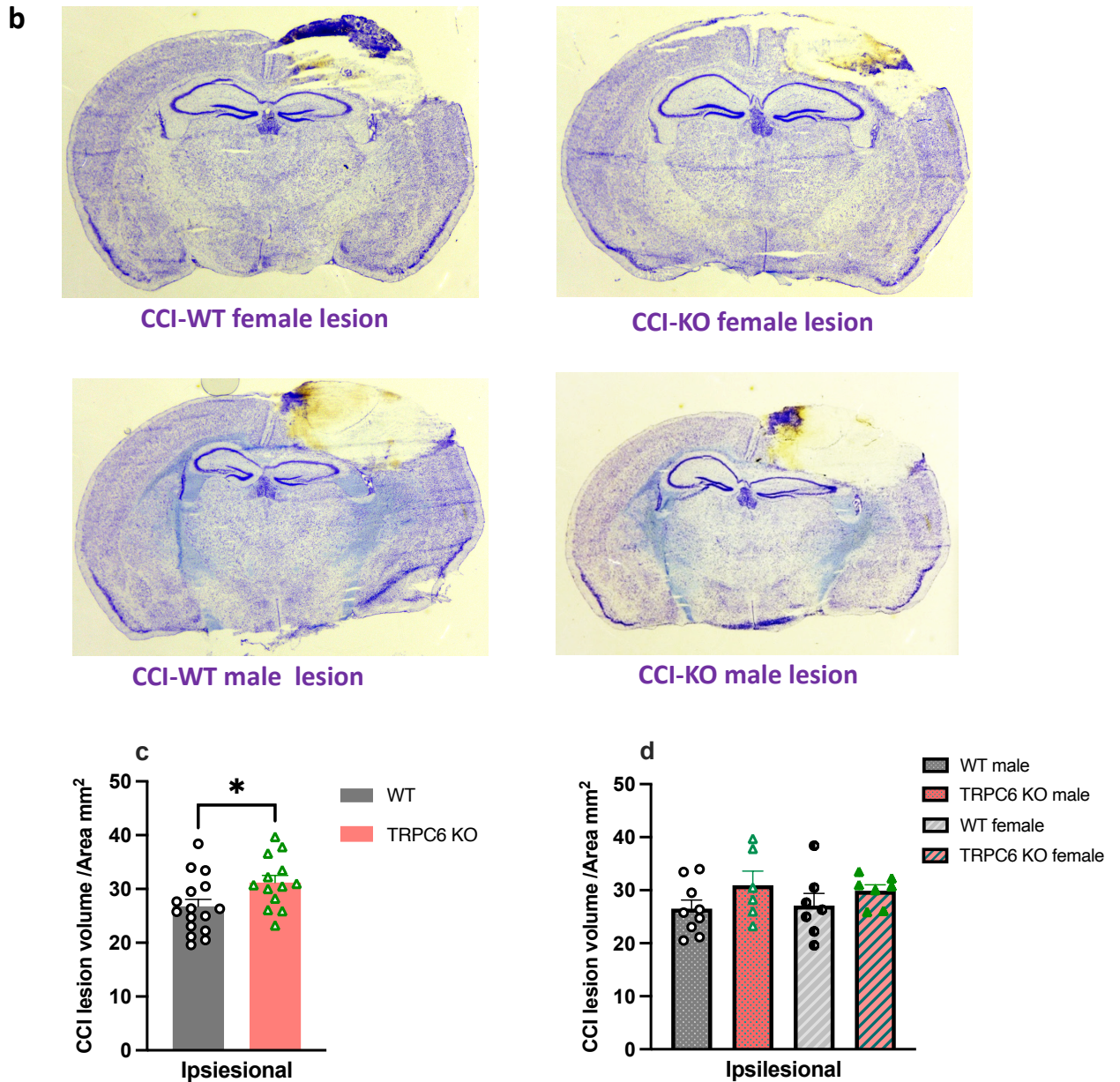
**Figure 13**: *TRPC6 deletion leads to increased lesion volume after CCI.* (**a**) A representative brain slice image shows the lesion's position on the right hemisphere (ipsilesional) and the left hemisphere as control (contralateral). (**b**) Cresyl violet stained slices showing the lesion volume in both WT and TRPC6 KO mice. (**c**) quantitative analysis of the lesion volume on the ipsilesional side showing significantly bigger lesions in the KO group. (**d**) quantitative analysis of lesion volume between males and females of each genotype indicating no significant difference sex-wise. Values represent mean ± SEM; pairwise comparisons were done using students' t-tests (*p<0.05, **P<0.001).

### 5.1.3 TRPC6 knockout did not affect the thickness of GCL, CA1, or CA3 layers in either ipsilesional or contralateral hemispheres

TBI can impact the hippocampus based on the severity and location of the injury. In the hippocampus, different regions are commonly affected by TBI, including the CA1 and CA3 layers. Additionally, the DG, a critical regulator of cortical input to the hippocampus, can suffer from long-term memory deficits and loss of GCs and other neurons. [170] This cell loss can reduce the GCL thickness and the overall volume of the DG. Nevertheless, TBI can cause changes in the structure and function of the remaining GCs, which can further impair the role of the DG and the hippocampus. The thickness of the outer molecular layer of the DG was measured in Nissl-stained sections after five dpi in all groups. The results demonstrated a considerable loss in the GCL in the ipsilesional hemisphere compared to the contralateral hemisphere in all groups following CCI (**Fig 24c**). However, the comparison between the ipsilesional hemispheres in WT and TRPC6 KO groups after CCI failed to show a significant difference (**Fig 24b**). The results were consistent when analyzing the ipsilesional hemisphere of each sex separately between the CCI and sham groups. (**Fig 24d, e**). To examine the potential impact of TBI on the CA1 and CA3 regions of the hippocampus, the thickness of these layers was compared between the contralateral and ipsilesional hemispheres. No significant loss was observed in either hemisphere after TBI, and no difference was found between the two genotypes. (**Fig 24f-k**)

**a**
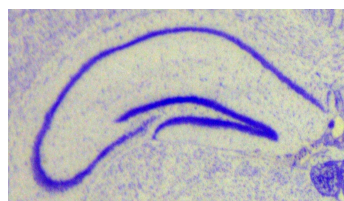


**CCI-WT hippocampus contra**   **CCI-WT hippocampus ipsi**
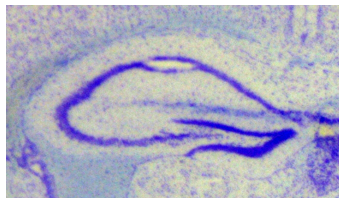
**CCI-KO hippocampus contra**   **CCI-KO hippocampus ipsi**
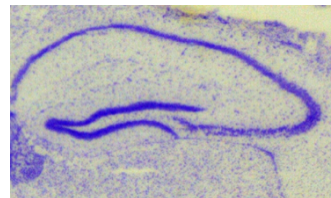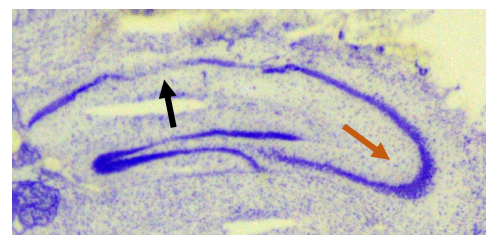
**CCI-WT hippocampus CA1 and CA3**
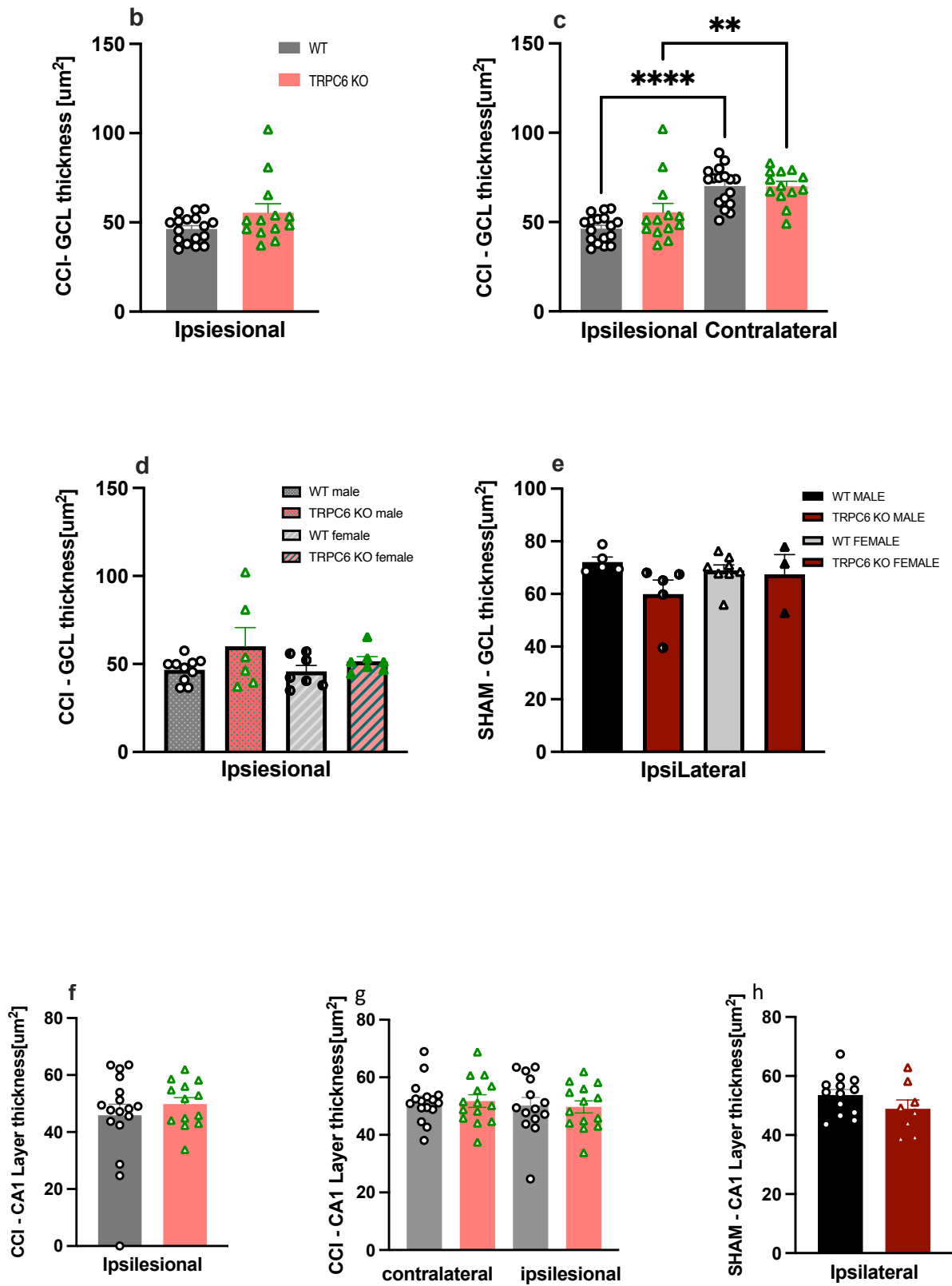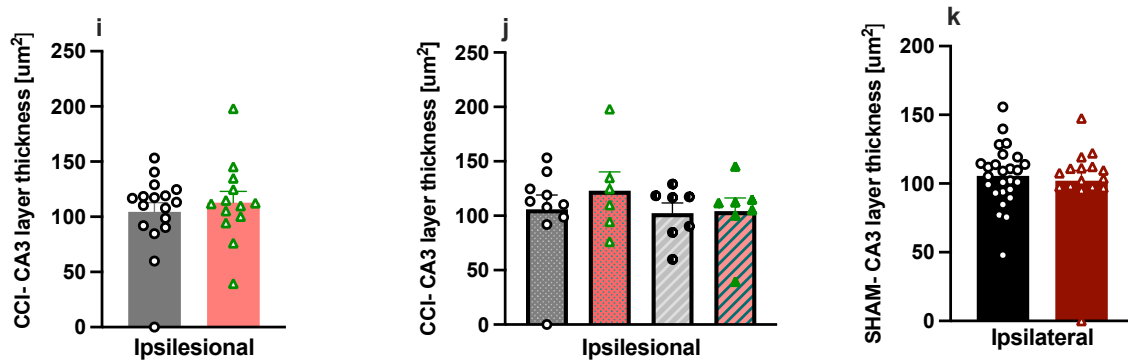
**Figure 14: TRPC6 deletion does not affect the thickness of GCL, CA1, or CA3 in either ipsi or contralateral regions**

(**a**) Image enlargements showing the hippocampus's ipsi- and contralesional GCL after CCI. Red arrows point to measurement regions of the thickness of the ipsilesional GCL; the black arrow points to the CA1 measurement region. The orange arrow points to the CA3 region (**b**) representative graph for the quantification of GCL thickness in the ipsilesional region of WT compared to TRPC6 KO (**c**) quantification of the GCL thickness of the ipsilesional region in every genotype sex specified (**d**) quantification of GCL thickness in the ipsilesional region compared to the contralateral region in each genotype, showing significant reduction in the ipsilesional region. (**e**) quantification of the GCL thickness of the ipsilateral region of sham animals in both genotypes, sex-specific showing no significant difference between any of the groups. (**f**)representative graph for the quantification of CA1layer thickness in the ipsilesional region of WT compared to TRPC6 KO (**g**) quantification of the CA1 layer thickness of the ipsilesional region in every genotype sex specified (**h**) quantification of CA1 layer thickness in the ipsilateral region of sham animals, WT compared to TRPC6 KO. (**i**) quantification of the CA3 layer thickness of the ipsilateral region of sham after CCI in WT compared to TRPC6 KO. (**j**) quantification of the CA3 layer thickness of the ipsilateral region of sham after CCI in WT compared to TRPC6 KO sex-specific. (**k**) representative graph showing the quantification of CA3 layer thickness in sham animals. Values represent mean ± SEM; pairwise comparisons were done using one-way ANOVA (*p<0.05, **P<0.001).

### 5.1.4  TRPC6 deletion has an impact on gliosis after CCI

GFAP (glial fibrillary acidic protein) and CD68 are proteins in various brain cells. GFAP is a significant component of the intermediate filaments in astrocytes that support and protect neurons. CD68, on the other hand, is a protein expressed in microglia, the brain immune cells that play a critical role in the brain's response to injury and disease[171]. There is a significant increase in the expression of both GFAP and CD68 in the brain following a traumatic brain injury. This rise is thought to be part of the brain's response to injury and may help repair and regenerate damaged neurons. Increased GFAP expression may help to stabilize astrocytes and maintain their structural integrity, whereas increased CD68 expression in microglia may help to remove debris and promote healing[172]. Overall, increased GFAP and CD68 expression after traumatic brain injury is thought to be part of the brain's response to injury and may aid recovery and repair.

qPCR analysis for the expression of GFAP of the different groups revealed a significant increase in the expression levels following CCI for WT animals but not for the TRPC6 KO (**Fig 25b**). Analyzing the data based on the sex differences surprisingly showed that the GFAP expression was significantly the highest after CCI in males but not in females of both genotypes. Furthermore, TRPC6 KO females in the sham group showed high expression compared to the females of the CCI group (**Fig 25a**). On the other hand, CD68 expression levels quantification showed a significant difference in both WT and TRPC6 KO following CCI compared to the sham groups. Interestingly, the sham WT group shows a higher expression trend than the sham TRPC6 KO group (**Fig 25d**). The quantification based on sex differences showed that the expression levels were higher after CCI as well in all groups, with high significance only between the CCI and sham WT females (**Fig 25c**).
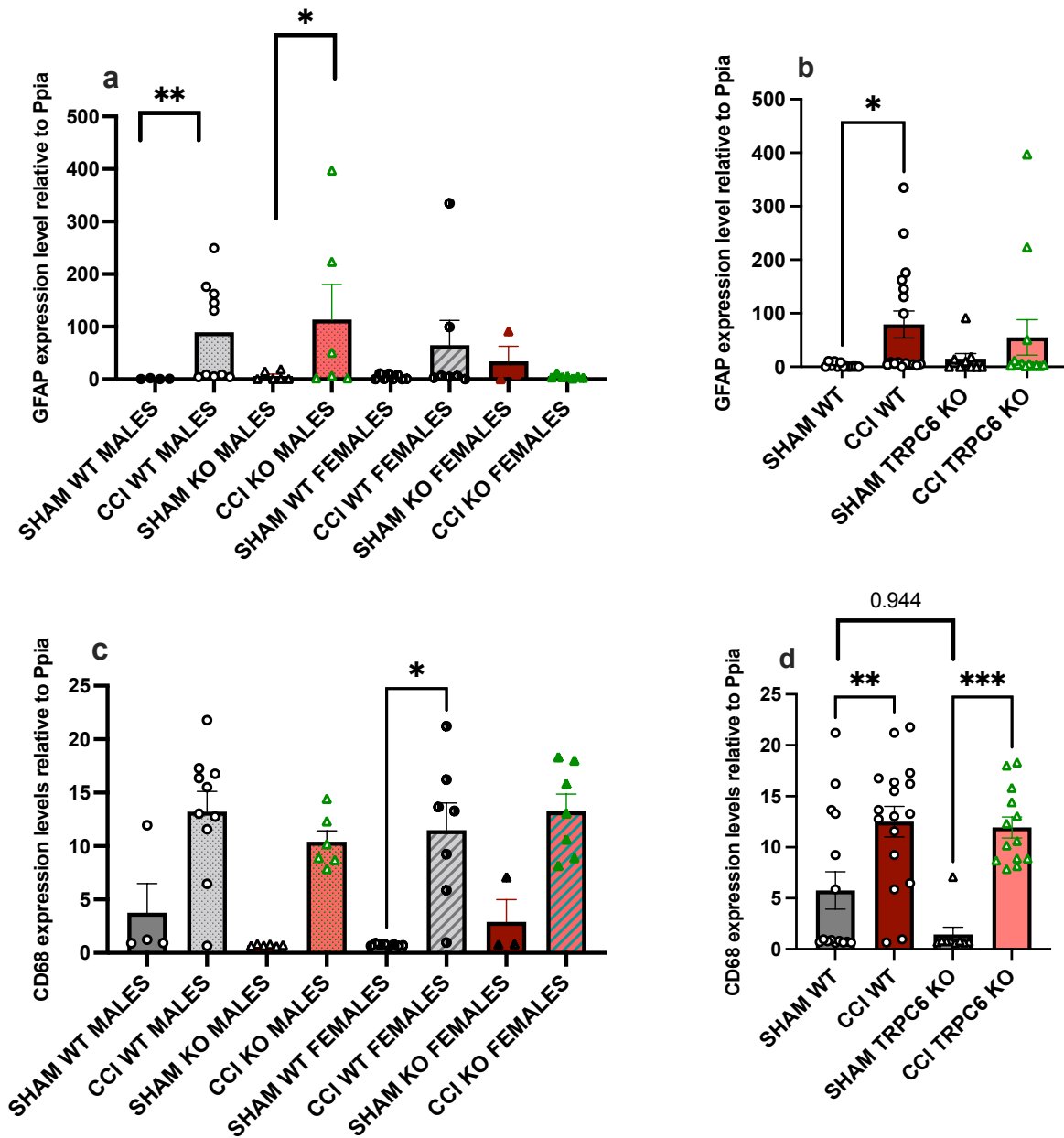
**Figure 15: TRPC6 deletion impacts the expression of gliosis after CCI.**

(**a, b**) mRNA expression levels of GFAP, astrocytes marker in sham and CCI groups, sex-specific. (**c, d**) mRNA expression levels of CD68, microglial marker in sham and CCI groups, sex-specific. Values are expressed relative to the reference Ppia. Values represent mean ± SEM; pairwise comparisons were done using one-way ANOVA (*p<0.05, **P<0.001). One outlier was identified and excluded by Rout's test.

### 5.1.5 Immunostainings show no difference in gliosis between WT and TRPC6 KO groups after CCI.

Triple immunostaining was performed using specific antibodies for GFAP, CD68, and the neuronal marker NeuN to confirm previous findings. The aim was to determine the co-localization of GFAP, CD68, and NeuN in brain tissues following traumatic brain injury. The results of this staining can provide insight into the relationship between astrocytes, microglia, and neurons in response to injury and aid in understanding the potential roles of GFAP and CD68 in the recovery and repair process the presence and absence of TRPC6. Images were taken from the whole brain slice as an overview from sham and CCI animals (**Fig 26a**), followed by a more detailed tile scan around the area of the hippocampus in both the ipsilesional and contralateral hemispheres. The CCI group, with a noticeable loss of the Neun staining in the DG and CA1, CA3 layers of the damaged hemisphere (**Fig 26c, g**). In conclusion, the data showed an increased GFAP and CD68 in the affected hemisphere after traumatic brain injury but no differences in expression levels between genotypes.

a

**SHAM WT male**

b

**CCI WT male**

c

**Dabi**

**Neu-n**

**CD68**

**GFAP**

d
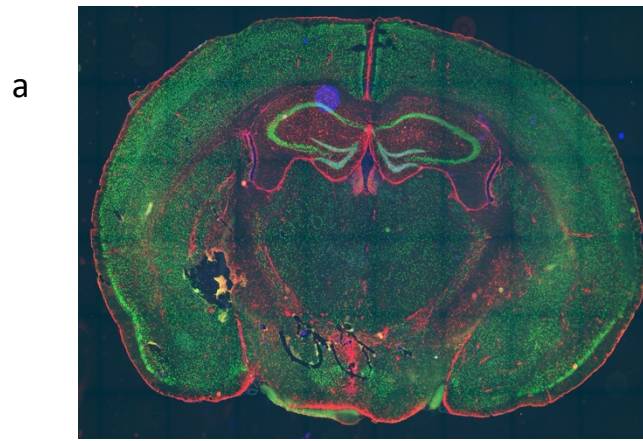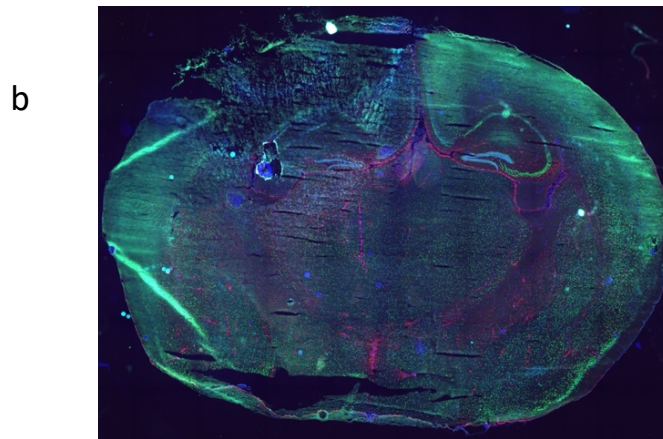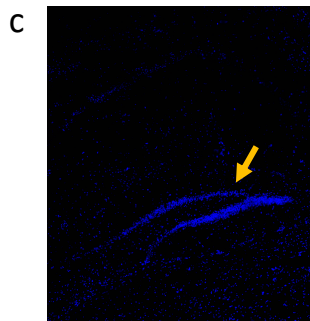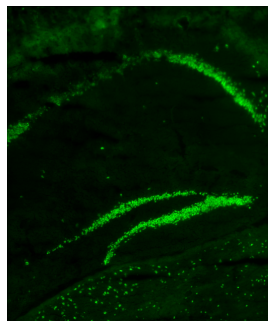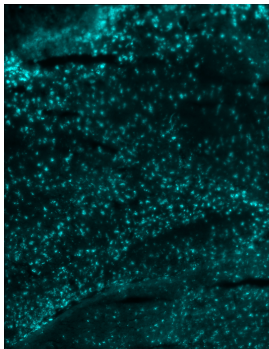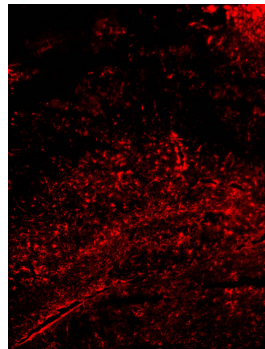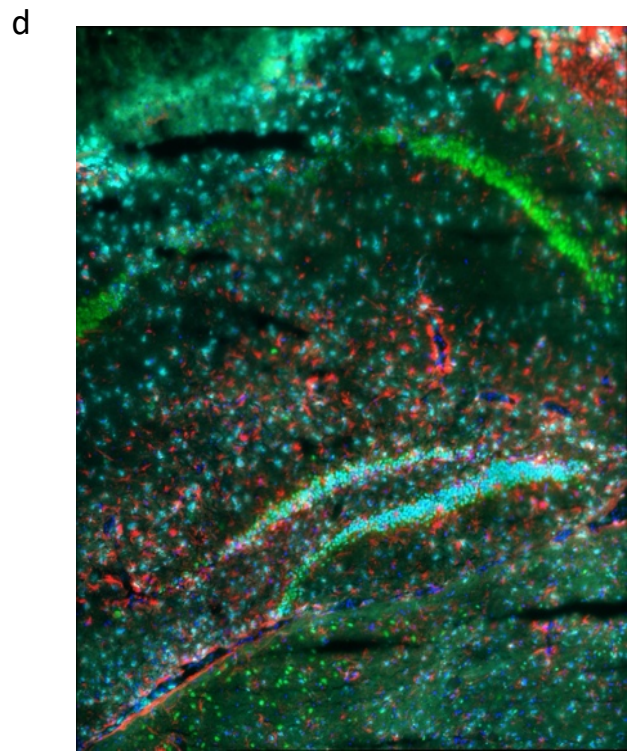
**Merged hippocampus**

**Ipsilesional hemishehere**

**CCI-WT male**

SHAM TRPC6 ko male

f
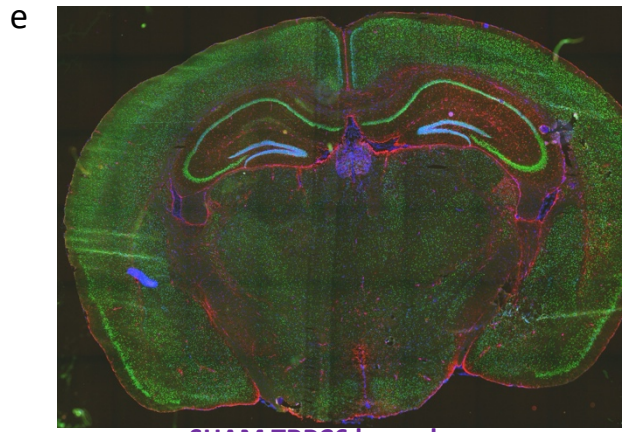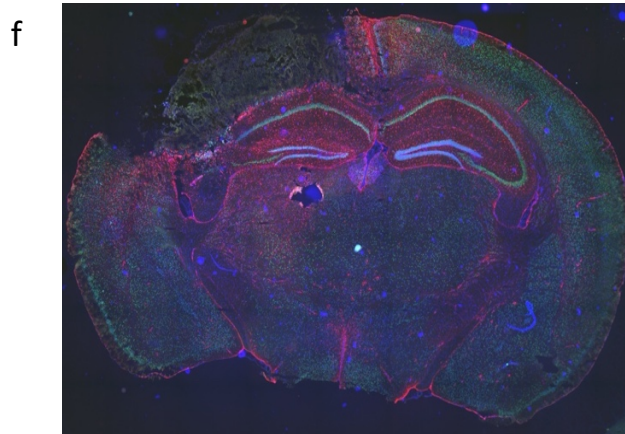


CCI TRPC6 ko male

g
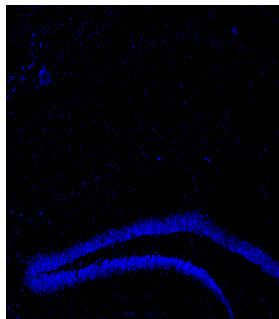


Dabi
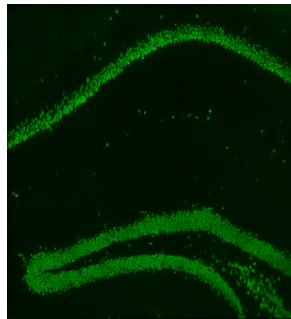
Neu-n
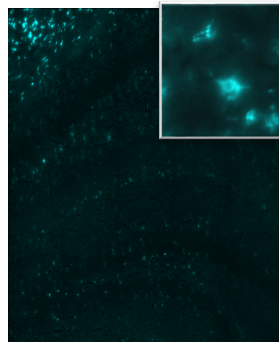
CD68
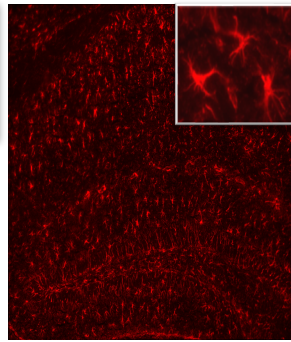
GFAP

h
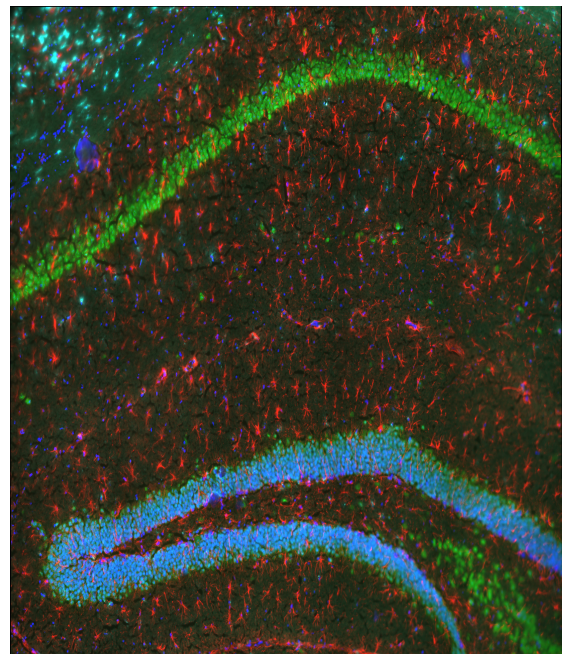


Merged hippocampus

Contralateral hemishehere

CCI-TRPC6 KO male
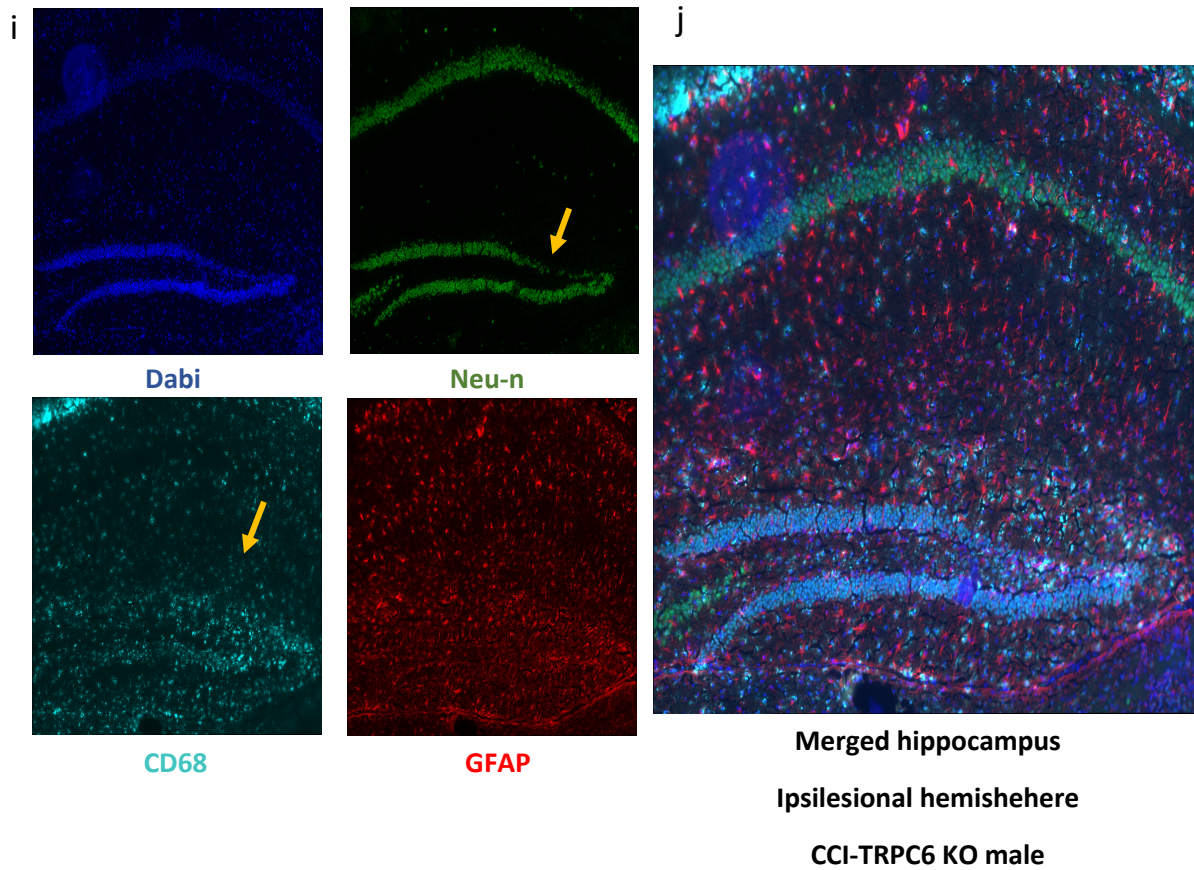
**Figure** *16: Immunostainings show no difference in gliosis between WT and TRPC6 KO groups after CCI. (a)* Representative images of triple immunostained brain sections of sham animals from WT male (**b**) overview of the whole brain slice of WT-male after CCI showing the distribution of astrocytes and microglia. (**c**) Tile scan showing neuN/CD68/GFAP triple-immunostaining in the brain tissue at 5 dpi. Dapi (blue), neuN(green), CD68 (cyan), and GFAP (red). (**d**) Tiles scan showing the hippocampus region from the ipsilesional region of WT-male after CCI. (**e,f**) overviews of the whole brain slice of the KO-male as sham and after CCI. Images were taken by Leica thunder microscope (**g, h**) Tile scan of the Hippocampal area of the contralateral side of KO-male after CCI (**I, j**) Tile scan from the hippocampus region of the ipsilesional region, showing the distribution of the microglia and astrocytes as well as neuronal degeneration.

## 5.2 Discussion

The prevalence of TBIs is rising, and there is more and more proof of systemic, long-term effects, which emphasizes the significance of creating novel ways and paradigms for treatment. Taking advantage of having a TRPC6 KO mouse model, the current study's objective was to precisely pinpoint how TRPC6 affected posttraumatic brain lesion growth, neurological function, and inflammatory markers in the brain.

The results showed that TBI caused significant neurological deficits, which improved over time. However, there was no significant difference between the TRPC6 KO mice and the control mice regarding neurological deficits.

For the first time, this study uncovered that TRPC6 deletion led to a significant increase in the volume of brain lesions caused by TBI, indicating that TRPC6 plays a role in mitigating the effects of the injury. Further, This research endeavors that after a TBI, the expression of two genes, GFAP and CD68, increased in the brain. These genes help repair and regenerate damaged neurons, stabilize astrocytes, and remove debris. The results revealed that the GFAP and CD68 expression increase was significant in WT mice but not in the KO after the injury. These findings suggest that TRPC6 may play a fundamental role in protecting the brain against TBI and may offer new avenues for developing treatments to reduce the effects of TBI.

Numerous models of focal lesions have been created to cause TBI in mice. This study used the CCI model as it permits the production of locally defined brain damage that reaches its peak extent two to three days after injury.[173] Within 24 hours of the trauma, the cerebral lesion spreads into the surrounding healthy parenchyma.[173] To incorporate a short time point and evaluate the size of the brain injury and neurological impairment, observation time points of 1,3 and 5 dpi were used, regarded as the initial stage of CCI.

Long-term cognitive rehabilitation and motor function difficulties are the most devastating consequences of human TBI.[174] Behavioral tests are widely used in pre-clinical research to evaluate the outcomes of TBI in animals. Despite making efforts to include results from some of the most commonly used behavioral tests, only a limited number of animal behavioral paradigms were utilized. Nevertheless, the results

provide valuable insights into the effects of TBI on animal behavior. My findings align with these clinical observations, as WT and TRPC6 KO mice demonstrated impaired neurological outcomes following TBI. However, the difference between the two genotypes was not pronounced.

Interestingly, the similarity of the poor neurological outcome after TBI does not correlate with the histopathological damage since TRPC6 KO mice had significantly more enormous lesion volumes after CCI compared to the TRPC6 WT. A recent study by J Walter et al. agreed with the same point with respect to the different methods used; they demonstrated that gait irregularities identified through the use of CatWalk XT1 analysis do not exhibit a correlation with the volume of unilateral lesions assessed through histological evaluation during the initial weeks after the induction of experimental TBI in mice using the CCI technique.[175] As a result, it is still being determined whether neurobehavioral testing adds significant extra information to the outcome assessed by histopathological parameters and whether it significantly contributes to the overall assessment of treatment effects. Given the possibility that impaired motor function is simply the direct result of focal histological damage, histological outcome assessment may be sufficient, rendering extensive neurobehavioral testing time and cost inefficient.

TBI was previously thought to be a static neurodegenerative disorder caused by an acute traumatic event, but clinical studies showed that trauma could cause chronic and progressive changes. Posttraumatic inflammation can last for years after the initial brain insult, even in areas far from the trauma site, and is linked to cognitive changes.

A significant number of neurobehavioral disabilities worsened over time in a prospective cohort of more than 200 TBI survivors followed for up to 12 to 14 years.[176] The initial phase of primary damage resulting from an insult to the brain comprises contusion and laceration, diffuse axonal injury, and intracranial hemorrhage. This triggers immediate (necrotic) cell death, followed by a prolonged secondary phase that involves a complex interplay of biological processes initiated at the time of injury, which may persist over days, weeks, and even months. These events are characterized by neuroinflammation, glutamate toxicity, ischemia, oxidative stress, astrocyte reactivity, blood-brain barrier changes, cellular dysfunction, and apoptosis. [177]

The results in this thesis demonstrated brain tissue loss and the creation of a lesion cavity in the ipsilesional hemispheres of both WT and TRPC6 KO after CCI, with more considerable lesion volume in the KO group compared to the WT. This result was not sex-specific.

According to various animal TBI models, including CCI injury, TBI causes neuronal apoptosis in the hippocampus. At seven days after TBI, hippocampal CA1, CA3, and DG neurons were significantly reduced in the ipsilateral injury site, according to one study by Myer et al.[114]. They demonstrated that severe CCI injury resulted in extensive neuronal death, rapid cortical tissue loss, and consistent degeneration of hippocampal regions. This data supports my findings since, at 5 days after CCI, a significant loss in the GCL thickness was observed in the ipsilesional hemisphere of both groups. However, no consequential loss was observed in the CA1 and CA3 layers, and no specific differences were found between the two genotypes. These hippocampus impairments may worsen over time, resulting in cognitive deficits. One limation of my study is the short recovery time. To evaluate the structural impairments further after experimental TBI, parameters to other aspects of secondary brain injury, such as edema formation or induction of de- and regenerative processes, in the long term would be of great interest.

In the central nervous system, TRPC6 is abundantly expressed and plays a crucial role in neuronal survival and development.[178] My data showed that TRPC6 KO brains exhibit larger lesion volume after TBI than WT. In line with these findings, growing data suggest that TRPC6 may act as a protective mechanism during an ischemic stroke, and its expression is dramatically reduced in neurons after exposure to ischemia, leading to ischemic neuronal death.[179]

Du et al. demonstrated that inhibiting TRPC6 calpain proteolysis protected rats from ischemic brain damage.[180] Moreover, Li et al. reported that TRPC6 inhibits NMDAR-induced $Ca^{2+}$ elevation and excitotoxicity and protects neurons from ischemic brain injury.[179] Surprisingly, TRPC6 has been implicated in the neuroprotective effect of BMSC and oxiracetam combination therapies in acute brain IR damage, as demonstrated by Wang et al.[181]

Several lines of evidence support their conclusion. First, TRPC6 was specifically degraded in transient ischemia, which occurred before and during neuronal cell death. On the other hand, suppression of TRPC6 degradation increases behavioral performance, decreases infarct size, and increases neuronal survival.

Second, the TRPC6 function was suppressed in ischemia models, and maintaining its expression provided neuroprotection through the CREB-dependent mechanism. The transcription factor CREB is downregulated because of TRPC6 degradation leading to neuron apoptosis. [179] Additionally, it was shown that a TRPC6 activator reduced neuronal death following an ischemic stroke, which was linked to increased phosphorylated CREB (p-CREB) activity.

Further, resveratrol, neuroprotectin D1, and the main compound in green tea, (−)-epigallocatechin-3-gallate, inhibit calpain-mediated TRPC6 proteolysis and activate MEK/ERK or CaMKIV-dependent CREB pathways, improving neurological status in experimental stroke patients.[182] Hyperforin, a TRPC6 activator, also contributes to neuroprotection after ischemic stroke by inhibiting TRPC6 degradation, which is accompanied by an increase in phosphorylated CREB in CaMKIV and Ras/MEK/ERK-dependent mechanisms.[182] Stem cell therapy for ischemic stroke is gaining popularity in the research community. Animal studies have shown that bone marrow-derived stromal cells (BMSCs) improve stroke outcomes, though the regulatory mechanisms are still unknown. Surprisingly, TRPC6 channels have been implicated in the neuroprotective effect of BMSCs and oxiracetam combination therapies in acute brain IR damage. Their overexpression in BMSCs improves neuronal functions in rats following ischemic stroke, which is linked to the BDNF/CREB pathway.[183]

Third, NMDARs mediated TRPC6 calpain proteolysis. After an ischemic stroke, excessive glutamate-mediated calpain stimulation leads to the overactivation of NMDA receptors, which promotes the proteolysis of TPRC6. [184] TRPC6 protects neurons from excitotoxicity by inhibiting the $Ca^{2+}$ overload caused by NMDA. It has been reported that by interacting with other receptors, NMDA activity can be modified. The dopamine D1 receptor, for example, interacts with NR2A subunits to suppress the NMDA current. Furthermore, NR2A and NR2B were phosphorylated more after cerebral ischemia. TRPC6 expression reduced NMDA receptor-mediated $Ca^{2+}$ neurotoxicity via

increasing TRPC6 activity in ischemic stroke.[185] It was suggested that TRPC6 might control the NMDA receptors' phosphorylation, which would reduce their function. Notably, the infarct amount of the TRPC6 transgenic (overexpressed TRPC6) mice was lower than that of their wild-type littermates, and the transgenic mice also had reduced mortality rates and superior behavioral performance.[186]

TRPC6 activation in the heart activates calcineurin, a phosphatase involved in the antiapoptotic effect against ischemic insults. Activated calcineurin inhibits NMDA currents in neurons by dephosphorylating NMDA receptors. TRPC6 could not consistently inhibit NMDA-induced $[Ca^{2+}]$ elevation in the presence of FK506. As a result, TRPC6 may inhibit NMDA receptor activity by increasing its dephosphorylation via calcineurin. [98]

What is known so far about the protective role of TRPC6 against stroke is somehow confirmed with my data and contradicts a study published by Chen X et al. in 2018, which stated that TRPC6 inhibition by Larixyl acetate could protect against traumatic brain injury-induced systemic endothelial dysfunction.[187] The authors evaluated the aortic arch of TRPC6 mutant mice for vascular reactivity and endothelial dysfunction after TBI but did not assess the effect on any neurological or cognitive function [187]. Notably, the TRPC6 knockout mice phenotype is characterized by having raised systemic blood pressure and enhanced vascular smooth muscle contractility.[188]

In the hippocampus, the DG typically serves as a "filter" or "gate," with sparse activity limiting the amount of information relayed to downstream areas. [189] One theory about TBI-induced cognitive deficits posits that this "DG gate" breaks down after injury, leading to excessive DG depolarization, which spreads to area CA3.[189]

After conducting Nissil staining experiments on brain slices, the data analysis revealed that the thickness of the GCL in the DG  of both WT and TRPC6 KO mice was significantly reduced following TBI. Interestingly, there were no significant differences in the reduction between the two types of mice. In contrast, the thickness of the CA1 and CA3 layers in the hippocampus showed no significant changes after TBI. This indicates that the effects of TBI on brain structures may vary depending on the specific area of the brain being studied.

Overall, these findings suggest that TBI can significantly impact the thickness of the granular layer in the DG, which could lead to cognitive impairments. However, the lack of changes in the CA1 and CA3 layers may indicate that these areas are more resilient to the effects of TBI.

It is well established that inflammatory processes in the brain after TBI contribute to extensive cell death and long-term tissue deterioration. Glial scar formation is composed primarily of astrocytes, microglia, endothelial cells, fibroblasts, and extracellular matrix[190], which are thought to be crucial in starting an inflammatory response after damage. They can secrete various cytokines, chemokines, and growth factors in response to injury. Ultimately, these modifications may impact the local microenvironment, deciding the degree of damage and eventual repair.[118] Also, Scarring is thought to act as a physical barrier to encapsulate damaged tissue, preventing toxic molecules from leaking into healthy tissue and invading cell types from gaining access after injury.

The data obtained from the lysates of damaged brain tissue following TBI showed exciting results regarding the levels of specific mRNAs, including GFAP and CD68. A general increase in these mRNAs was observed in the TBI groups compared to the sham groups, indicating that molecular changes occur following TBI. Notably, the levels of GFAP were found to be significantly elevated in the TBI group of WT compared to the sham group of the same genotype. This is a compelling finding as it suggests that GFAP may serve as a potential marker of TBI. In contrast, the TBI group of TRPC6 KO did not exhibit a significant increase in GFAP levels compared to their sham counterparts. However, further analysis revealed that this might be because female mice in the KO group did not exhibit any elevation of GFAP after TBI.

These findings have significant implications for understanding the molecular mechanisms underlying TBI and identifying potential biomarkers for diagnosis and monitoring of TBI. Furthermore, the results suggest that TRPC6 may regulate GFAP expression after TBI and that gender-specific differences exist in this effect.

The findings in this thesis are supported by the fact that At 1, 3, and 7 days following damage in a mouse CCI model, GFAP-positive astrocytes were found to proliferate,

with the most significant number occurring on day 3. These astrocytes, which were hypertrophic and had expanded processes, were proximal to the lesion. These findings show that astrocytes have a primarily proliferative response following experimental TBI that peaks in the acute period.[191] Furthermore, CD68 (ED1) is used as a marker to confirm microglial activation, and CD68 immunoreactivity is seen following both mouse and human TBI.[192]

Interestingly, a recent publication by Liu L at al. showed that after ischemia/reperfusion (IR) injury, there was a substantial reduction in TRPC6 protein in both cultured astrocytes and cerebral cortices. Besides, astrocytes and the brain were protected against IR damage by HYP9 or TRPC6 overexpression, which inhibited TRPC6 downregulation. These findings suggest that the TRPC6 supports neuroprotection during cerebral ischemia by encouraging astrocyte survival. [193]

While the findings of my study support the observed lack of significant elevation of GFAP levels in the TBI group of female TRPC6 KO mice, it is essential to note that this finding contrasts the effects seen in the TBI group of male  KO mice. An apparent elevation in the astrocytic reaction was observed in the latter group after TBI. These results may be explained by the fact that TRPC6 deletion did not impact the expression of astrocytes in male mice but rendered them unhealthy following TBI. This observation underscores the complex molecular changes following TBI and highlights the potential differences in the underlying mechanisms between male and female mice.

There is a shortage of research investigating the impact of sex on inflammation in response to CNS injury. Despite the growing recognition of the importance of considering sex differences in disease pathophysiology, the existing literature on the subject is still limited.

Villapol et al. investigated the spatial and temporal neuroinflammatory changes following experimental TBI. Their study uncovered exciting insights into the divergent response of males and females to TBI. Within the first seven days following injury, male mice exhibited a rapid and pronounced activation of cortical microglia and macrophages, with a prominent activated phenotype. This response involved the production of pro-inflammatory cytokines (IL-1b and TNFa) and anti-inflammatory cytokines (Arg1 and TGFb), which exhibited a single-phase, sustained peak from 1 to 7 days. In contrast, female mice displayed a less robust microglia/macrophage

phenotype, with a biphasic pro-inflammatory response peaking at 4 hours and 7 days and a delayed anti-inflammatory mRNA peak at 30 days. Interestingly, female mice were found to be protected against acute cell loss following TBI, while male mice exhibited enhanced astrogliosis, neuronal death, and increased lesion volume 7 days post-injury.[194]

This neuroprotective effect seen in females following TBI might be due to the female hormones estrogen and progesterone. Bodhankar et al. discovered that microglia from female mice had a lower inflammatory status than male mice after middle cerebral artery occlusion in a stroke model. Furthermore, preclinical studies of ischemia-reperfusion models in rats have shown that sex steroids 17b-estradiol and progesterone can suppress microglial activation and downregulate associated pro-inflammatory cytokines in male and ovariectomized females to a comparable extent.[195]

On the other hand, in a controlled cortical impact model, Bruce-Keller et al. found no difference in cortical tissue sparing between males, intact females, ovariectomized females, and ovariectomized females with estrogen supplementation, implying that the amount of estrogen in female subjects did not alter injury severity. In their model, microglial activation in the hippocampus was similar in males and females and was unaffected by basal estrogen levels or estrogen supplementation.[195]

The fact that many of the data presented above contradict each other emphasizes the high likelihood that sex differences in TBI exist and that more focused research is required. TBI is complex, heterogeneous, and variable for each patient; failing to include sex as a complex variable in the pathophysiology of TBI would undoubtedly be an oversight.

It is important to note that the disparities in gliosis expression following TBI between WT and knockout KO subjects cannot be solely attributed to sex differences. Instead, evidence suggests that decreased hormone levels in females are accompanied by TRPC6 channel downregulation in some neurological diseases.

Q. Song et al. in their study demonstrated that estradiol treatment increased the downregulation of TRPC6 and BDNF in hippocampal neurons in the rat

perimenopausal depression model; BDNF/TrkB signaling pathway inhibitor (K252a) could reverse the effects of estrogen, and TRPC6 agonist could upregulate the reduced expressions of TRPC6 and BDNF caused by estradiol in combination with K252a. Their findings suggest that estrogen treatment can protect hippocampal neurons from injury in the rat perimenopausal depression model, with the underlying mechanisms involving an increase in the BDNF/TRPC6 pathway.[196]

My data, with respect to other studies which are in line or against, highlighting the impact of TRPC6 deletion on astrocytic and microglial protective effects after TBI, which may lead to larger lesion volumes than in WT mice, has left us intrigued about the potential gender-specific mechanisms underlying these effects. Could the absence of TRPC6 have different consequences for males and females, and if so, what are the underlying mechanisms?

Addressing these engaging questions would require a closer examination of the effects of astrocytic TRPC6 on TBI neurons. By delving deeper into the complex interplay between these factors, we may uncover critical insights into the gender-specific effects of TRPC6 deletion on astrocytic and microglial protective effects in TBI. Such insights could pave the way for more personalized approaches to treating this debilitating condition, ultimately helping to improve outcomes for all individuals affected by TBI. As we eagerly await further research in this area, we can only imagine the exciting discoveries ahead.

# 6  <u>Conclusion and future perspective</u>

The findings presented in this thesis provide strong evidence that the deletion of TRPC6 is closely associated with significant changes in the hippocampal structure and function. The study utilized TRPC6 KO mice to demonstrate that the absence of this gene leads to abnormal maturation and morphological changes in the granular cells of the DG, as well as disrupted expression and protein phosphorylation of genes essential for neuronal survival and synaptic plasticity in the hippocampus. The observed hypo-excitability and lack of LTP in these granular cells are particularly noteworthy, as they highlight the critical role that TRPC6 plays in regulating synaptic plasticity, which is essential for normal neural function. Additionally, this study's results align with the concept that TRPC6 is involved in changes in synaptic plasticity regarding dendritic development, changes in spine shape, and an increase in excitatory synapses[149], adding to the credibility of the findings.

This thesis also sheds new light on the critical role that TRPC6 plays in TBI. For the first time, the study demonstrated that TRPC6 deletion escalates TBI's pathogenicity, leading to a significant lesion volume and altered astrocytic activation following injury. Remarkably, while prior research has extensively investigated TRPC6's role in ischemic stroke [186], this study is the first to implicate TRPC6 in the pathogenesis of TBI. These novel findings add to the growing body of evidence supporting the critical role that TRPC6 plays in maintaining normal neural function and protecting against injury-induced damage.

Further studies are required to demonstrate the mechanisms behind the complex role of TRPC6 in hippocampal function and TBI progression. It is interesting to see whether the altered maturation of granular cells of the DG is accompanied by altered neurogenesis or if it is a de-maturation phenomenon and what are the exact molecular pathways behind it. Moreover, more studies are needed to clarify the relationship between TRPC6 and NMDA receptors and whether the hypo-excitability seen in the TRPC6 KO brains is associated with different NMDA or calcium homeostasis expression levels.

With regard to the TBI, further studies would be important to investigate the effects of TRPC6 deletion on long-term injury with more intentions to gender specificity, which would be the essential theoretical basis for the discovery of drugs that prevents TRPC6 degradation after injury.

# 7 Bibliography

1.  Emir, T. L. R. Neurobiology of TRP channels. *Neurobiology of TRP Channels* 1–327 (2017) doi:10.4324/9781315152837.

2.  breif history of trp.pdf.

3.  Jia, Y. T. ; & Yichang. *Transient Receptor Potential Canonical Channels and Brain Diseases*. *Transient Receptor Potential Canonical Channels and Brain Diseases* vol. 976 (2017).

4.  Himmel, N. J. & Cox, D. N. "Transient receptor potential channels: current perspectives on evolution. *Proceedings of the Royal Society B: Biological Sciences* **287**, 1–9 (2020).

5.  Clapham, D. E., Runnels, L. W. & Strübing, C. The TRP ion channel family. *Nat Rev Neurosci* **2**, 387–396 (2001).

6.  Morelli, M. B., Amantini, C., Liberati, S., Santoni, M. & Nabissi, M. Send Orders of Reprints at reprints@benthamscience.net TRP Channels: New Potential Therapeutic Approaches in CNS Neuropathies. *CNS & Neurological Disorders-Drug Targets* **12**, 274–293 (2013).

7.  Steinritz, D., Stenger, B., Dietrich, A., Gudermann, T. & Popp, T. TRPs in tox: Involvement of transient receptor potential-channels in chemical-induced organ toxicity—A structured review. *Cells* **7**, 1–22 (2018).

8.  Wes, P. D. *et al.* TRPC1, a human homolog of a Drosophila store-operated channel. *Proc Natl Acad Sci U S A* **92**, 9652–9656 (1995).

9.  Zhu, X., Chu, P. B., Peyton, M. & Birnbaumer, L. Molecular cloning of a widely expressed human homologue for the Drosophila trp gene. *FEBS Lett* **373**, 193–198 (1995).

10. Chen, X., Sooch, G., Demaree, I. S., White, F. A. & Obukhov, A. G. cells Transient Receptor Potential Canonical (TRPC) Channels: Then and Now. doi:10.3390/cells9091983.

11. Sawamura, S., Shirakawa, H., Nakagawa, T., Mori, Y. & Kaneko, S. TRP channels in the brain: What are they there for? in *Neurobiology of TRP Channels* (2017). doi:10.4324/9781315152837.

12. Lavanderos, B. *et al.* TRP Channels Regulation of Rho GTPases in Brain Context and Diseases. *Front Cell Dev Biol* **8**, 1–23 (2020).

13. Li, J. *et al.* The structure of TRPC ion channels. *Cell Calcium* **80**, 25–28 (2019).

14. Wang, H. *et al.* TRPC channels: Structure, function, regulation and recent advances in small molecular probes. *Pharmacology and Therapeutics* Preprint at https://doi.org/10.1016/j.pharmthera.2020.107497 (2020).

15. Duan, J. *et al.* Cryo-EM structure of TRPC5 at 2.8-Å resolution reveals unique and conserved structural elements essential for channel function. *Sci Adv* **5**, 1–12 (2019).

16. Fan, C., Choi, W., Sun, W., Du, J. & Lu, W. Structure of the human lipid-gated cation channel TRPC3. *Elife* **7**, 1–14 (2018).

17. Bacsa, B., Tiapko, O., Stockner, T. & Groschner, K. Mechanisms and significance of Ca2+ entry through TRPC channels. *Curr Opin Physiol* **17**, 25–33 (2020).

18. Curcic, S., Tiapko, O. & Groschner, K. Photopharmacology and opto-chemogenetics of TRPC channels-some therapeutic visions. *Pharmacol Ther* **200**, 13–26 (2019).

19. Kwon, Y., Hofmann, T. & Montell, C. Integration of Phosphoinositide- and Calmodulin-Mediated Regulation of TRPC6. *Mol Cell* **25**, 491–503 (2007).

20. Kim, H. *et al.* The roles of G proteins in the activation of TRPC4 and TRPC5 transient receptor potential channels. *Channels* **6**, 333–343 (2012).

21. Miehe, S. *et al.* The phospholipid-binding protein SESTD1 is a novel regulator of the transient receptor potential channels TRPC4 and TRPC5. *Journal of Biological Chemistry* **285**, 12426–12434 (2010).

22. Zhu, M. X. Multiple roles of calmodulin and other Ca2+-binding proteins in the functional regulation of TRP channels. *Pflugers Arch* **451**, 105–115 (2005).

23. Liu, C. H. *et al.* Arrestin-biased AT1R agonism induces acute catecholamine secretion through TRPC3 coupling. *Nat Commun* **8**, 1–17 (2017).

24. Saleh, S. N., Albert, A. P. & Large, W. A. Activation of native TRPC1/C5/C6 channels by endothelin-1 is mediated by both PIP3 and PIP2 in rabbit coronary artery myocytes—Journal *of Physiology* **587**, 5361–5375 (2009).

25. Itsuki, K. *et al.* PLC-mediated PI(4,5)P2 hydrolysis regulates activation and inactivation of TRPC6/7 channels. *Journal of General Physiology* **143**, 183–201 (2014).

26. Myeong, J. Y. *et al.* Close spatio-association of the transient receptor potential canonical 4 (TRPC4) channel with Gαi in TRPC4 activation process. *Am J Physiol Cell Physiol* **308**, C879–C889 (2015).

27. Bousquet, S. M., Monet, M. & Boulay, G. Protein kinase C-dependent phosphorylation of transient receptor potential canonical 6 (TRPC6) on serine 448 causes channel inhibition. *Journal of Biological Chemistry* **285**, 40534–40543 (2010).

28. Wang, H. *et al.* TRPC channels: Structure, function, regulation and recent advances in small molecular probes. *Pharmacology and Therapeutics* vol. 209 Preprint at https://doi.org/10.1016/j.pharmthera.2020.107497 (2020).

29. Jardin, I., Nieto, J., Salido, G. M. & Rosado, J. A. TRPC6 channel and its implications in breast cancer: an overview. *Biochim Biophys Acta Mol Cell Res* **1867**, 118828 (2020).

30. Goel, M., Sinkins, W. G. & Schilling, W. P. Selective association of TRPC channel subunits in rat brain synaptosomes. *Journal of Biological Chemistry* **277**, 48303–48310 (2002).

31. Tang, Q. *et al.* Structure of the receptor-activated human TRPC6 and TRPC3 ion channels. *Cell Research* vol. 28 746–755 Preprint at https://doi.org/10.1038/s41422-018-0038-2 (2018).

32. Estacion, M., Sinkins, W. G., Jones, S. W., Applegate, M. A. B. & Schilling, W. P. Human TRPC6 expressed in HEK 293 cells forms non-selective cation channels with limited Ca2+ permeability. *Journal of Physiology* vol. 572 359–377 Preprint at https://doi.org/10.1113/jphysiol.2005.103143 (2006).

33. Inoue, R. *et al. The Transient Receptor Potential Protein Homologue TRP6 Is the Essential Component of Vascular 1-Adrenoceptor-Activated Ca 2-Permeable Cation Channel*. http://www.circresaha.org (2001).

34. Dryer, S. E. & Kim, E. Y. Permeation and rectification in canonical transient receptor potential-6 (TRPC6) channels. *Front Physiol* **9**, 1–10 (2018).

35. Azumaya, C. M., Sierra-Valdez, F., Cordero-Morales, J. F. & Nakagawa, T. Cryo-EM structure of the cytoplasmic domain of murine transient receptor potential cation channel subfamily C member 6 (TRPC6). *Journal of Biological Chemistry* **293**, 10381–10391 (2018).

36. Bai, Y. *et al.* Structural basis for pharmacological modulation of the TRPC6 channel. *Elife* **9**, 1–18 (2020).

37. Hofmann, T. *et al.* Direct activation of human TRPC6 and TRPC3 channels by diacylglycerol. *Nature* **397**, 259–263 (1999).

38. Leuner, K. *et al.* Simple 2,4-diacylphloroglucinols as classic transient receptor potential-6 activators - Identification of a novel pharmacophore. *Mol Pharmacol* **77**, 368–377 (2010).

39. Leuner, K. *et al.* Hyperforin—a key constituent of St. John's wort specifically activates TRPC6 channels. *The FASEB Journal* vol. 21 4101–4111 Preprint at https://doi.org/10.1096/fj.07-8110com (2007).

40. Williams, J. W. & Holsinger, T. St John's for depression, worts and all. *Bmj* **330**, E350 (2005).

41. Mony, T. J., Elahi, F., Choi, J. W. & Park, S. J. Neuropharmacological Effects of Terpenoids on Preclinical Animal Models of Psychiatric Disorders: A Review. *Antioxidants* vol. 11 Preprint at https://doi.org/10.3390/antiox11091834 (2022).

42. Zanoli, P. Role of hyperforin in the pharmacological activities of St. John's wort. *CNS Drug Rev* **10**, 203–218 (2004).

43. Roshanravan, H., Kim, E. Y. & Dryer, S. E. 20-hydroxyeicosatetraenoic acid (20-HETE) modulates canonical transient receptor potential-6 (TRPC6) channels in podocytes. *Front Physiol* **7**, 1–12 (2016).

44. Yamaguchi, Y., Iribe, G., Nishida, M. & Naruse, K. Role of TRPC3 and TRPC6 channels in the myocardial response to stretch: Linking physiology and pathophysiology. *Prog Biophys Mol Biol* **130**, 264–272 (2017).

45. Kim, E. Y., Roshanravan, H. & Dryer, S. E. Changes in podocyte TRPC channels evoked by plasma and sera from patients with recurrent FSGS and by putative glomerular permeability factors. *Biochim Biophys Acta Mol Basis Dis* **1863**, 2342–2354 (2017).

46. Jiang, Y. *et al.* Topotecan prevents hypoxia-induced pulmonary arterial hypertension and inhibits hypoxia-inducible factor-1α and TRPC channels. *International Journal of Biochemistry and Cell Biology* **104**, 161–170 (2018).

47. Tai, Y., Feng, S., Du, W. & Wang, Y. Functional roles of TRPC channels in the developing brain. *Pflugers Arch* **458**, 283–289 (2009).

48. Sun, Y., Sukumaran, P., Bandyopadhyay, B. C. & Singh, B. B. Physiological function and characterization of TRPCs in neurons. *Cells* vol. 3 455–475 Preprint at https://doi.org/10.3390/cells3020455 (2014).

49. Insausti, R. & Amaral, D. G. Hippocampal Formation. in *The Human Nervous System: Second Edition* 871–914 (Elsevier Inc., 2003). doi:10.1016/B978-012547626-3/50024-7.

50. Shavitt, T., Johnson, I. N. S. & Batistuzzo, M. C. Hippocampal formation volume, its subregions, and its specific contributions to visuospatial memory tasks. *Brazilian Journal of Medical and Biological Research* **53**, 1–9 (2020).

51. Fanselow, M. S. & Dong, H. W. Are the Dorsal and Ventral Hippocampus Functionally Distinct Structures? *Neuron* vol. 65 7–19 Preprint at https://doi.org/10.1016/j.neuron.2009.11.031 (2010).

52. Schultz, C. & Engelhardt, M. Anatomy of the hippocampal formation. in *The Hippocampus in Clinical Neuroscience* vol. 34 6–17 (S. Karger AG, 2014).

53. Dudek, S. M., Alexander, G. M. & Farris, S. Rediscovering area CA2: Unique properties and functions. *Nature Reviews Neuroscience* vol. 17 89–102 Preprint at https://doi.org/10.1038/nrn.2015.22 (2016).

54. Schultz, C. & Engelhardt, M. Anatomy of the hippocampal formation. in *The Hippocampus in Clinical Neuroscience* vol. 34 6–17 (S. Karger AG, 2014).

55. Canto, C. B., Wouterlood, F. G. & Witter, M. P. What does the anatomical organization of the entorhinal cortex tell us? *Neural Plasticity* vol. 2008 Preprint at https://doi.org/10.1155/2008/381243 (2008).

56. Amaral, D. G., Scharfman, H. E. & Lavenex, P. *The dentate gyrus: fundamental neuroanatomical organization (dentate gyrus for dummies).*

57. Scharfman, H. E. & Myers, C. E. Hilar mossy cells of the dentate gyrus: A historical perspective. *Frontiers in Neural Circuits* Preprint at https://doi.org/10.3389/fncir.2012.00106 (2012).

58. Kriegstein, A. & Alvarez-Buylla, A. The glial nature of embryonic and adult neural stem cells. *Annual Review of Neuroscience* vol. 32 149–184 Preprint at https://doi.org/10.1146/annurev.neuro.051508.135600 (2009).

59. Houser, C. R. Interneurons of the dentate gyrus: an overview of cell types, terminal fields and neurochemical identity. *Prog Brain Res* **163**, 217–233 (2007).

60. Lovett-Barron, M. *et al.* Regulation of neuronal input transformations by tunable dendritic inhibition. *Nat Neurosci* **15**, 423–430 (2012).

61. Savic´, N. ˘ A., Savic´, S., Pedarzani, P. & Sciancalepore, M. *Medium Afterhyperpolarization and Firing Pattern Modulation in Interneurons of Stratum Radiatum in the CA3 Hippocampal Region.* www.jn.physiology.org (2001).

62. Pedroni, A., Minh, D. D., Mallamaci, A. & Cherubini, E. Electrophysiological characterization of granule cells in the dentate gyrus immediately after birth. *Front Cell Neurosci* **8**, 1–9 (2014).

63. Gould, E. *Serotonin and Hippocampal Neurogenesis. Neuropsychopharmacology* vol. 21 (1999).

64. Duan, X., Kang, E., Liu, C. Y., Ming, G. li & Song, H. Development of neural stem cell in the adult brain. *Current Opinion in Neurobiology* vol. 18 108–115 Preprint at https://doi.org/10.1016/j.conb.2008.04.001 (2008).

65. Oomen, C. A., Bekinschtein, P., Kent, B. A., Saksida, L. M. & Bussey, T. J. Adult hippocampal neurogenesis and its role in cognition. *Wiley Interdisciplinary*

*Reviews: Cognitive Science* vol. 5 573–587 Preprint at https://doi.org/10.1002/wcs.1304 (2014).

66. Steiner, B. *et al.* Type-2 cells as link between glial and neuronal lineage in adult hippocampal neurogenesis. *Glia* **54**, 805–814 (2006).

67. Nicola, Z., Fabel, K. & Kempermann, G. Development of the adult neurogenic niche in the hippocampus of mice. *Front Neuroanat* **9**, (2015).

68. Semënov, M. v. Adult Hippocampal Neurogenesis Is a Developmental Process Involved in Cognitive Development. *Front Neurosci* **13**, (2019).

69. Kempermann, G., Song, H. & Gage, F. H. Neurogenesis in the adult hippocampus. *Cold Spring Harb Perspect Med* **5**, (2015).

70. Kitabatake, Y., Sailor, K. A., Ming, G. li & Song, H. Adult Neurogenesis and Hippocampal Memory Function: New Cells, More Plasticity, New Memories? *Neurosurgery Clinics of North America* vol. 18 105–113 Preprint at https://doi.org/10.1016/j.nec.2006.10.008 (2007).

71. Marín-Burgin, A., Mongiat, L. A., Pardi, M. B. & Schinder, A. F. Unique processing during a period of high excitation/inhibition balance in adult-born neurons. *Science (1979)* **335**, 1238–1242 (2012).

72. Lopez-Rojas, J. & Kreutz, M. R. Mature granule cells of the dentate gyrus-Passive bystanders or principal performers in hippocampal function? *Neurosci Biobehav Rev* **64**, 167–174 (2016).

73. Nagy, G. A. *et al.* DAG-sensitive and Ca2+ permeable TRPC6 channels are expressed in dentate granule cells and interneurons in the hippocampal formation. *Hippocampus* (2013) doi:10.1002/hipo.22081.

74. Hagenston, A. M. & Baing, H. Calcium signaling in synapse-to-nucleus communicationl. *Cold Spring Harb Perspect Biol* **3**, (2011).

75. Gualdani, R. & Gailly, P. How TRPC channels modulate hippocampal function. *Int J Mol Sci* **21**, 1–19 (2020).

76. Tai, Y. *et al.* TRPC6 channels promote dendritic growth via the CaMKIV-CREB pathway. *J Cell Sci* **121**, 2301–2307 (2008).

77. Xie, R. *et al.* AAV Delivery of shRNA Against TRPC6 in Mouse Hippocampus Impairs Cognitive Function. *Front Cell Dev Biol* **9**, (2021).

78. Gao, Y. Y. *et al.* Canonical transient receptor potential channels and their modulators: biology, pharmacology and therapeutic potentials. *Archives of Pharmacal Research* vol. 44 354–377 Preprint at https://doi.org/10.1007/s12272-021-01319-5 (2021).

79. Sawamura, S., Shirakawa, H., Nakagawa, T., Mori, Y. & Kaneko, S. TRP Channels in the Brain. in *Neurobiology of TRP Channels* (2019). doi:10.4324/9781315152837-16.

80. Zeng, C., Tian, F. & Xiao, B. TRPC Channels: Prominent Candidates of Underlying Mechanism in Neuropsychiatric Diseases. *Molecular Neurobiology* vol. 53 631–647 Preprint at https://doi.org/10.1007/s12035-014-9004-2 (2016).

81. Thapak, P., Vaidya, B., Joshi, H. C., Singh, J. N. & Sharma, S. S. Therapeutic potential of pharmacological agents targeting TRP channels in CNS disorders. *Pharmacological Research* vol. 159 Preprint at https://doi.org/10.1016/j.phrs.2020.105026 (2020).

82. Friedland, K. & Harteneck, C. Hyperforin: To be or not to be an activator of TRPC(6). *Rev Physiol Biochem Pharmacol* **169**, 1–24 (2015).

83. Duman, C. H. & Duman, R. S. Spine synapse remodeling in the pathophysiology and treatment of depression. *Neurosci Lett* **601**, 20–29 (2014).

84. Kim, Y. J. & Kang, T. C. The role of TRPC6 in seizure susceptibility and seizure-related neuronal damage in the rat dentate gyrus. *Neuroscience* **307**, 215–230 (2015).

85. Selkoe, D. J. *Alzheimer Disease: Mechanistic Understanding Predicts Novel Therapies*. https://annals.org (2004).

86. Griffith, T. N., Varela-Nallar, L., Dinamarca, M. C. & Inestrosa, N. C. *Neurobiological Effects of Hyperforin and its Potential in Alzheimer's Disease Therapy*. *Current Medicinal Chemistry* vol. 17 (2010).

87. Inestrosa, N. C. *et al.* Tetrahydrohyperforin prevents cognitive deficit, Aβ deposition, tau phosphorylation and synaptotoxicity in the APPswe/PSEN1ΔE9

model of Alzheimer's disease: A possible effect on APP processing. *Transl Psychiatry* **1**, (2011).

88.  Lu, R., He, Q. & Wang, J. TRPC channels and Alzheimer's disease. in *Advances in Experimental Medicine and Biology* vol. 976 73–83 (Springer New York LLC, 2017).

89.  Channels, T. TRPC Channels and Alzheimer's Disease. (2017) doi:10.1007/978-94-024-1088-4.

90.  Hyder, A. A., Wunderlich, C. A., Puvanachandra, P., Gururaj, G. & Kobusingye, O. C. *The impact of traumatic brain injuries: A global perspective*. *NeuroRehabilitation* vol. 22 (2007).

91.  Mckee, A. C. & Daneshvar, D. H. The neuropathology of traumatic brain injury. in *Handbook of Clinical Neurology* vol. 127 45–66 (Elsevier B.V., 2015).

92.  Reis, C. *et al.* What's new in traumatic brain injury: Update on tracking, monitoring and treatment. *Int J Mol Sci* **16**, 11903–11965 (2015).

93.  Khoshnam, S. E., Winlow, W., Farzaneh, M., Farbood, Y. & Moghaddam, H. F. Pathogenic mechanisms following ischemic stroke. *Neurological Sciences* vol. 38 1167–1186 Preprint at https://doi.org/10.1007/s10072-017-2938-1 (2017).

94.  Qin, C. *et al.* Signaling pathways involved in ischemic stroke: molecular mechanisms and therapeutic interventions. *Signal Transduction and Targeted Therapy* vol. 7 Preprint at https://doi.org/10.1038/s41392-022-01064-1 (2022).

95.  Shekhar, S. *et al.* Novel mechanistic insights and potential therapeutic impact of trpc6 in neurovascular coupling and ischemic stroke. *International Journal of Molecular Sciences* vol. 22 1–15 Preprint at https://doi.org/10.3390/ijms22042074 (2021).

96.  Du, W. *et al.* Inhibition of TRPC6 degradation suppresses ischemic brain damage in rats. *Journal of Clinical Investigation* **120**, 3480–3492 (2010).

97.  Shen, H., Pan, J., Pan, L. & Zhang, N. TRPC6 inhibited NMDA current in cultured hippocampal neurons. *Neuromolecular Med* (2013) doi:10.1007/s12017-013-8226-1.

98.  Du, W. *et al.* Inhibition of TRPC6 degradation suppresses ischemic brain damage in rats. *Journal of Clinical Investigation* **120**, 3480–3492 (2010).

99.  Lin, Y. *et al.* Neuroprotective effect of resveratrol on ischemia/reperfusion injury in rats through TRPC6/CREB pathways. *Journal of Molecular Neuroscience* **50**, 504–513 (2013).

100. Li, W. *et al.* Over-Expression of TRPC6 via CRISPR Based Synergistic Activation Mediator in BMSCs Ameliorates Brain Injury in a Rat Model of Cerebral Ischemia/Reperfusion. *Neuroscience* **415**, 147–160 (2019).

101. Zhang, J., Mao, X., Zhou, T., Cheng, X. & Lin, Y. IL-17A contributes to brain ischemia reperfusion injury through calpain-TRPC6 pathway in mice. *Neuroscience* **274**, 419–428 (2014).

102. Liu, L. *et al.* Novel Targets for Stroke Therapy: Special Focus on TRPC Channels and TRPC6. *Frontiers in Aging Neuroscience* vol. 12 Preprint at https://doi.org/10.3389/fnagi.2020.00070 (2020).

103. Hughes, N. *et al.* The prevalence of traumatic brain injury among young offenders in custody: A systematic review. *Journal of Head Trauma Rehabilitation* vol. 30 94–105 Preprint at https://doi.org/10.1097/HTR.0000000000000124 (2015).

104. Maas, A. I. R. & Lingsma, H. F. *Predicting outcome after traumatic brain injury.* (2015).

105. Najem, D. *et al. Downloaded from www.nrcresearchpress. Biochem. Cell Biol* www.nrcresearchpress.com.

106. Osier, N. & Dixon, C. E. The controlled cortical impact model of experimental brain trauma: Overview, research applications, and protocol. in *Methods in Molecular Biology* vol. 1462 177–192 (Humana Press Inc., 2016).

107. Xiong, Y., Mahmood, A. & Chopp, M. Animal models of traumatic brain injury. *Nature Reviews Neuroscience* vol. 14 128–142 Preprint at https://doi.org/10.1038/nrn3407 (2013).

108. Paterno, R., Folweiler, K. A. & Cohen, A. S. Pathophysiology and Treatment of Memory Dysfunction After Traumatic Brain Injury. *Current Neurology and*

*Neuroscience Reports* vol. 17 Preprint at https://doi.org/10.1007/s11910-017-0762-x (2017).

109. Gupta, A., Elgammal, F. S., Proddutur, A., Shah, S. & Santhakumar, V. Decrease in tonic inhibition contributes to increase in dentate semilunar granule cell excitability after brain injury. *Journal of Neuroscience* **32**, 2523–2537 (2012).

110. Andrews, K., Josiah, S. S. & Zhang, J. The therapeutic potential of neuronal K-Cl co- transporter KCC2 in Huntington's disease and its comorbidities. *International Journal of Molecular Sciences* vol. 21 1–21 Preprint at https://doi.org/10.3390/ijms21239142 (2020).

111. Bonislawski, D. P., Schwarzbach, E. P. & Cohen, A. S. Brain injury impairs dentate gyrus inhibitory efficacy. *Neurobiol Dis* **25**, 163–169 (2007).

112. Larkin, M. C., Lykken, C., Tye, L. D., Wickelgren, J. G. & Frank, L. M. Hippocampal output area CA1 broadcasts a generalized novelty signal during an object-place recognition task. *Hippocampus* **24**, 773–783 (2014).

113. Paterno, R., Folweiler, K. A. & Cohen, A. S. Pathophysiology and Treatment of Memory Dysfunction After Traumatic Brain Injury. *Current Neurology and Neuroscience Reports* vol. 17 Preprint at https://doi.org/10.1007/s11910-017-0762-x (2017).

114. Myer, D. J., Gurkoff, G. G., Lee, S. M., Hovda, D. A. & Sofroniew, M. v. Essential protective roles of reactive astrocytes in traumatic brain injury. *Brain* **129**, 2761–2772 (2006).

115. di Giovanni, S. *et al. Cell cycle inhibition provides neuroprotection and reduces glial proliferation and scar formation after traumatic brain injury.* https://www.pnas.org (2005).

116. Karve, I. P., Taylor, J. M. & Crack, P. J. The contribution of astrocytes and microglia to traumatic brain injury. *Br J Pharmacol* **173**, 692–702 (2016).

117. Loane, D. J., Kumar, A., Stoica, B. A. & Faden, A. I. *Progressive Neurodegeneration After Experimental Brain Trauma: Association With Chronic Microglial Activation.* https://academic.oup.com/jnen/article/73/1/14/2917532 (2013).

118. Karve, I. P., Taylor, J. M. & Crack, P. J. The contribution of astrocytes and microglia to traumatic brain injury. *Br J Pharmacol* **173**, 692–702 (2016).

119. Jeon, J. *et al.* Contribution of TRPC Channels in Neuronal Excitotoxicity Associated With Neurodegenerative Disease and Ischemic Stroke. *Front Cell Dev Biol* **8**, (2021).

120. Hummel, R. *et al.* Single intracerebroventricular progranulin injection adversely affects the blood–brain barrier in experimental traumatic brain injury. *J Neurochem* **158**, 342–357 (2021).

121. Thal, S. C., Wyschkon, S., Pieter, D., Engelhard, K. & Werner, C. Selection of endogenous control genes for normalization of gene expression analysis after experimental brain trauma in mice. *J Neurotrauma* **25**, 785–794 (2008).

122. Conforti, L. Patch-Clamp Techniques. in *Cell Physiology Source Book: Essentials of Membrane Biophysics* 369–381 (Elsevier, 2011). doi:10.1016/B978-0-12-387738-3.00020-2.

123. Hummel, R. *et al.* Administration of all-trans retinoic acid after experimental traumatic brain injury is brain protective. *Br J Pharmacol* **177**, 5208–5223 (2020).

124. Cole, J. T. *et al.* Craniotomy: True sham for traumatic brain injury, or a sham of a sham? *J Neurotrauma* **28**, 359–369 (2011).

125. Navari, R. M., Wei, E. P., Kontos, H. A. & Patterson, J. L. *Comparison of the Open Skull and Cranial Window Preparations in the Study of the Cerebral Microcirculation*.

126. Hamm, R. J., Pike, B. R., O'dell, D. M., Lyeth, B. G. & Jenkins2, L. W. *The Rotarod Test: An Evaluation of Its Effectiveness in Assessing Motor Deficits Following Traumatic Brain Injury*.

127. Montgomery, ". *THE RELATION BETWEEN FEAR INDUCED .BY NOVEL STTMULATfON AND EXPLORATORY BEHAVIOR*.

128. Zhou, J. *et al.* Critical role of TRPC6 channels in the formation of excitatory synapses. *Nat Neurosci* **11**, 741–743 (2008).

129. Nagy, G. A. *et al.* DAG-sensitive and Ca2+ permeable TRPC6 channels are expressed in dentate granule cells and interneurons in the hippocampal formation. *Hippocampus* **23**, 221–232 (2013).

130. Hagihara, H., Takao, K., Walton, N. M., Matsumoto, M. & Miyakawa, T. Immature dentate gyrus: An endophenotype of neuropsychiatric disorders. *Neural Plast* **2013**, (2013).

131. Heiser, J. H. *et al.* TRPC6 channel-mediated neurite outgrowth in PC12 cells and hippocampal neurons involves activation of RAS/MEK/ERK, PI3K, and CAMKIV signaling. *J Neurochem* **127**, 303–313 (2013).

132. Tanis, K. Q., Duman, R. S. & Newton, S. S. CREB Binding and Activity in Brain: Regional Specificity and Induction by Electroconvulsive Seizure. *Biol Psychiatry* **63**, 710–720 (2008).

133. Tai, Y. *et al.* TRPC6 channels promote dendritic growth via the CaMKIV-CREB pathway. *J Cell Sci* **121**, 2301–2307 (2008).

134. Fortin, D. A. *et al.* Brain-derived neurotrophic factor activation of CaM-kinase kinase via transient receptor potential canonical channels induces the translation and synaptic incorporation of GluA1-containing calcium-permeable AMPA receptors. *Journal of Neuroscience* **32**, 8127–8137 (2012).

135. Bird, C. M. & Burgess, N. The hippocampus and memory: Insights from spatial processing. *Nature Reviews Neuroscience* vol. 9 182–194 Preprint at https://doi.org/10.1038/nrn2335 (2008).

136. Lopez-Rojas, J. & Kreutz, M. R. Mature granule cells of the dentate gyrus-Passive bystanders or principal performers in hippocampal function? *Neuroscience and Biobehavioral Reviews* vol. 64 167–174 Preprint at https://doi.org/10.1016/j.neubiorev.2016.02.021 (2016).

137. Reid, C. A. & Clements, J. D. Postsynaptic expression of long-term potentiation in the rat dentate gyrus demonstrated by variance-mean analysis. *Journal of Physiology* **518**, 121–130 (1999).

138. Bromer, C. *et al.* Long-term potentiation expands information content of hippocampal dentate gyrus synapses. *Proc Natl Acad Sci U S A* **115**, E2410–E2418 (2018).

139. Collitti-Klausnitzer, J., Hagena, H., Dubovyk, V. & Manahan-Vaughan, D. Preferential frequency-dependent induction of synaptic depression by the lateral perforant path and of synaptic potentiation by the medial perforant path inputs to the dentate gyrus. *Hippocampus* **31**, 957–981 (2021).

140. Kim, K.-R. *et al.* Calbindin regulates Kv4.1 trafficking and excitability of dentate granule cells via CaMKII-dependent phosphorylation Lead contact. doi:10.1101/2021.02.26.433035.

141. Walton, N. M. *et al.* Detection of an immature dentate gyrus feature in human schizophrenia/bipolar patients. *Transl Psychiatry* **2**, (2012).

142. Hagihara, H. *et al.* Expression of progenitor cell/immature neuron markers does not present definitive evidence for adult neurogenesis. *Molecular Brain* vol. 12 Preprint at https://doi.org/10.1186/s13041-019-0522-8 (2019).

143. Li, C. xin *et al.* β-arrestin 2 is essential for fluoxetine-mediated promotion of hippocampal neurogenesis in a mouse model of depression. *Acta Pharmacol Sin* **42**, 679–690 (2021).

144. Karádi, K. *et al.* Correlation between calbindin expression in granule cells of the resected hippocampal dentate gyrus and verbal memory in temporal lobe epilepsy. *Epilepsy and Behavior* **25**, 110–119 (2012).

145. Radic, T. *et al.* Differential postnatal expression of neuronal maturation markers in the dentate gyrus of mice and rats. *Front Neuroanat* **11**, (2017).

146. Roy, A., Millen, K. J. & Kapur, R. P. Hippocampal granule cell dispersion: A non-specific finding in pediatric patients with no history of seizures. *Acta Neuropathol Commun* **8**, (2020).

147. Griesi-Oliveira, K. *et al.* Modeling non-syndromic autism and the impact of TRPC6 disruption in human neurons. *Mol Psychiatry* **20**, 1350–1365 (2015).

148. Griesi-Oliveira, K. *et al.* Modeling non-syndromic autism and the impact of TRPC6 disruption in human neurons. *Mol Psychiatry* **20**, 1350–1365 (2015).

149. Zhou, J. *et al.* Critical role of TRPC6 channels in the formation of excitatory synapses. *Nat Neurosci* (2008) doi:10.1038/nn.2127.

150. Heiser, J. H. *et al.* TRPC6 channel-mediated neurite outgrowth in PC12 cells and hippocampal neurons involves activation of RAS/MEK/ERK, PI3K, and CAMKIV signaling. *J Neurochem* **127**, 303–313 (2013).

151. Amidfar, M., de Oliveira, J., Kucharska, E., Budni, J. & Kim, Y. K. The role of CREB and BDNF in neurobiology and treatment of Alzheimer's disease. *Life Sciences* vol. 257 Preprint at https://doi.org/10.1016/j.lfs.2020.118020 (2020).

152. Su, B., Ji, Y. S., Sun, X. L., Liu, X. H. & Chen, Z. Y. Brain-derived neurotrophic factor (BDNF)-induced mitochondrial motility arrest and presynaptic docking contribute to BDNF-enhanced synaptic transmission. *Journal of Biological Chemistry* (2014) doi:10.1074/jbc.M113.526129.

153. Lee, D. Y. Roles of mTOR Signaling in Brain Development. *Exp Neurobiol* **24**, 177–185 (2015).

154. Nikbakht, F., Hashemi, P., Vazifekhah, S. & Babaei, J. F. Investigating the mechanism of antiepileptogenic effect of apigenin in kainate temporal lobe epilepsy: possible role of mTOR. *Exp Brain Res* (2023) doi:10.1007/s00221-023-06557-1.

155. el Hamdaoui, Y. *et al.* Analysis of hyperforin (St. John's wort) action at TRPC6 channel leads to the development of a new class of antidepressant drugs. *Mol Psychiatry* (2022) doi:10.1038/s41380-022-01804-3.

156. Mertens, J. *et al.* Differential responses to lithium in hyperexcitable neurons from patients with bipolar disorder. *Nature* **527**, 95–99 (2015).

157. Guo, Y., Su, Z. J., Chen, Y. K. & Chai, Z. Brain-derived neurotrophic factor/neurotrophin 3 regulate axon initial segment location and affect neuronal excitability in cultured hippocampal neurons. *J Neurochem* **142**, 260–271 (2017).

158. Shen, H., Pan, J., Pan, L. & Zhang, N. TRPC6 inhibited NMDA current in cultured hippocampal neurons. *Neuromolecular Med* **15**, 389–395 (2013).

159. Kim, D. S., Ryu, H. J., Kim, J. E. & Kang, T. C. The reverse roles of transient receptor potential canonical channel-3 and -6 in neuronal death following pilocarpine-induced status epilepticus. *Cell Mol Neurobiol* **33**, 99–109 (2013).

160. *Epilepsy*. (Exon Publications, 2022). doi:10.36255/exon-publications-epilepsy.

161. Kim, J.-E., Park, H., Choi, S.-H., Kong, M.-J. & Kang, T.-C. TRPC6-Mediated ERK1/2 Activation Increases Dentate. *Cells* **8**, 1376 (2019).

162. Kim, J. E., Park, J. Y. & Kang, T. C. TRPC6-mediated ERK1/2 activation regulates neuronal excitability via subcellular Kv4.3 localization in the rat hippocampus. *Front Cell Neurosci* **11**, 1–16 (2017).

163. Nayak, M. *et al.* Epigenetic signature in neural plasticity: the journey so far and journey ahead. *Heliyon* vol. 8 Preprint at https://doi.org/10.1016/j.heliyon.2022.e12292 (2022).

164. Palmer, A. & Good, M. Hippocampal synaptic activity, pattern separation and episodic-like memory: Implications for mouse models of Alzheimer's disease pathology. in *Biochemical Society Transactions* vol. 39 902–909 (2011).

165. Barnes, C. A., Rao, G. & Houston, F. P. LTP induction threshold change in old rats at the perforant path-granule cell synapse. *Neurobiology of Aging* vol. 21 613–620 Preprint at https://doi.org/10.1016/S0197-4580(00)00163-9 (2000).

166. Beis, D., Schwarting, R. K. W. & Dietrich, A. Evidence for a supportive role of classical transient receptor potential 6 (TRPC6) in the exploration behavior of mice. *Physiol Behav* **102**, 245–250 (2011).

167. Zernov, N. *et al.* New Positive TRPC6 Modulator Penetrates Blood–Brain Barrier, Eliminates Synaptic Deficiency and Restores Memory Deficit in 5xFAD Mice. *Int J Mol Sci* **23**, (2022).

168. Smith, D. H. *et al. A Model of Parasagittal Controlled Cortical Impact in the Mouse: Cognitive and Histopathologic Effects. JOURNAL OF NEUROTRAUMA* vol. 12 (1995).

169. Krämer, T. J. *et al.* Depletion of regulatory T cells increases T cell brain infiltration, reactive astrogliosis, and interferon-γgene expression in acute experimental traumatic brain injury. *J Neuroinflammation* **16**, (2019).

170. Clark, L. R. *et al.* Mild Traumatic Brain Injury Induces Transient, Sequential Increases in Proliferation, Neuroblasts/Immature Neurons, and Cell Survival: A Time Course Study in the Male Mouse Dentate Gyrus. *Front Neurosci* **14**, (2021).

171. Hol, E. M. & Pekny, M. Glial fibrillary acidic protein (GFAP) and the astrocyte intermediate filament system in diseases of the central nervous system. *Current Opinion in Cell Biology* vol. 32 121–130 Preprint at https://doi.org/10.1016/j.ceb.2015.02.004 (2015).

172. Arcuri, C., Mecca, C., Bianchi, R., Giambanco, I. & Donato, R. The pathophysiological role of microglia in dynamic surveillance, phagocytosis and structural remodeling of the developing CNS. *Frontiers in Molecular Neuroscience* vol. 10 Preprint at https://doi.org/10.3389/fnmol.2017.00191 (2017).

173. Timaru-Kast, R. *et al.* Influence of Age on Brain Edema Formation, Secondary Brain Damage and Inflammatory Response after Brain Trauma in Mice. *PLoS One* **7**, (2012).

174. Bramlett, H. M. & Dietrich, W. D. Long-Term Consequences of Traumatic Brain Injury: Current Status of Potential Mechanisms of Injury and Neurological Outcomes. *J Neurotrauma* **32**, 1834–1848 (2015).

175. Walter, J. *et al.* Focal lesion size poorly correlates with motor function after experimental traumatic brain injury in mice. *PLoS One* **17**, (2022).

176. Loane, D. J., Kumar, A., Stoica, B. A. & Faden, A. I. *Progressive Neurodegeneration After Experimental Brain Trauma: Association With Chronic Microglial Activation*. www.jneuropath.com (2013).

177. Yang, L. Y. *et al.* Post-traumatic administration of the p53 inactivator pifithrin-α oxygen analogue reduces hippocampal neuronal loss and improves cognitive deficits after experimental traumatic brain injury. *Neurobiol Dis* **96**, 216–226 (2016).

178. Tai, Y. *et al.* TRPC6 channels promote dendritic growth via the CaMKIV-CREB pathway. *J Cell Sci* **121**, 2301–2307 (2008).

179. Li, H. *et al.* TRPC6 inhibited NMDA receptor activities and protected neurons from ischemic excitotoxicity. *J Neurochem* **123**, 1010–1018 (2012).

180. Du, W. *et al.* Inhibition of TRPC6 degradation suppresses ischemic brain damage in rats. *Journal of Clinical Investigation* **120**, 3480–3492 (2010).

181. Wang, J., Sun, R., Li, Z. & Pan, Y. Combined bone marrow stromal cells and oxiracetam treatments ameliorates acute cerebral ischemia/reperfusion injury through TRPC6. *Acta Biochim Biophys Sin (Shanghai)* **51**, 767–777 (2018).

182. Lin, Y. *et al.* Neuroprotective effect of resveratrol on ischemia/reperfusion injury in rats through TRPC6/CREB pathways. *Journal of Molecular Neuroscience* **50**, 504–513 (2013).

183. Li, W. *et al.* Over-Expression of TRPC6 via CRISPR Based Synergistic Activation Mediator in BMSCs Ameliorates Brain Injury in a Rat Model of Cerebral Ischemia/Reperfusion. *Neuroscience* **415**, 147–160 (2019).

184. Wang, J., Sun, R., Li, Z. & Pan, Y. Combined bone marrow stromal cells and oxiracetam treatments ameliorates acute cerebral ischemia/reperfusion injury through TRPC6. *Acta Biochim Biophys Sin (Shanghai)* **51**, 767–777 (2018).

185. Lin, Y. *et al.* Hyperforin attenuates brain damage induced by transient middle cerebral artery occlusion (MCAO) in rats via inhibition of TRPC6 channels degradation. *Journal of Cerebral Blood Flow and Metabolism* **33**, 253–262 (2013).

186. Huang, J. TRPC channels and stroke. in *Advances in Experimental Medicine and Biology* vol. 976 61–71 (Springer New York LLC, 2017).

187. Chen, X. *et al.* The TRPC6 inhibitor, larixyl acetate, is effective in protecting against traumatic brain injury-induced systemic endothelial dysfunction. *J Neuroinflammation* (2019) doi:10.1186/s12974-019-1407-6.

188. Dietrich, A. *et al.* Increased Vascular Smooth Muscle Contractility in TRPC6 − / − Mice . *Mol Cell Biol* **25**, 6980–6989 (2005).

189. Folweiler, K. A., Samuel, S., Metheny, H. E. & Cohen, A. S. Diminished dentate gyrus filtering of cortical input leads to enhanced area ca3 excitability after mild traumatic brain injury. *J Neurotrauma* **35**, 1304–1317 (2018).

190. Silver, J. & Miller, J. H. Regeneration beyond the glial scar. *Nature Reviews Neuroscience* vol. 5 146–156 Preprint at https://doi.org/10.1038/nrn1326 (2004).

191. Susarla, B. T. S., Villapol, S., Yi, J. H., Geller, H. M. & Symes, A. J. Temporal patterns of cortical proliferation of glial cell populations after traumatic brain injury in mice. *ASN Neuro* **6**, 159–170 (2014).

192. Graeber, M. B. & Stre'rt, W. J. Microglia: Immune Network in the CNS. *Brain Pathology* vol. 1 2–5 Preprint at https://doi.org/10.1111/j.1750-3639.1990.tb00630.x (1990).

193. Liu, L. *et al.* TRPC6 Attenuates Cortical Astrocytic Apoptosis and Inflammation in Cerebral Ischemic/Reperfusion Injury. *Front Cell Dev Biol* **8**, (2021).

194. Villapol, S., Loane, D. J. & Burns, M. P. Sexual dimorphism in the inflammatory response to traumatic brain injury. *Glia* **65**, 1423–1438 (2017).

195. Caplan, H. W., Cox, C. S. & Bedi, S. S. Do microglia play a role in sex differences in TBI? *Journal of Neuroscience Research* vol. 95 509–517 Preprint at https://doi.org/10.1002/jnr.23854 (2017).

196. Carver, C. M. *et al.* Neuroprotective Effects of Estrogen Through BDNF-Transient Receptor Potential Channels 6 Signaling Pathway in the Hippocampus in a Rat Model of Perimenopausal Depression. **14**, 1–15 (2022).

# 8  <u>Figures and Tables</u>

## 8.1  Figures

All figures were created using BioRender.com.

## 8.2  Tables

# Curriculum vitae

███████████████████████████

██████████████████████████████

███████████████████████████

████████████████████████████████

████████████████████████████████

████████████████████████████████

████████████████████

████████████████████████████████████████

████████████████████████████████

## Education

██████████████████████████████████████████████
████████████████████████████████████████████

██████████████████████████████████████████████
████████████████████████████████████
███████████████

██████████████████████████████████████████████
████████████████████████████████████
███████████████

██████████████████████████████████████████████
█████████████████████████████████████████████.

## Scientific career

██████████████████████████████████████████████
███████████████

██████████████████████████████████████████████
█████████

██████████████████████████████████████████████
███████████████

██████████████████████████████████████████████
██████████████

██████████████████████████████████████████████
████████████████████████████

## Conferences and workshops

██████████████████████████████████████████████████████
████████████████████████████████

████████████████████████████████████████████████████████
████████████████████

████████████████████████████████████████████████████████
████████████████████████████████████████████████
████████████████████████████████████████████████

████████████████████████████████████████████████████████
████████████████████████████████████████████████
████████████████████████████████████████████████
████████████████████████████████████████████████
███████

████████████████████████████████████████████████████████
████████████████████████████████████████████████

████████████████████████████████████████████████████████
████████████████████████████████████████████████
████████████████████████████████████████

████████████████████████████████████████████████████████
████████████████████████████████████████████████

## Publications

████████████████████████████████████████████████████████
████████████████████████

████████████████████████████████████████████████████████

████████████████████████████████████████████████████████

████████████████████████████████████████████████████████

████████████████████████████████████████████████████████

████████████████████████████████████████████████████

████████████████████████████████████████████████████████
████████████████████████████████████████████████

████████████████████████████████████████████████████████

██████████████████████

████████████████████████████████████████████████████

████████████████████████████████████████████████████████
████████████████████████████████████████████████
████████████████

Salma Hamed

Mainz, March 2023